

(2)

AD-A239 297



OA 11606

DTIC
S
AUG 6 1991
C
D

July 1991

Applications of Wavelets to Radar Data Processing

Final Technical Report

CLIN 0002AA

Approved for public release;
distribution unlimited.

AIR FORCE OF SCIENTIFIC RESEARCH (AFOSR)
NOTICE OF TRANSMITTAL TO DTIC
This technical report has been reviewed and is
approved for public release IAW AFM 200-12
instructions, as indicated.
Charles W. Miller
AFOSR Program Manager

Principal Investigator
Mr. Charles Stirman

Program Manager
Dr. Arje Nachman

Sponsored by
Defense Advanced Research Projects Agency
DARPA Order No. 7450
Monitored by AFOSR Under Contract No. F49620-90-C-0050

Martin Marietta Electronics,
Information, and Missiles Group
P.O. Box 555837
Orlando, Florida 32855-5837

91-06902

91 8 05 110

REPORT DOCUMENTATION PAGE

Form Approved
OMB No. 0704-0188

Public reporting burden for this collection of information is estimated to average 1 hour per response, including the time for reviewing instructions, searching existing data sources, gathering and maintaining the data needed, and completing and reviewing the collection of information. Send comments regarding this burden estimate or any other aspect of this collection of information, including suggestions for reducing this burden, to Washington Headquarters Services, Directorate for Information Operations and Reports, 1215 Jefferson Davis Highway, Suite 1204, Arlington, VA 22202-4302, and to the Office of Management and Budget, Paperwork Reduction Project (0704-0188), Washington, DC 20503

1. AGENCY USE ONLY (Leave blank)		2. REPORT DATE	3. REPORT TYPE AND DATES COVERED FINAL 27 Aug 90 to 26 Apr 91	
4. TITLE AND SUBTITLE APPLICATIONS OF WAVELETS TO RADAR DATA PROCESSING			5. FUNDING NUMBERS F49620-90-C-0050 61101E 7450/00	
6. AUTHOR(S) MR. CHARLES STIRMAN				
7. PERFORMING ORGANIZATION NAME(S) AND ADDRESS(ES) MARTIN MARIETTA CORPORATION MISSILE SYSTEMS P.O. BOX 555837 ORLANDO, FL 32855-5837			8. PERFORMING ORGANIZATION REPORT NUMBER AFOSR-TR 91-0285 AFOSR-TR 91 0686	
9. SPONSORING / MONITORING AGENCY NAME(S) AND ADDRESS(ES) AFOSR/WM Bldg 410 Bolling AFB DC 20332-6448			10. SPONSORING / MONITORING AGENCY REPORT NUMBER F49620-90-C-0050	
11. SUPPLEMENTARY NOTES				
12a. DISTRIBUTION / AVAILABILITY STATEMENT Approved for public release; distribution unlimited. . .			12b. DISTRIBUTION CODE	
13. ABSTRACT (Maximum 200 words) In this study, the recent mathematical theory of wavelets was introduced to the engineering problems of designing radar systems, radar processors, and radar algorithms. The goal was to make radars more efficient or more effective by the use of wavelets. To understand why particular possible applications of wavelets to radars were examined, it is necessary to understand some background information on both radars and wavelets theory.				
14. SUBJECT TERMS			15. NUMBER OF PAGES	
			16. PRICE CODE	
17. SECURITY CLASSIFICATION OF REPORT UNCLASSIFIED	18. SECURITY CLASSIFICATION OF THIS PAGE UNCLASSIFIED	19. SECURITY CLASSIFICATION OF ABSTRACT UNCLASSIFIED	20. LIMITATION OF ABSTRACT UL	

OA 11606

July 1991

Applications of Wavelets to Radar Data Processing



Handwritten "A-1" and a checkmark in a box.

Final Technical Report

CLIN 0002AA

Principal Investigator
Mr. Charles Stirman

Program Manager
Dr. Arje Nachman

Sponsored by
Defense Advanced Research Projects Agency
DARPA Order No. 7450
Monitored by AFOSR Under Contract No. F49620-90-C-0050

Martin Marietta Electronics,
Information, and Missiles Group
P.O. Box 555837
Orlando, Florida 32855-5837

FINAL TECHNICAL REPORT

CLIN 0002AA

APPLICATIONS OF WAVELETS TO RADAR DATA PROCESSING

ARPA Order 7450

Program Code OD20

Name of Contractor - Martin Marietta Corporation
Missile Systems

Effective Date of Contract - August 27, 1990

Contract Expiration Date - July 26, 1991

Amount of Contract Dollars - \$192,806

Contract Number - F49620-90-C-0050

Principal Investigator - Mr. Charles Stirman
407-356-2573

Program Manager - Dr. Arje Nachman
202-767-5025

Title of Work - Applications of Wavelets to Radar Data
Processing

Sponsored by
Defense Advanced Research Projects Agency
DARPA Order No. 7450
Monitored by AFOSR Under Contract No. F49620-90-C-0050

The views and conclusions contained in this document are those of the authors and should not be interpreted as necessarily representing the official policies or endorsements, either expressed or implied, of the Defense Advanced Research Projects Agency or the U.S. government.

TABLE OF CONTENTS

1	SUMMARY	1
	1.0 Final Report Summary	1
2	WAVELETS METHODS	6
	2.0 Compactly Supported Wavelets	6
	2.1 The Scaling Function, Wavelets, and the Wavelet Transform	9
	2.2 The Scaling Function	10
	2.3 Wavelets	13
	2.4 The Wavelet Transform	15
	2.5 The Computational Complexity of Wavelet Transforms	17
3	RADAR METHODS AND MAIN RESULTS	20
	3.0 Basic Radar System Operation	20
	3.1 The Millimeter Radar Data Base	21
	3.2 Wavelet Approximation to the FFT	29
	3.3 Target Length Estimation	34
	3.4 Wavelet Target Classification Results	39
	3.5 Fine Range Resolution by Wavelets	41
4	ADDITIONAL RESULTS	43
	4.0 Supplemental Results	43
	APPENDICES	72
	A. List of Symbols	72
	B. Wavelet Transform Theory	73
	B.1 Wavelets and Wavelet Transforms	73
	B.2 Wavelet Approximation to the Fourier Transform	77
	B.3 Computational Complexity of the Wavelet Approximation to the Fourier Transform	82
	C. Phase Unwrapping	88
	D. Martin Marietta Radar Data and Pulse Compression Processing	95
	D.1 Time-Frequency Pulse Compression	96
	D.2 Characteristics of the Millimeter Wave Radar Data used in this Study	99
	E. Baseline Target Extent Calculation Method	106
	BIBLIOGRAPHY	107

FIGURES

2.1	Scaling Functions
2.2	Wavelets
2.3	Wavelet Transform
2.4	Sub-band Tree Structure
2.5-2.6	Wavelet Transform Computational Complexity
3.1	Radar Block Diagram
3.2	Wavelet Impact Areas
3.3-3.6	Wavelet Reconstruction of Target Profiles
3.7-3.11	Wavelet FFT Approximation Results
3.12-3.15	Target Length Estimation Results
3.16	Wavelet Classifier Results
3.17	Wavelet Waveforms for Radars
4.1-4.3	Wavelet Reconstruction of a Trihedral
4.4-4.6	Wavelet Reconstruction of two Dihedrals
4.7-4.18	Truck Even Polarization Length Estimation Results
4.19-4.30	Truck Odd Polarization Length Estimation Results
4.31-4.42	Tank Even Polarization Length Estimation Results
4.43-4.54	Tank Odd Polarization Length Estimation Results
B.1-B.3	Wavelet FFT Approximation Computations
C.1-C.8	Phase Unwrapping Comparisons
D.1-D.9	Radar Data Plots

1.0 Final Report Summary

Technical Problem

The technical problem addressed by this contract was to determine the feasibility of exploiting the emerging mathematical theory of wavelets in radar system applications. The work to be done was divided into three tasks.

1. Perform a preliminary systems benefit study. Address the complete radar processing problem including the applicability of wavelets to the various processing elements: prescreeener, fast Fourier transform (FFT), classifier, and automatic target recognizer (ATR).
2. Define and develop appropriate wavelet methods for radar applications.
3. Determine the stability of the wavelet transform image. Make a comparison of wavelet transforms and FFT signatures for each of three targets: a set of calibrated corner reflectors of known radar cross section and spacing, an M60 tank, and an M35 truck.

Three specific potential applications of wavelets methods to radar systems were identified for investigation.

1. Use wavelets to transform the data that forms the input to the radar's ATR algorithms.
2. Modify a typical radar system so that if a wavelet transform (which is faster than an FFT) replaces the FFT (which is currently used), the output is still a high range resolution target profile.
3. Develop a wavelet approximation to an FFT such that the wavelet approximation is sufficiently accurate and faster than an FFT.

Methodology

In this study, the recent mathematical theory of wavelets was introduced to the engineering problems of designing radar systems, radar processors, and radar algorithms. The goal was to make radars more efficient or more effective by the use of wavelets. To understand why particular possible applications of wavelets to radars were examined, it is necessary to understand some background information on both radars and wavelets theory. These topics are discussed briefly in the following paragraphs. Also, the Martin Marietta radar data that was used in this study is described, and some description is given of typical processing methods for this data.

Modern radar systems transmit and receive frequency-stepped radio frequency (RF) waveforms. The radar signal processor transforms the received data by using an FFT. Since the FFT forms a matched filter with the frequency-stepped waveforms, the vector whose components are the magnitudes of the complex data output from the FFT forms a high range resolution profile (HRRP) of the objects in the radar beam. These HRRPs are the inputs to the radar's ATR

processor. Both FFT and ATR calculations are computation intensive and impose difficult and costly requirements on the radar signal processor. Wavelet methods were examined for potential efficiency improvements in FFT or ATR processors as well as for potential ATR performance improvements.

Investigations utilized Martin Marietta's short pulse, frequency-stepped, fully calibrated 35 Ghz radar data. This data utilized two transmit (right hand circular and left hand circular) and two receive (right hand circular and left hand circular) radar polarizations (right and left circular) and resulted in a complete polarization set of four receive-transmit pairs. Transmitting right or left and receiving the opposite yields "odd" polarized returns. If the receiver has the same polarization sense as the transmitter, the return is an "even" polarization. The data is coherent which allows creation of HRRPs. Figures 3.3 through 3.6 show odd and even HRRPs. There are radar looks at an M60 tank and an M35 truck at every hundredth of a degree of aspect in this data set. A radar look consists of 64 coherent, frequency stepped time samples for the four receive-transmit polarization pairs. Each polarization of each radar look can be processed through an FFT to produce an HRRP of the vehicle in the radar's view. Compactly supported wavelets are a family of recently discovered (1986) mathematical functions that have been successfully applied to problems in image compression, audio compression, vision analysis, and transient signal analysis. The wavelet methods used on this contract employed compactly supported wavelets that generated orthonormal bases. Particular wavelets used were denoted D2, D4, D6, and D8 in honor of Ingrid Daubechies, who developed the theory of orthonormal bases of compactly supported wavelets. The D2 wavelet is also known as the Haar wavelet. A wavelet basis consists of a "scaling function" $\phi(x)$ that is the solution to a recursion equation derived from orthogonal subspace projection mathematics, a basic wavelet function $w_{00}(x)$ that is derived from the scaling function, and a countably infinite collection of wavelet functions $w_{jk}(x)$ that are dilations (frequency changes) and translations (time shifts) of the basic wavelet function. The recursion equation is given by

$$\phi(x) = \sum c_k \phi(2x-k)$$

and the wavelet functions are defined by

$$w_{00}(x) = \sum (-1)^k c_{1-k} \phi(2x-k)$$

$$w_{jk}(x) = 2^{j/2} w_{00}(2^j x - k).$$

Some specific linear operations involving the recursion coefficients c_k can compute wavelet coefficients and wavelet approximations to functions very rapidly since only a few of the c_k are nonzero.

Not all wavelets have compact support nor do they all generate orthogonal bases. However, throughout this report the terms wavelets and compactly supported wavelets are used interchangeably, and wavelet bases are assumed to be orthogonal. Results presented were produced using specific compactly supported wavelets.

Technical Results

Results clearly demonstrate that, under certain circumstances, wavelets methods can improve radar system performance. These wavelet results and their radar system applications are summarized below and described in detail in Sections 3.2, 3.3, 3.4, and 3.5 of this report.

The radars considered in this study were millimeter wave (MMW) radars, but results obtained are also applicable to radars of other wave lengths. MMW radars are typically either pulse radars with short radar pulse lengths or frequency modulated continuous waveform (FMCW) with long radar pulse lengths. There is a major difference between these two types of MMW radars as far as wavelets applications are concerned. This is due to the fact that if one wants a given range resolution in the HRRP, one must compute an FFT of very large dimension for an FMCW radar but a relatively small FFT for a pulse radar.

The most significant application of wavelet methods to radars involves the radar's ATR algorithms' capability and complexity. The data base of full polarization, calibrated, coherent MMW radar returns from tanks and trucks was used for this study. This data base also contained radar looks at the calibration reflectors consisting of a single trihedral and a pair of dihedrals of known radar cross section. The major goal was to reduce the dimension of the HRRP radar data vector without losing information that is important to the ATR. There are three distinct reasons why this dimension reduction could improve the ATR.

1. The reduced dimension that serves as the input to the ATR may allow use of a more complex and effective (higher order polynomial classifier, for example) classifier or target-clutter discriminator algorithm within the computational limitations of the ATR digital signal processor.
2. Reduced dimension may make the choice of the type of ATR classifier and/or target-clutter discriminator obvious; consequently, ATR performance could be improved.
3. Even if reduced dimension does not suggest a change in the type of classifier or discriminator algorithm, it may greatly reduce the number of computations required by the ATR thereby increasing the speed and decreasing the hardware requirements of the ATR.

As a test case for the ability of wavelets to reduce HRRP dimension, one feature - "target length" - was examined. For this effort, Martin Marietta defined the problem and monitored the results while our subcontractor, Aware, Inc., provided the wavelets expertise and produced the results. Wavelet algorithms and typical target length estimation techniques were applied to the radar HRRP data base. Results showed that when appropriate wavelet methods were applied

with the D4 or D6 wavelet basis, vector dimension could be reduced by a factor of four with essentially no loss in ability to estimate target length. The main results are given in Section 3.3 and additional details are presented in Section 4.0 and Appendix E.

Next a brief, two class target classification study was conducted by Martin Marietta to see if it is feasible to improve radar target classification signal processing by wavelet methods, either by improving classifier percent correct classification (PCC) in the presence of noise (added to the very clean radar target data) or by decreasing the number of computations required by the classifier processor, or both. In this study, the features used by the classifier were particular wavelet coefficients produced by the target HRRP. Classifier overall PCC was improved in realistic signal/interference situations by up to 6 percentage points, and computations were decreased by a factor of 10. These results clearly indicate that it is feasible to improve radar classifier processors by wavelet methods. Details of this study are given in Section 3.4.

A second application of wavelet methods to a radar system consists of replacing the radar's FFT by a wavelet transform (WT). This results in a more efficient processor for two reasons. An FFT requires on the order of $N \log_2(N)$ multiplies, but a WT requires only on the order of N multiplies. Also, an FFT uses complex*complex multiplies, which requires 4 real multiplies, 1 add, and 1 subtract, but the waveform proposed for the WT radar application is processed by a WT with only real*real multiplies. The output of the WT will still be an HRRP if the radar transmitter and receiver can be modified so that the received, sampled waveform data vector is a matched filter with the WT, just as the current frequency stepped radar data vector is a matched filter with an FFT. This wavelet radar application would improve either pulse or FMCW radar digital processor efficiency. Details of this WT radar application and an example are given in Section 3.5.

Another wavelet radar application consists of using a wavelet fast Fourier transform approximation (WFFT), derived by Aware, Inc., instead of using an FFT. This procedure does not require any modification to the radar transmitter or receiver but does require changes in the radar digital processor. A number of versions of WFFT's were examined. The fastest version of a WFFT is faster than an FFT in creating a target range profile if the target length (in post-FFT cells) is less than one fourth of the FFT dimension. In cases when the target would occupy more than one fourth of the post-FFT cells, the FFT will be at least as fast as the WFFT. Consequently, the WFFT does not appear to be useful for typical MMW pulse radars but would be useful in typical FMCW radars which sample relatively long waveforms to produce the data vectors that are input to large FFTs (or WFFTs). A discussion of this WFFT vs. FFT comparison follows in Section 3.2. Additional details are given in Appendices B.2

and B.3.

Further Research

This wavelets radar applications feasibility study has pointed out several areas for further useful research.

Wavelet dimension reduction capabilities may improve other radar ATR algorithms, either by improving stability versus signal-to-interference and/or by decreasing computational complexity. Also, wavelets methods may prove even more useful in two-dimensional ATR applications such as synthetic array radar, infrared imaging, or electro-optical imaging.

If there is an FMCW system whose targets are small in length relative to the radar pulse length, this study indicates that it would be appropriate for that system to further investigate implementing WFFTs rather than FFTs.

Several questions remain concerning the possible use of WTs to replace FFTs in a radar. What wavelet basis produces the radar waveform that is most appropriate for transmission and reception by a radar system such that the WT would output HRRPs? Can such a system be built? Is the increased efficiency of the WT (over the FFT) sufficient to offset the cost of the changes required in the transmitter and receiver?

Acknowledgement

We are indebted to Howard Resnikoff and Charles Smith along with their staff at Aware, Inc. for their time and effort expended in support of this contract. It was their expertise in wavelet technology and their willingness to entertain a myriad of fundamental questions which permitted Martin Marietta to formulate and successfully complete a meaningful feasibility study in applicability of wavelet methods to radar systems.

Several sections (2.0 through 2.5, 3.2, 3.3, 4.0, and the Appendices) are based on input received from Aware, Inc. However, conclusions and results as they relate to the ATR classifier are solely those of Martin Marietta.

2.0 Compactly Supported Wavelets

A major reason for conducting this study is the remarkable results being obtained through the application of compactly supported (zero outside a finite interval) wavelets to signal processing. Compactly supported wavelets are a class of mathematical functions that were discovered in 1986. Some of the particular advantages of wavelet signal processing methods are:

- o Wavelet transforms are computationally efficient. The number of arithmetic operations required to perform a wavelet transform is linearly proportional to the number of input data points. The computational complexity of the more traditional Fast Fourier Transform (FFT) is proportional to the number of input data points times the logarithm (base 2) of the number of input data points. For large problems, the wavelet methods require only a fraction of the number of operations required by the traditional methods. This advantage increases as the problem size increases. In addition, wavelet transform algorithms can be directly implemented in very large scale integration (VLSI) logic devices, and they are fully parallelizable.
- o Wavelet transform methods can analyze signals in both the time and frequency domains. The relative resolution of the time and frequency components can be flexibly adapted to the problem at hand. The selection of the appropriate time-frequency resolution can be done upfront at system design time or it can be accomplished with real-time adaptive algorithms. The traditional Fourier transform suffers from very poor (or nonexistent) time resolution. This particularly limits its usefulness in the analysis of time-limited (i.e., transient) signals. There have been attempts to modify the Fourier technique in various ways to overcome this limitation, but all of the methods introduce some additional complexities and compromises. Wavelet methods offer a very natural means to perform time-frequency signal analysis.
- o Wavelets provide the flexibility to choose a particular wavelet function that is "customized" to the specific application. This is possible since compactly supported wavelets are an infinite family of complete orthogonal basis functions. This flexibility to choose basis functions can not be matched with the Fourier transform for it uses only a single set of basis functions - the complex exponentials (i.e., the sine and cosine functions.)

Compactly supported wavelets are a complete and orthogonal set of basis functions for the set of all finite energy discrete signals. The wavelet transform is invertible, energy-preserving and linear. The wavelet transform is a processing method which analyzes both continuous streams of input data and blocks of data. A multiplier 2 wavelet basis consists of a scaling function, a

basic wavelet and a collection of smaller wavelets. The smaller wavelets are created by "shrinking" the basic wavelet by a factors of 2 and shifting (or translating) them by scaled integer distances. Thus the collection of smaller wavelets are $1/2$ and $1/4$ and $1/8$ (and so on) the size of the basic wavelet. Whenever the "wavelet length" shrinks by a factor of two, the "wavelet frequency" can be thought of as doubling. This shrinkage factor is sometimes called scale or scale level. Wavelet basis functions are all related by multiples of the constant ratio (2 : 1). The basic wavelet is computed from the scaling function. The selection of the scaling function determines all of the remaining basis functions. A remarkable fact is that there are an infinite number of scaling functions, each of which defines a complete wavelet basis. This provides tremendous flexibility in selecting basis functions which are appropriate for different systems.

In general, the computational complexity of wavelet methods is $O(n)$, which means that the computational complexity is of order n . The efficiency is the direct result of the simplicity of the wavelet transform process. The process starts by separating the signal information in the smallest wavelets from information in all the larger wavelets scales. Details are given in Section 2.4. The output of the first stage is processed again by the same method and is repeated for each successive scale. This recursive structure reduces the amount of data to be processed at each successive level by a factor of two which reduces the computational cost for each successive transform level. Information which varies rapidly over just a few data points is separated from information which varies over many points. The procedure is stopped at the largest wavelet of interest.

The outputs of the wavelet transform are coefficients which represent the similarity of the signal (as a function of time) to the wavelets of different shrinkage factors and times. The output of a wavelet transform can be plotted on a grid that has time on the x-axis (or t-axis) and shrinkage factor on the y-axis. This grid is called phase space and is used to graphically display the relationships between signal information at different shrinkage factors and times.

It is helpful to compare and contrast the wavelet transform with the well known Fourier transform. The Fourier transform is also invertible, energy-preserving and linear. The Fourier basis functions are orthogonal and complete for the entire set of finite energy discrete signals.

The Fourier transform separates signal information by frequency. The Fourier transform requires an a priori choice of input data block size. The Fourier basis functions are constant frequency complex exponential functions each of which persists as long as the block size. The basis functions are uniformly spaced in frequency. The frequencies are separated by a constant interval rather than a constant ratio. Since all of the basis functions are as long as the input data block, they all have the same (lack of) time resolution. The output of a Fourier transform contains information about how the energy in the signal is distributed among the frequencies in the signal. However information about how the energy is distributed in time, about

when it occurred, is not available in the Fourier transform representation. All that can be inferred is that the frequency was present somewhere in the block and what fraction of the signal energy it accounted. The computational complexity of the fast Fourier transform (for the commonly used Cooley-Tukey algorithm) is $O(n \log_2(n))$.

The Fourier transform separates signal information into uniformly spaced frequency components. The Fourier transform has fine frequency resolution and a complete lack of time resolution. Increasing the input data block size increases the range of frequencies which the Fourier method can resolve, but decreases the time information available from a signal.

In summary, the primary difference between the Fourier transform and the wavelet transform is in how each separates signal information between time and frequency or a frequency related parameter, shrinkage factor. Wavelet transforms separate signal information by shrinkage factor and time. The number of shrinkage factors used and the number of times resolved are jointly limited by the input data block size. There are an infinite number of wavelet basis from which an appropriate basis can be selected. The computational complexity of the wavelet transform is $O(n)$, less than the Fourier transform $O(n \log_2(n))$.

2.1 The Scaling Function, Wavelets, and the Wavelet Transform

Wavelet methods separate the components of a signal by time and a shrinkage factor that is related to frequency. With a wavelet transform, both the time resolution, or "correlation length", and the shrinkage factor resolution vary logarithmically.

The wavelet technique takes into account the reciprocal relationship between time and frequency (or any type of structure which is expressed across multiple data points). To identify or locate the position of a particular shape, such as an oscillation, in a set of data, one must look for relationships among the data values; a structure or an oscillation exists only across a set of data, and not in a single point value. A number has no frequency, no structure. Conversely, properties which exist throughout a set of data cannot be said to have a particular location within that set. Wavelet signal representation techniques take this trade-off into account by allowing small sets of data to be combined and correlated to derive structural or shape information about that subset, without requiring a complete transformation of the signal into a particular type of structural information, the way a Fourier transform does. Thus, unlike the Fourier transform one is allowed to exchange a small amount of temporal resolution for a small amount of information.

It is no accident that these properties are reflected in the characteristics of many natural signals. Signals with time varying characteristics, like speech, music, seismic signals and underwater acoustic signals are all best analyzed by a system capable of resolving both frequency and time. Furthermore, many signal-producing phenomena have octave band structure due to the presence of harmonics within the signal and respond well to wavelet analysis. Transient events also respond well to wavelet analysis in that the identification of precisely located phenomena, such as the sharp onset of a signal, requires the ability to resolve its location in time with a very short wavelength, while the characteristics of later, more persistent, parts of the signal may require the ability to identify longer wave shapes.

Scaling functions, wavelets, and the wavelet transform are discussed in more detail in the next three sections and also in Appendix B.

2.2 The Scaling Function

The scaling function is at the core of any wavelet based representation of a signal. We will discuss only compactly supported wavelets in this report. The scaling function has three essential properties. The first is that it is compactly supported. This means that the scaling function is exactly zero outside a bounded region of the real line. The scaling function is only locally non zero.

The second essential property is that the scaling function is orthogonal to integer translates of itself. The importance of this will become clear a little later. The third property is that the scaling function is intimately related to smaller, or scaled versions of itself. This relationship is expressed concisely by the scaling equation:

$$\phi(x) = \sum_{k=0}^{N-1} \alpha_k \phi(2x - k) \quad (2.1)$$

where $\phi(x)$ is the scaling function. The function $\phi(2x)$ is a smaller, scaled down (by a factor of two), version of $\phi(x)$. The scaling equation states that $\phi(x)$ is equal to a weighted sum of these small versions of itself. The numbers α_k , of which only finitely many (N , which is an even number here) are non zero, are called the scaling coefficients. N is the size of the wavelet system. The support of ϕ , the region on which it is non zero, is the interval $[0, N-1]$. The coefficients α_k must satisfy certain conditions in order for the scaling function to exist and satisfy the scaling equation. There turns out to be an infinite number of sets of scaling coefficients for every even $N > 2$. It is the choice of the α_k , from among this set, which determines the detailed shape of $\phi(x)$.

Scaling functions are commonly selected from the class of Daubechies functions, which have several important characteristics. They are relatively smooth and have certain approximation properties (i.e., vanishing moments). These systems will be referred to as D2 (which is also the "Haar") D4, D6, D8...Dn, where n is the size of the system. The first four Daubechies scaling functions are shown in Figure 2.1.

The scaling function is the basic unit from which a level of detail is constructed. This is done by considering the set of functions which can be represented as a linear combination of shifted versions of the scaling function. That is, we define a collection of functions at "scale level" j , which we write V_j to be the set of functions which are linear combinations of the functions $\phi(2^j x - k)$, where k is an integer. The factor 2^j multiplying x has the effect of shrinking the support of ϕ to the interval from 0 to $(N - 1)/2^j$, and the shift by k moves these small functions around. Thus a function's components at scale level j are expressed by the equation:

$$f_j(x) = \sum_{k \in \mathbb{Z}} c_{j,k} \phi(2^j x - k) \quad (2.2)$$

where f_j is the part of f resolvable at the scale level j .

This idea can also be expressed by stating that V_j is the space spanned by the set

$$\{\phi(2^j x - k) \mid k \in \mathbb{Z}\} . \quad (2.3)$$

This set of functions forms an orthonormal basis for V_j . Functions in V_j are uniquely expressible as linear combinations of the basis functions, and the basis functions all have unit "energy". Thus the set of functions $\{\phi(2^j x - k)\}$ form an orthogonal set of "templates" for V_j .

The effect of performing a transform with such a set of basis functions is to identify, within the signal, those parts or components which are similar to the basis functions at the given scale level. Similarly, a Fourier transform has oscillatory functions as a basis, and identifies the relative contribution of each frequency to the overall signal.

With shifted versions of the scaling function as a basis, the wavelet transform will identify components which are similar to a particular shifted copy of the scaling function; that is, representations of a function in the scaling function basis identifies features locally in time, since the scaling function is compactly supported, and locally in scale level, because the scaling function has structure.

There is another, equally good, set of orthogonal "templates" for this scale level V_j . This set of "templates" gives a different type of information than the one presented above. In our previous basis, all of the resolution within the scale level j was in the temporal domain: each coordinate corresponded to a position in time. The new basis will trade some of this temporal resolution for some additional structural information; for each scale level it will give us two sets of coefficients, one set which represents large structure, while the other set represents small ("fine") structure. The process extracts or filters out the components of the scale level j which cannot be regarded as part of the coarser scale level, $j - 1$.

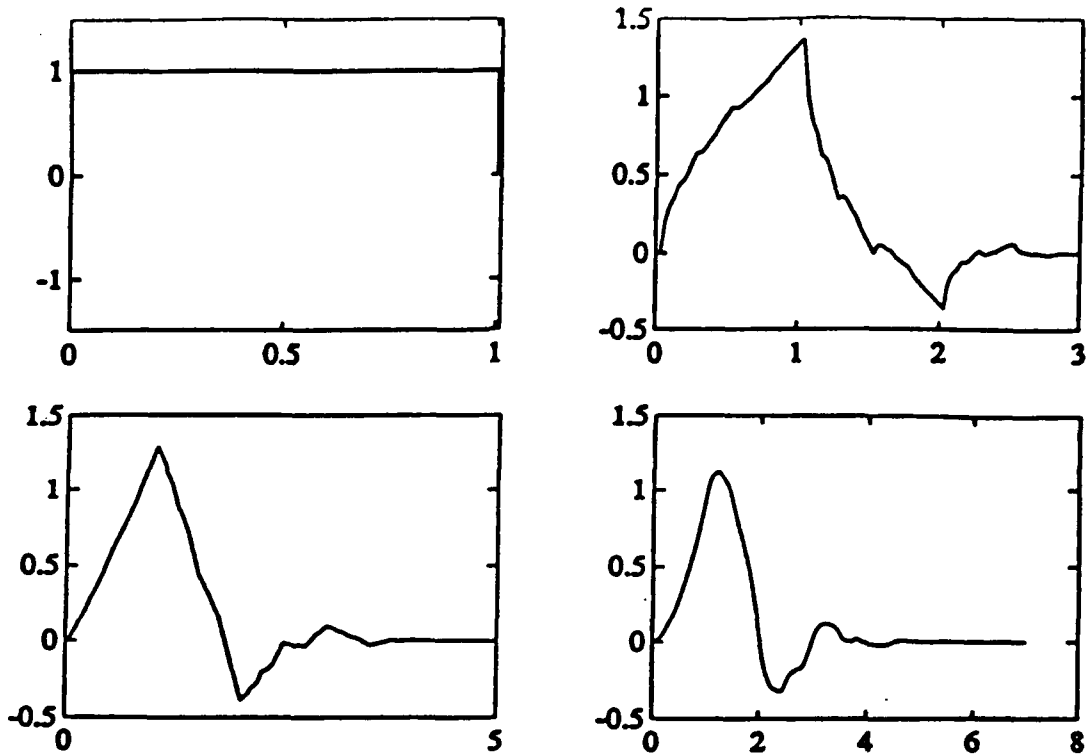


Figure 2.1: Four Examples of Scaling Functions (clockwise from upper left) "Haar", "Daubechies-4", "Daubechies-8", "Daubechies-6".

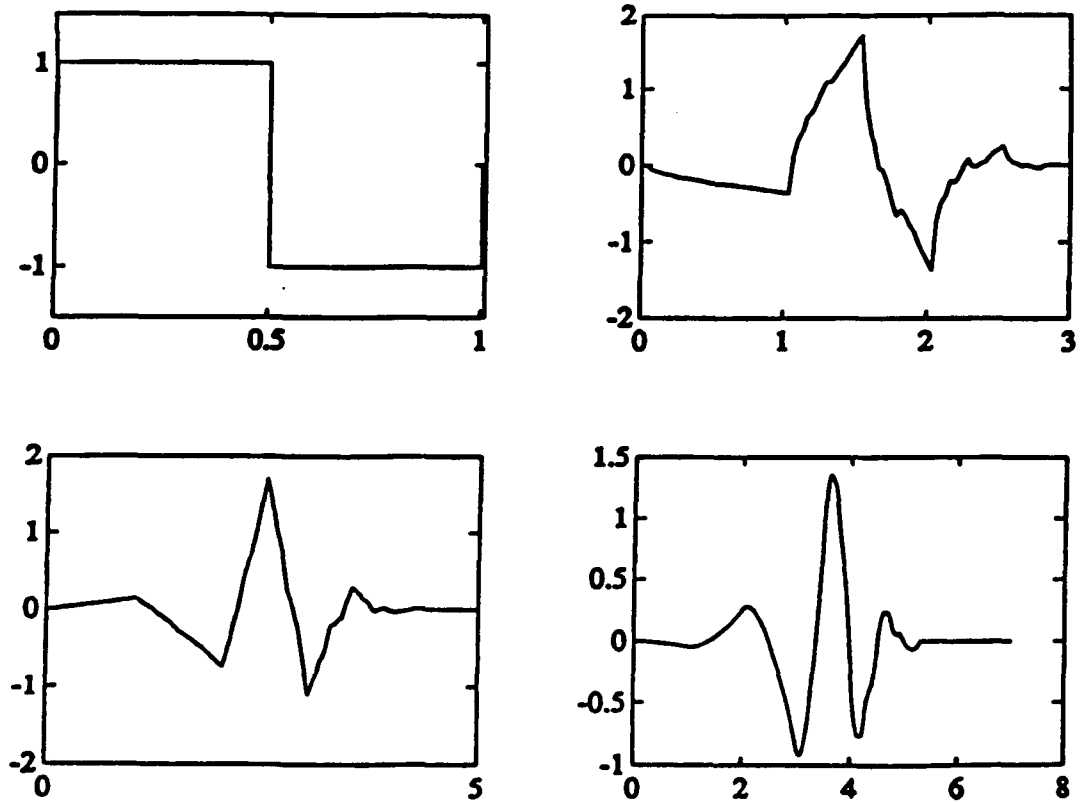


Figure 2.2: Four Examples of Wavelets (clockwise from upper left) "Haar", "Daubechies-4", "Daubechies-8", "Daubechies-6".

2.3 Wavelets

This idea of dividing the scale level V_j into a coarser version of itself, V_{j-1} , and a difference space, which we will call W_{j-1} , can be compactly expressed as an orthogonal splitting of the space V_j into two perpendicular spaces V_{j-1} and W_{j-1} :

$$V_j = V_{j-1} \oplus W_{j-1}. \quad (2.4)$$

The reason this can be done efficiently comes from the scaling equation. Since $\phi(x)$ can be expressed as a linear combination of translated versions of $\phi(2x)$ the coarser scale level V_{j-1} is contained within the finer scale level V_j :

$$V_{j-1} \subset V_j \quad (2.5)$$

Repetition of the argument shows that

$$V_{j-1} \subset V_j \subset V_{j+1} \subset V_{j+2} \dots \quad (2.6)$$

The difference space, W_{j-1} , contains all that remains when the coarser scale information is removed. However, since W_{j-1} is contained in V_j , it is also expressible as a linear combination of translates of $\phi(2^j x)$.

The actual set of functions that are used to span the space W_{j-1} are the orthonormal basis formed by the functions

$$\psi(2^j x) = \sum_{k=0}^{N-1} (-1)^k \alpha_{N-k-1} \phi(2^{j+1} x - k) \quad (2.7)$$

or in the case of $j = 0$,

$$\psi(x) = \sum_{k=0}^{N-1} (-1)^k \alpha_{N-k-1} \phi(2x - k) \quad (2.8)$$

Notice that the signs now alternate in the sum, and the order of the coefficients α_k has been reversed ($k \rightarrow N - k - 1$). These changes make $\psi(x)$ orthogonal to $\phi(x)$. The full basis for W_j is formed by taking shifted versions of ψ , i.e., Basis $(W_j) = \{2^{j/2} \psi(2^j x - k) | k \text{ an integer}\}$. The support of $\psi(x)$ is easily seen to be the same as the support of $\phi(x)$, and this is true for the shrunken versions as well, that is, the support of $\psi(2^j x - k)$ is the same as the support of $\psi(2^j x - k)$. The normalization term $2^{j/2}$ maintains unit energy in the functions. Figure 2.2 shows the wavelets which correspond to the scaling functions presented in Figure 2.1.

Thus the transformation from the first representation of V_j , where f_j was expressed as a linear combination of shifted versions of $\phi(2^j x)$, to the new representation, where f_j is expressed as a sum of translates of $\phi(2^{j-1} x)$ and translates of $\psi(2^{j-1} x)$, gives us new information about the shapes and structures, perhaps frequencies, present in f_j . This is at the expense of some temporal

resolution, because the new basis functions are twice as long. The new basis incorporates the inter-relationships among larger subsets of the data, providing correlative information. As a result of the spectral refinement, there has been a loss of temporal resolution.

The scaling function, being the origin for all of the spaces V_j , forms the connection between these spaces via the scaling equation, equation 2.1. The basic wavelet, ψ , represents the differences between the scale levels.

2.4 The Wavelet Transform

The exchange of temporal resolution in V_j for scale resolution in the division of V_j into V_{j-1} and W_{j-1} forms the basic unit of the Wavelet transform. Since the definition is independent of scale level, it can be repeatedly applied in the same way. Furthermore, the operations involved in the transformation require only the expansion coefficients of the function $f(x)$ in the basis at the current scale, and not the actual values of the function. The computation is very simple and efficient because of the close link between the functions ϕ and ψ .

The basic operation involved in a wavelet transform is the conversion of temporal resolution into structural or spectral information. This basic single step, essentially a filter, exchanges half the temporal resolution of a signal for twice the "frequency" resolution; the product of the two remains the same. More importantly, this operation can be repeated to gain any desired level of detail in the structural or spectral realm, while only imposing a reciprocal loss of resolution in the temporal domain. This is in sharp contrast to Fourier transform techniques, where one either gets all the available frequency information, or none of it, with no intermediate stages of knowledge available.

The wavelet transform allows one to move gradually between the two extremes present in the Fourier transform, successively gaining shape or structure information. In a sense, the wavelet transform interpolates between the frequency, or structure, domain and the temporal domain. This step by step transformation can be understood in terms of trade-offs between relative time resolution and relative frequency resolution.

Since the transform is defined in terms of operations on the coefficients of the representation, and not the actual values of the scaling or wavelet functions, the output from a single stage of the transform is exactly what the next stage requires for input. This easily pipelined, recursive structure is what makes the wavelet transform rapidly computable. While many such structures are made possible by the wavelet transform, one in particular, the one-sided or Mallat transform, has proven to be exceptionally useful in analyzing signals. Figure 2.3 shows one operation of the wavelet transform. The second operation uses the "low pass" (see Figure 2.4) output coefficients from the first stage as the input for the second stage, etc. The number of data points at each level is reduced by a factor of two by the conversion of temporal information into spectral information.

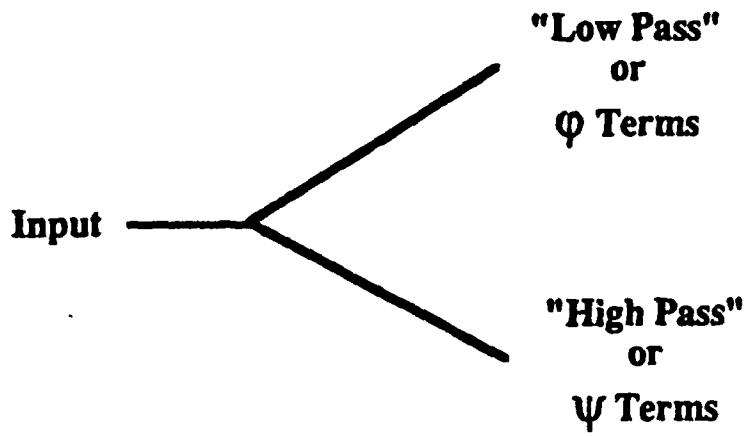


Figure 2.3: One Operation of the Wavelet Transform

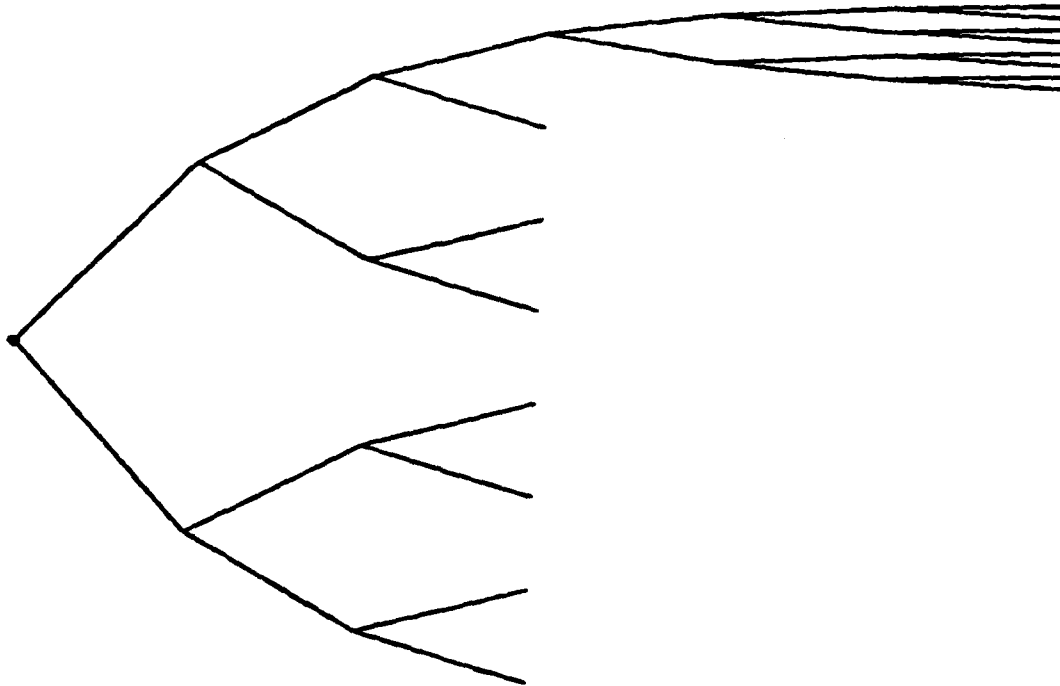


Figure 2.4: Tree Structure for the Partial Sub-band Tree Analysis.

2.5 The Computational Complexity of Wavelet Transforms

This section is concerned with the computational efficiency of wavelet-based analysis techniques. The computational complexity of several types of wavelet transforms is developed and comparisons are made to the computational complexity of the FFT. Both pre- and post-processing requirements are ignored. It is assumed that the output from the wavelet transform or FFT is the desired result. The input block size is the factor which determines the computational cost. The first case is a wavelet transform which resolves only a portion $R=1/2^J$ of the total bandwidth, and resolves it as finely as possible using recursive wavelet techniques. The simplest example of such a transform is the familiar Mallat Transform, which calculates the decomposition of a signal on the basis of scale, i.e., it "homes in" on low frequencies. This fundamental structure requires

$$\text{OPS(Mallat)} = \alpha(K)N(1-1/2^J) \text{ \# of operations} \quad (2.9)$$

where $\alpha(K)=(K+1)$ multiplies and (K) additions per output point. The number of input data is N , and J is the finest level calculated; that is, the basic wavelet decomposition operation is applied J times. The number of nonzero coefficients is K , which we have also called the length of the wavelet coefficient matrix. Note that whatever the depth of the decomposition, the operation count never exceeds $\alpha(K)N$. This operation count also applies to any wavelet transform which "zooms in" on a single location in phase space, allowing other side-bands to remain unchanged. These are not partial wavelet transforms: each is a complete representation in a wavelet basis. Each is, however, a partial frequency decomposition. That is a powerful advantage because only what is required need be calculated.

In applications where one wishes to resolve frequencies (or some other structure) to some pre-specified resolution (say $1/2^J$), and one is interested in a small number of sub-bands, wavelets are very computationally efficient. This case includes the Mallat Transform, and any other wavelet processing scheme which generates only a small subset of the finest resolution cells.

If the application requires that the temporal resolution existing in a subband be converted to frequency or structure information, the wavelet transform can be further applied in a uniform fashion to derive this information, as in Figure 2.4. Since the formula for this case, equation 2.10, is rather complicated, comparisons were made with the complexity of an FFT calculation for the full bandwidth of the signal, and for consistency the wavelet transform was also carried to its full resolution within the resolved subband. Since there are essentially no savings possible with an FFT for resolving only a portion of all subbands, the full complexity of $3n+n\log_2 n$ was used for comparison.

If we define

1. N = the number of data points;
2. K = the size of the wavelet filter (assumed to be constant throughout the procedure) and $\alpha(K)$ is the computational cost for the fixed filter length;
3. R = the portion of the bandwidth of the signal which is resolved (assumed to be $1/2^L$ for some L);
4. J = the finest level of resolution (the width of the frequency bands resolved is $1/2^J$),

then the number of operations required to generate the desired results, along with all of the remaining results that are required to have a complete representation, is:

$$\alpha(K)N(1+R(J-2+\log_2(R))/2) \quad (2.10)$$

The comparison is summarized by Figures 2.5 and 2.6, ($\alpha(K)$ counts the number of real multiplies) which show the filter length for which the two techniques are equally complex for a variety of values of R . See Figure 2.4 for an example of such a decomposition.

Figures 2.5 and 2.6 relate increased wavelet computations due to increased number of coefficients, K , to wavelet superiority versus FFT (in terms of computations required), which increases as the data block size increases.

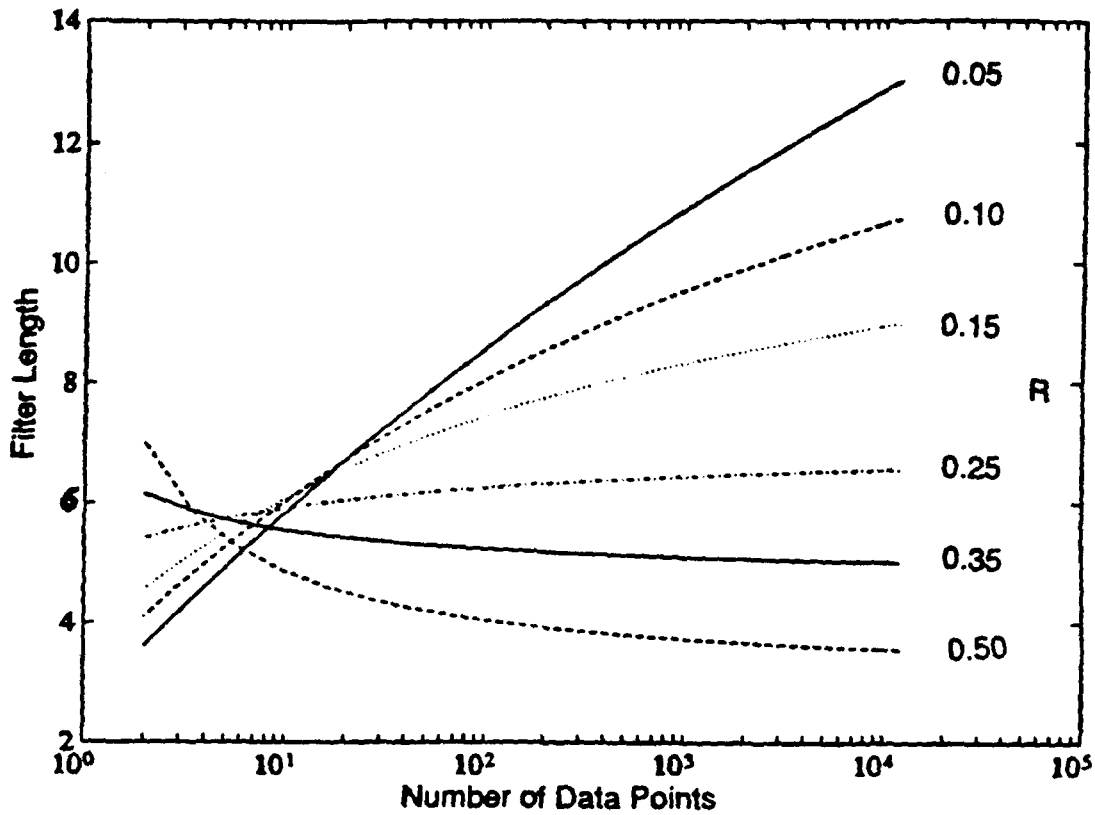


Figure 2.5: Computational complexity of the Wavelet Transform vs. the FFT: Filter Length vs. N for equivalent complexity for various values of R .

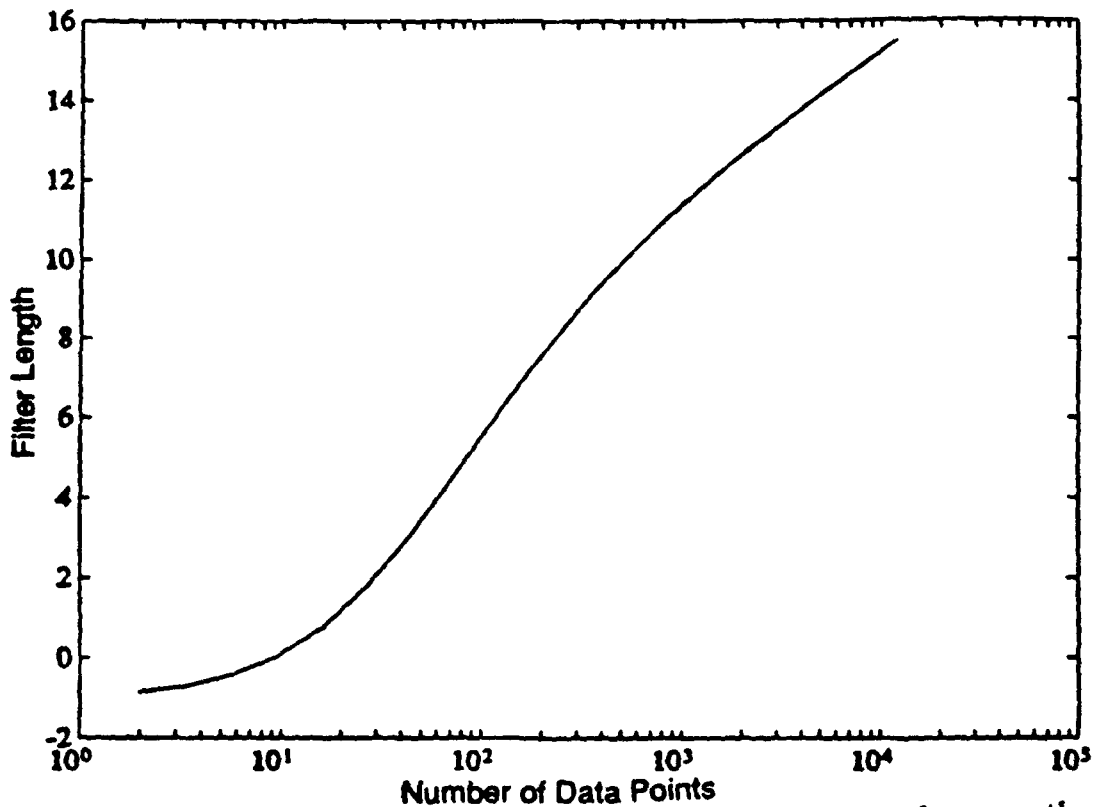


Figure 2.6: Computational complexity of the Wavelet Transform vs. the FFT: Filter Length vs. N for equivalent complexity for fixed target size of 32 bins. $R = 32/N$.

3.0 Basic Radar System Operation

Radar is an active sensor system that transmits electromagnetic energy and interprets the echoes reflected from objects. Objects in the propagation path scatter this energy in directions determined by the physical and electromagnetic characteristics of the object. The reflected energy is then received, processed, and perhaps interpreted by the radar system. Since electromagnetic energy propagates with a (nearly) constant velocity in the atmosphere, the round trip travel time t from the radar to an object and back again can be converted to distance by the formula

$$r = ct/2 \quad (3.1)$$

where r is the range to the object and c is the speed of light.

Radars are built for many purposes. Some are used to detect objects such as aircraft, ships, or tanks. Others are used to provide weapon guidance information. Still others are used to map the surface of the earth or for weather forecasting. In the first two cases, users are interested in the energy reflected from the "target" and they desire that it be separated from energy received from the earth or sources of clutter. Similarly, a "target" radar signal may be corrupted by "noise" which is undesired or extraneous energy received with the signal of interest. The total noise level present in a radar depends on many factors including the weather, operation of nearby electrical equipment (either friendly or hostile) and many other factors. The radar data processing requirements will vary from system to system depending on the intended use.

Radar processors may have to perform any or all of the following tasks. "Detection" means that the radar has found some object that may possibly be a target based upon some very fast data processing procedure designed to eliminate most noise and homogeneous clutter. One such process is called CFAR (for "constant false alarm rate") where thresholds are set to eliminate desired percentages of noise. "Discrimination" is the process of separating detected targets from detected clutter. "Classification" is the process of identifying particular types of targets (some of which may be more important as a missile target than others - for example, tanks versus trucks). Also, the radar may perform "tracking" which includes computing and frequently updating target position and motion information.

3.1 The Millimeter Wave Radar Data Base

Millimeter wave (MMW) radar systems are particularly well suited for use in tactical missile systems because they are physically small and their short wavelengths provide excellent target range resolution in nearly all weather conditions. Missile sensors are usually used only once; so, they must be inexpensive. Also, MMW radars have some resistance to electronic countermeasures (i.e., jamming). A typical MMW radar block diagram is given in Figure 3.1, and areas that wavelets methods might apply to are highlighted in Figure 3.2.

The radar data used in studies on this contract was taken by a 35 Ghz MMW radar. This data base contained coherent radar looks at a trihedral (which is visible when the transmitter - receiver polarization is "odd"), looks at two dihedrals (which are visible when the transmitter - receiver polarization is "even") separated in range, looks at many 360 degrees of azimuth aspect angles of an M60 tank, and an M35 truck. The trihedral (representing odd bounce scattering) is visible when the transmitter-receiver are "odd" or of opposite sense (transmitting right hand circular polarized energy and receiving left hand circular polarized energy or vice-versa). The dihedrals (representing even bounce scattering) are visible when the transmitter-receiver polarizations are "even" or of the same sense (transmitting right and receiving right or transmitting left and receiving left).

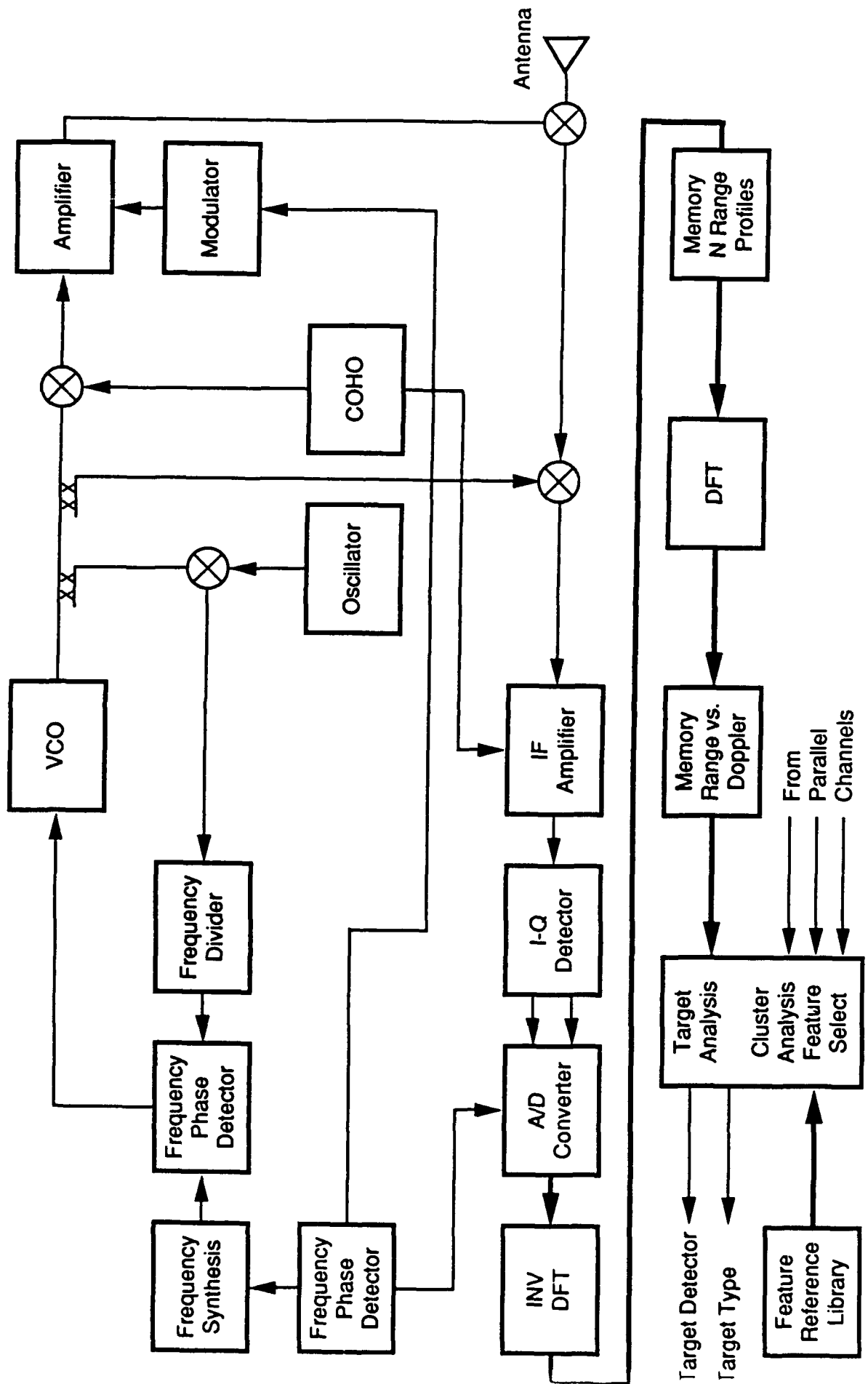
Each polarization of a radar look consists of 63 frequency stepped pulses transmitted at and received from the same target or area of ground. A 64 point (one zero added) FFT then forms a matched filter with the received radar frequency stepped pulse train. That is, phase change (due to a point scatterer) in the pulse train will "match" one of the columns of a discrete Fourier transform (DFT) matrix. In that way, the original pulse length that was twice 63 feet (for round trip travel) is subdivided to about one foot range resolution by FFT processing. The result is called a high range resolution profile (HRRP). This method of achieving high range resolution allows the use of fairly long pulses. That in turn allows long range target detection with low peak power radar transmitters. There are two "odd" polarization HRRPs and two "even" polarization HRRPs available from each radar look. Additional details of this data base are given in Appendix D.

Typical (head-on aspect) HRRPs and partial wavelet reconstructions using the D2 (Haar) wavelet basis and 50%, 25%, and 10% of the coefficients to reconstruct the original (100%) HRRP are shown in Figures 3.3 through 3.6. Figure 3.3 is a plot of the results for an even polarization M60 tank. Figure 3.4 is a plot for the odd polarization M60. Figure 3.5 is a plot of the results for an even polarization M35 truck. Figure 3.6 is a plot of the results for an odd polarization M35. It can be seen from these figures that

reasonably fine structure is preserved along with the target extent, even when only 25% of the wavelet coefficients are used to reconstruct the original target image. This reduces target image dimension by a factor of four. It is conjectured that features from the reconstructed image may be more robust than features from the original image. The next phase of this contract will investigate this conjecture in detail.

MMW RADAR BLOCK DIAGRAM

Figure 3.1:



WAVELET IMPACT AREAS

Figure 3.2:

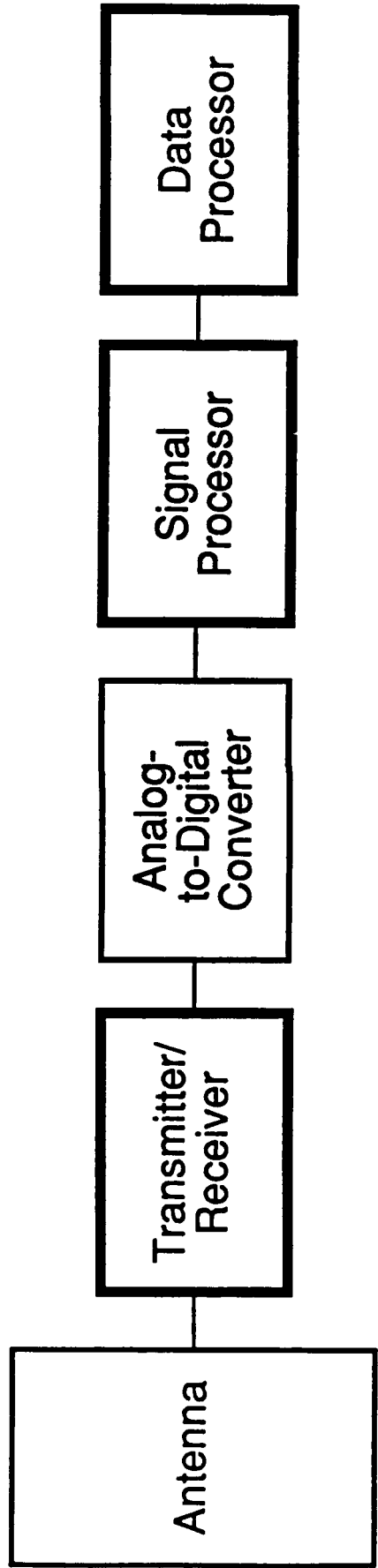


Figure 3.3: D2 RECONSTRUCTED M60 - EVEN

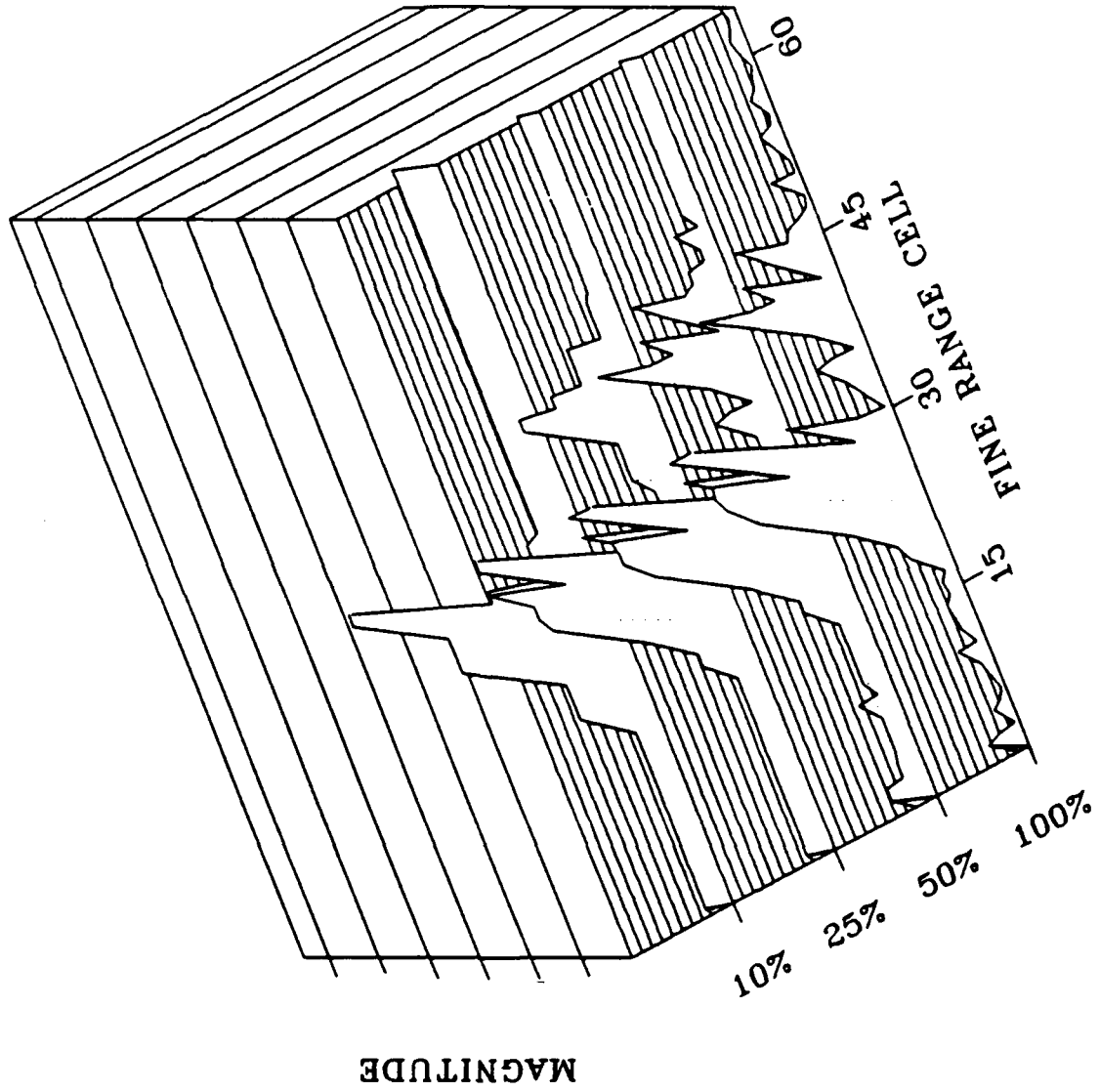


Figure 3.4: D2 RECONSTRUCTED M60 - ODD

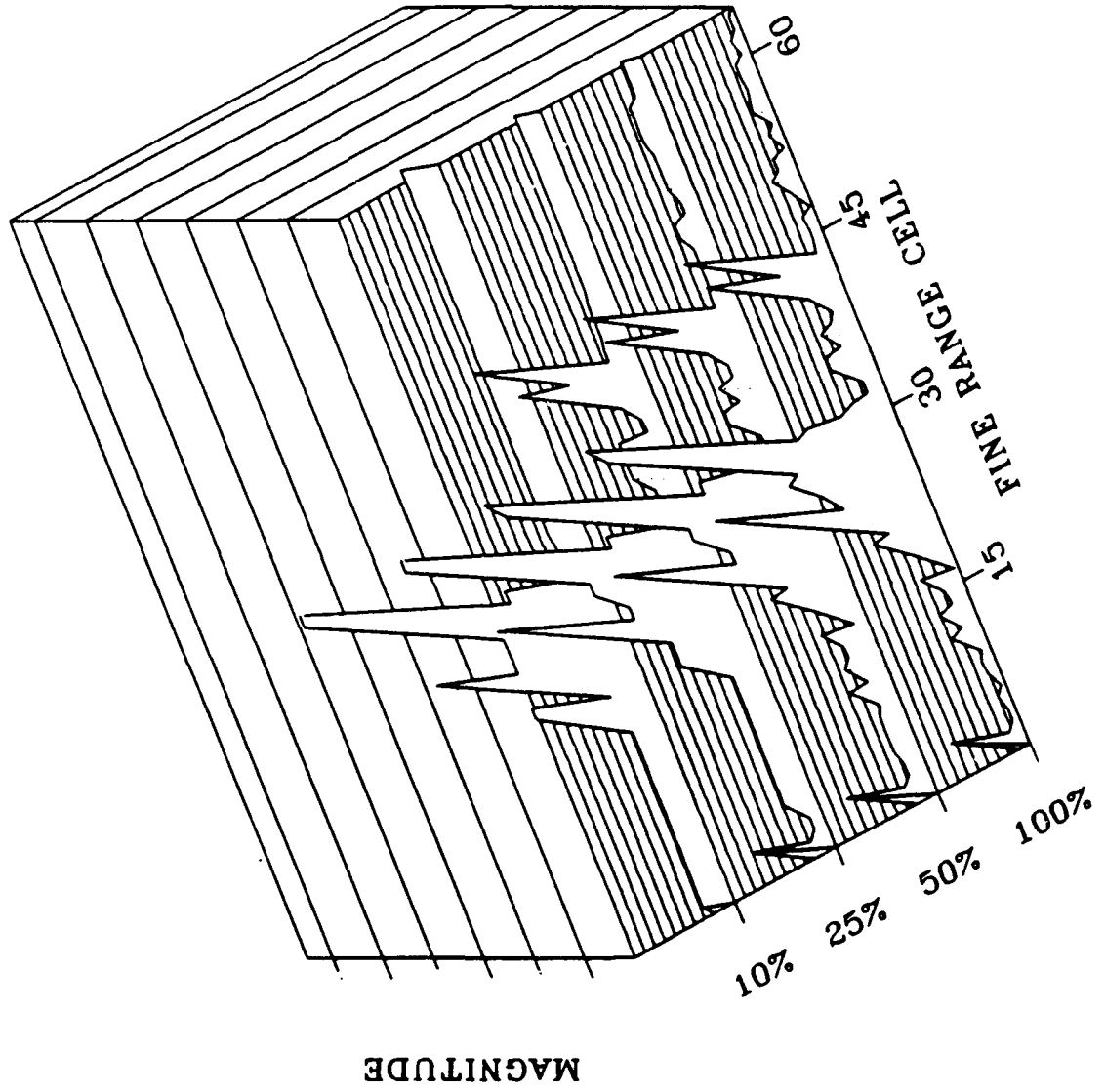


Figure 3.5: D2 RECONSTRUCTED M35 - EVEN

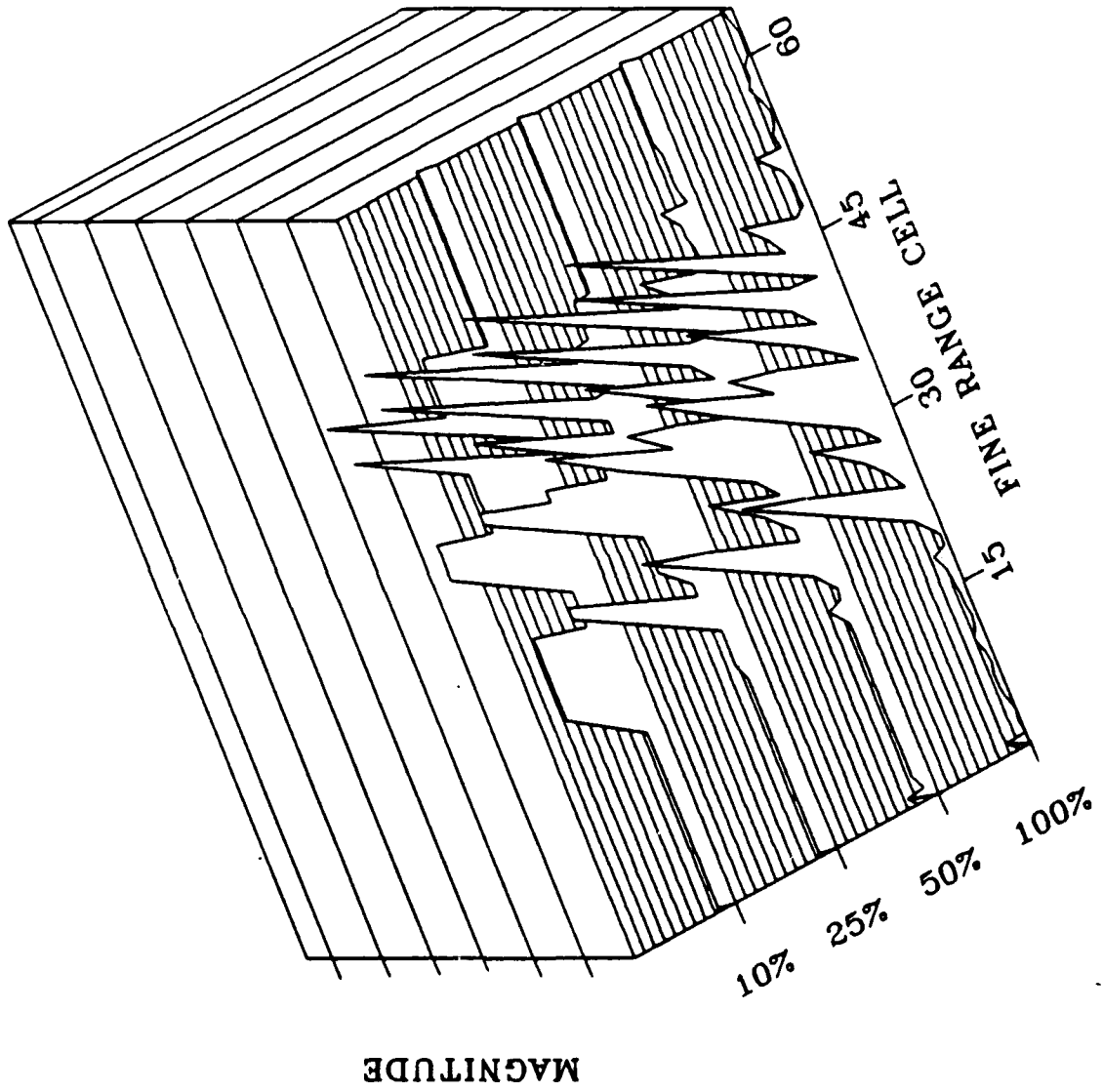
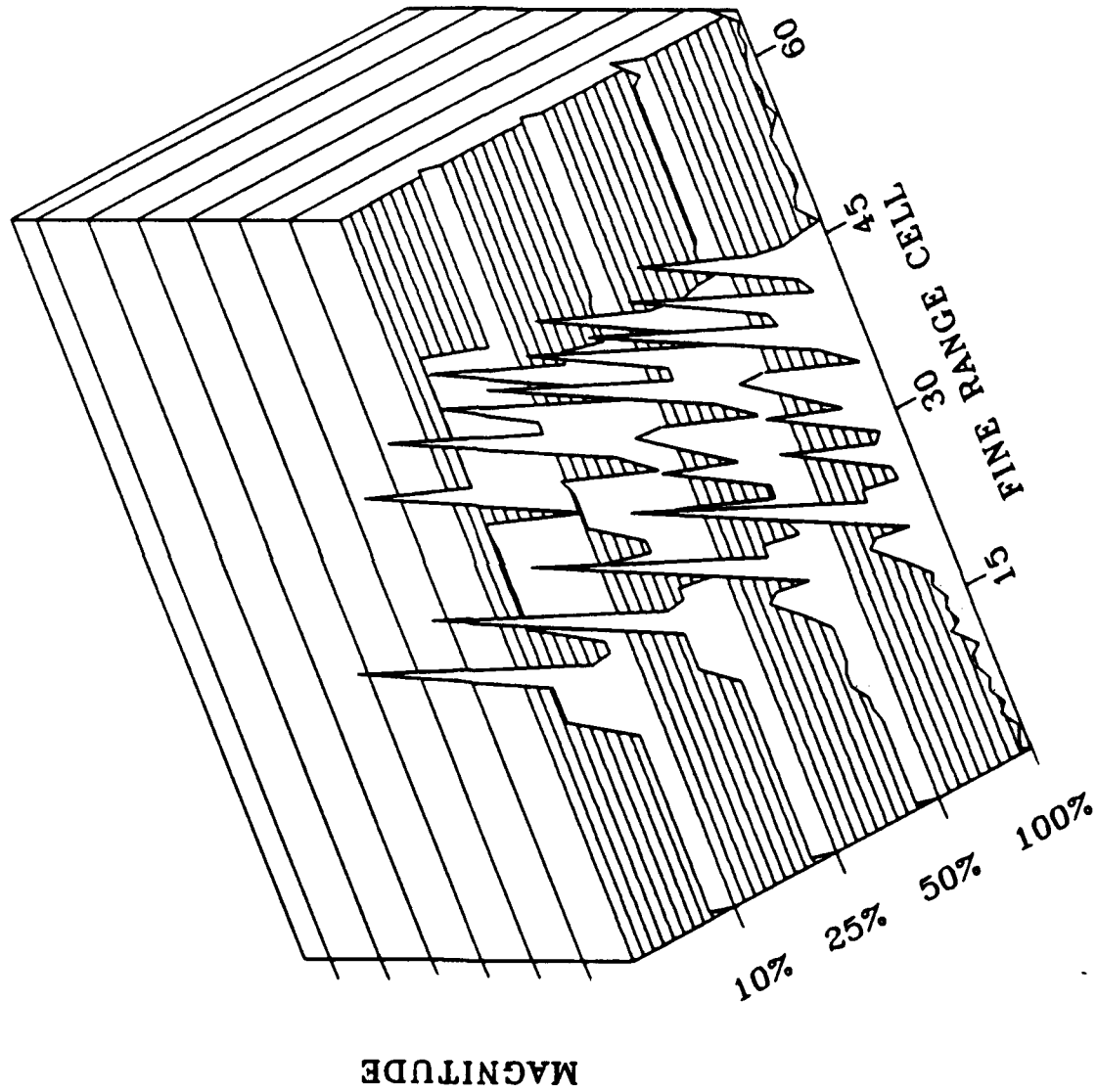


Figure 3.6: D2 RECONSTRUCTED M35 - ODD



3.2 Wavelet Approximation to the FFT

Several studies were conducted using the radar data to develop and demonstrate wavelet processing methods for approximating the Fourier transform and extracting target features. The experiments ranged from simple demonstrations of the methods, which proved that they could be performed, to a series of trials to evaluate the sensitivity of the methods to the choice of wavelet basis functions and target signature variations. The sensitivity of these methods to the selection of basis functions is important, in part because the choice of basis function directly influences the computational complexity of the method. The sensitivity to signature variation is important because the military targets (i.e., tank and truck) exhibit significant signature fluctuations as a function of viewing angle.

This section reports the results of these studies which were performed to assess the basic feasibility of performing wavelet approximations to the discrete Fourier transform (DFT). The mathematical details of wavelet transform theory are discussed in Appendix B.1, and details of wave transform approximations to Fourier transforms are in Appendix B.2.

The method we chose to quantify the error of approximation is the ratio of the mean squared error, to the total energy in the signal. This method is sensitive to any loss of target energy by the approximation method and the normalization allows the direct comparison of different signals.

Figure 3.7 illustrates the normalized error of approximation as a function of the number of wavelet terms retained in the wavelet FFT approximation formula (B.30). Note that, for this M60 tank scattering profile, the error of approximation decreases very rapidly in the first 5 or 6 terms followed by a more gradual and steady convergence to zero. This behavior is typical of the method applied to other target profiles, as illustrated in Figure 3.8. The convergence of this method for each of the target profiles (which vary in aspect or viewing angle) is rapid and consistent. The method shows little sensitivity to changes in aspect angle and therefore to target signature variations.

Figure 3.9 is a plot of the error for a number of wavelet bases. The functions considered ranged from a 2 coefficient wavelet basis (the Haar basis) to an eight coefficient wavelet basis (Daubechies - 8.) There is very little difference in their performance. This surprising result indicates that the approximating wavelet basis does not have to be chosen very carefully and that the computational advantages of short wavelets can be fully exploited in this application.

In the previous cases, the wavelet terms which were retained in the approximation were the wavelet coefficients with the largest absolute value. They were determined by sorting the wavelet coefficients. Sorting is an expensive computational process which would quickly eliminate any computational advantage wavelets would have relative to Fourier methods. There is an alternative formulation of the wavelet approximation to the Fourier transform which uses all of the wavelet coefficients at a given scale (Eq. B.33) rather than coefficients selected by

Daubechies 6 Wavelet / L - L Polarization

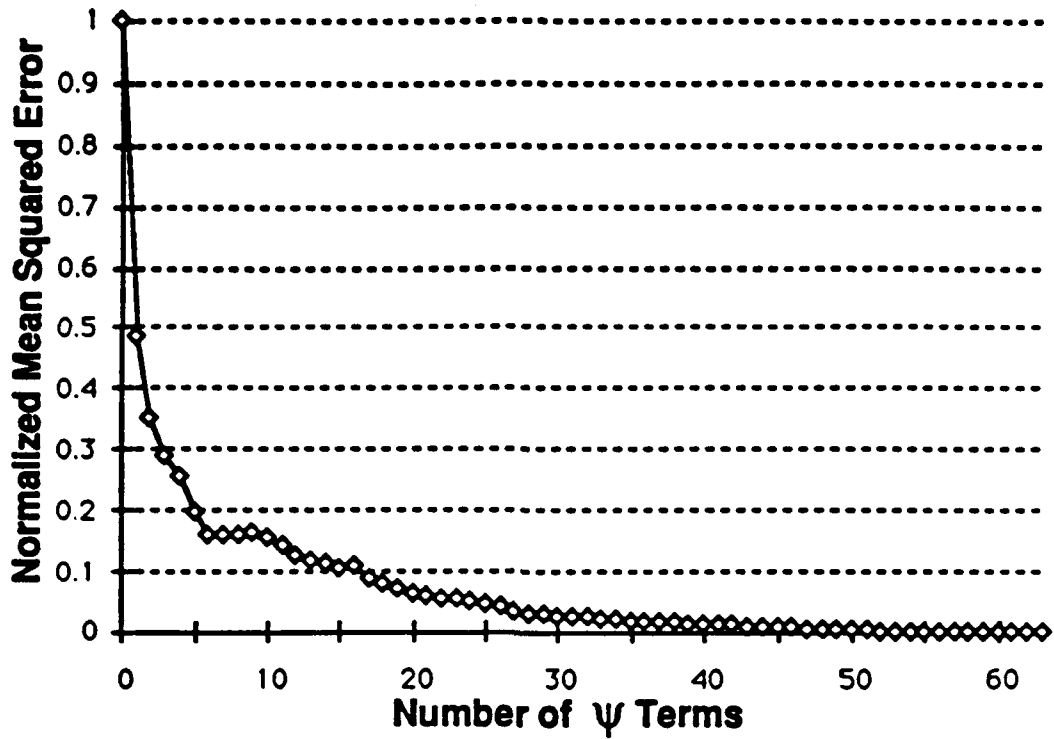


Figure 3.7: Error of Approximation versus Number of Wavelet (ψ) Terms.

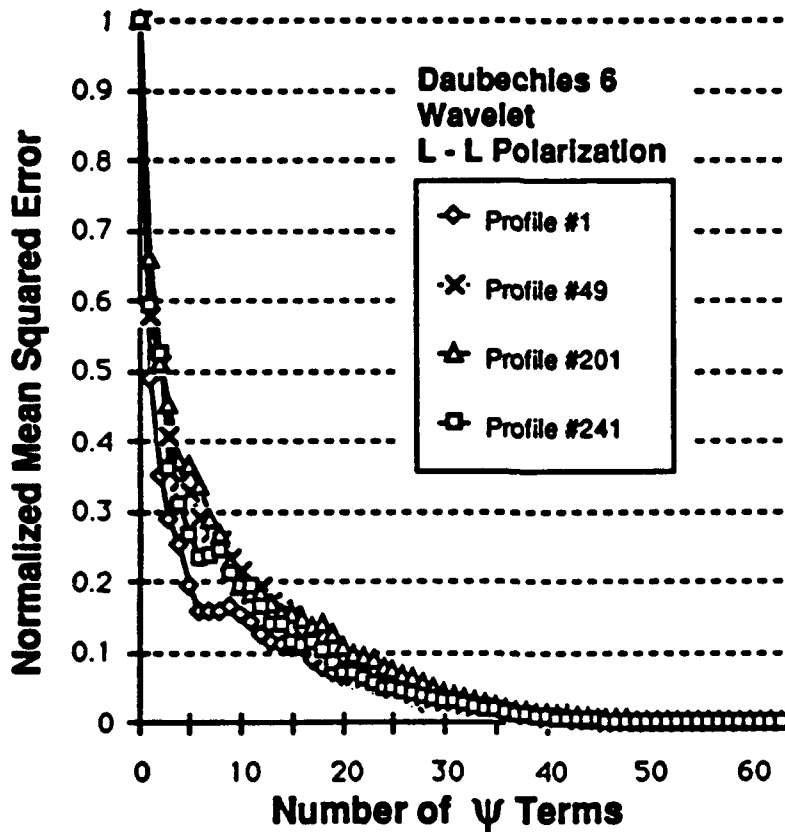


Figure 3.8: Error of Approximation versus Number of Wavelet (ψ) Terms for Selected Target Profiles.

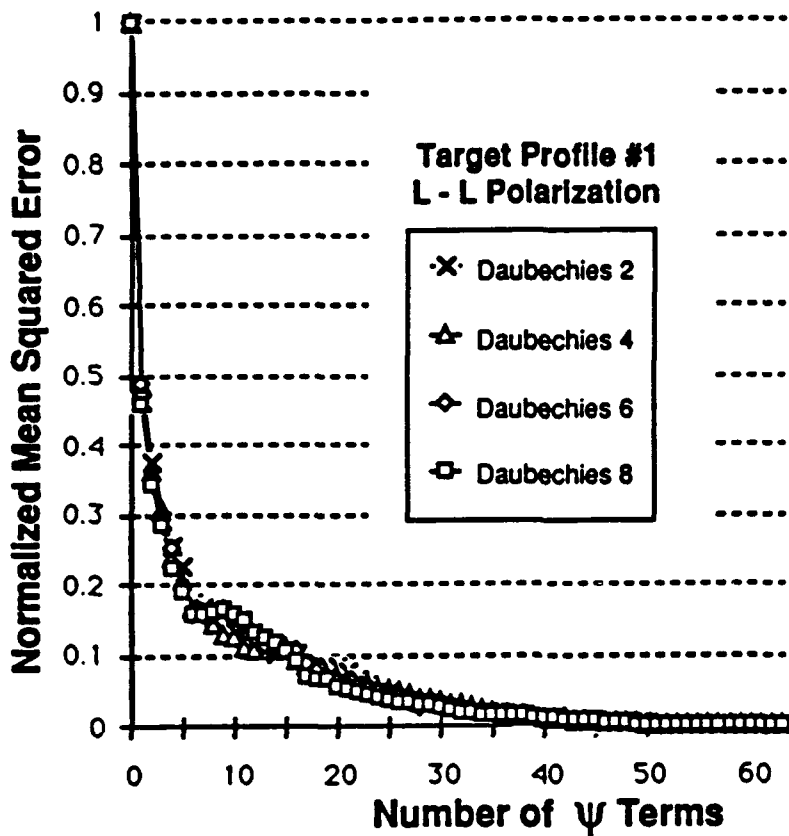


Figure 3.9: Error of Approximation versus Number of Wavelet (ψ) Terms for Selected Wavelet Bases.

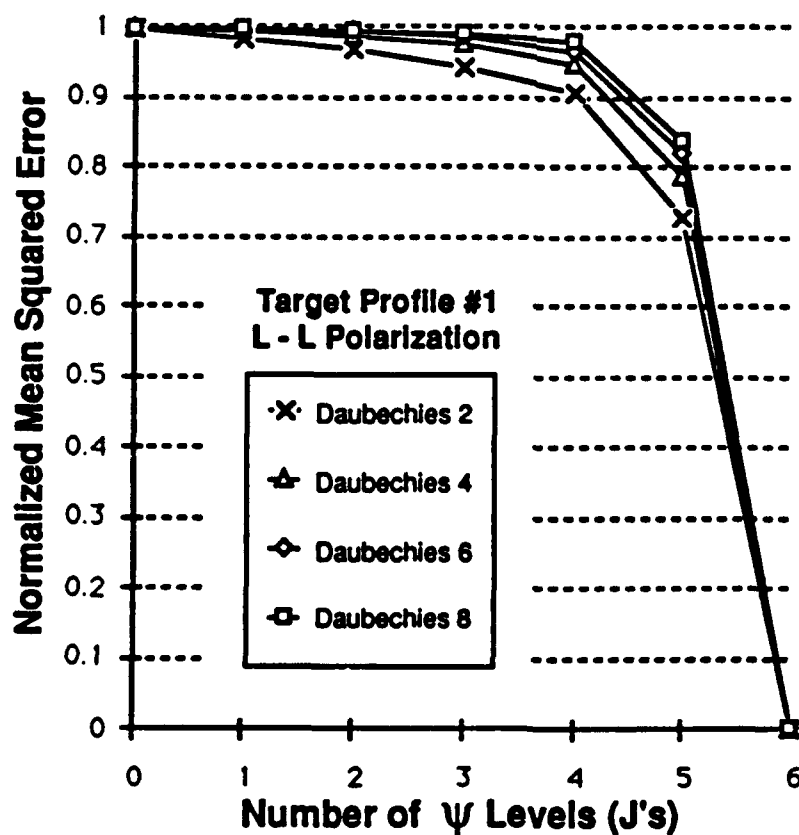


Figure 3.10: Error of Approximation versus Scale (ψ) Levels for Selected Wavelet Bases.

magnitude. An experiment was performed to evaluate the feasibility of eliminating entire scales from the approximation. Figure 3.10 shows the results for several wavelet basis functions. The approximation is very poor until the smallest scale wavelet coefficients are included. This means that the energy was distributed in wavelet coefficients across all scales.

The results of the previous experiment motivated a search for a method to preprocess the radar data so that the target energy could be placed into predictable scale levels and thereby eliminate the need to select (or sort) the most significant wavelet coefficients. This led us to adapt a method called "phase unwrapping" to this problem. Appendix C describes the mathematical details of the procedure. When it is applied to the radar data, the target energy is concentrated into the lowest scale levels and the approximation method can discard the highest scale level terms with little loss of information. This significantly reduces the computational complexity of the method. Figure 3.11 illustrates the reduction in error it produced.

In conclusion, it is feasible to apply the wavelet approximation to the Fourier transform to the millimeter wave sensor problem of producing HRRPs. The error of approximation can be controlled to any level desired by adjusting the number of wavelet terms retained in the approximation. The computational complexity of the wavelet methods for wavelet support lengths of 6 or less are comparable to the Fast Fourier Transform for the radar data used in this study, which is processed in blocks of 63 complex data points. The target data is contained in a relatively large fraction (1/2 to 1/3) of the output data points which requires that a large fraction of the wavelet coefficients be retained in the approximation. This increases the computation required for the wavelet methods. The target extent varies from about 10 fine range resolution cells to 30 range resolution cells. The error of approximation was about 0.10 (Norm. MSE) when 16 terms were retained and was less than 0.05 (Norm. MSE) when 32 terms were retained. It should be noted that the 8 term approximations contain over 80% of the original target energy, but have relatively severe "shape" distortion.

Since the wavelet methods offer no computational advantage and produce some error, they are probably not an appropriate choice for this particular radar data processing problem due to the small number of data points to process. However, if the data came from, for example, an FMCW (with a long pulse length) that performed 1024 point FFT's, yielding one foot range resolution, tank and truck detections, which are 10 to 30 feet long, depending on aspect, could be very efficiently processed by wavelet FFT approximation. Additional comparison results are given in Appendix B.3.

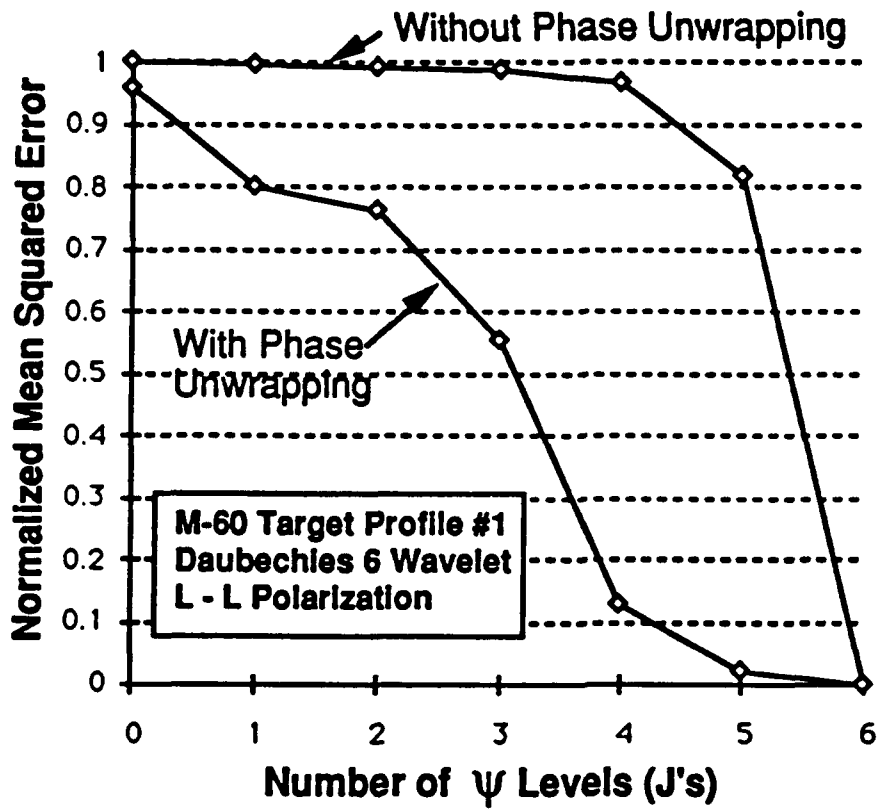


Figure 3.11: Error of Approximation versus Scale (ψ) Levels for Phase Unwrapped Target

3.3 Target Length Estimation

This section presents the results of experiments conducted on the radar data to develop and investigate the capabilities of wavelet based feature extraction methods. Of particular interest was the feasibility of performing feature extraction with a wavelet based approach and the stability of the method with respect to target signature variations due to change of aspect angle.

The feature which was selected for analysis was target extent which is the length of the target image in the high resolution radar range data. This feature is important because it requires that both the "front" and "back" of the target be determined. Target classification algorithms need this information to delimit the region in the high resolution radar data which contains the target detail. The performance of the wavelet methods is compared to a baseline method described in appendix E.

The following procedure was used to measure the stability of the target extent methods.

1. Calculate the target extent for a large number of aspect angles. The entire target data sets available to the subcontractor were used for the results presented in this report.
2. Divide the results into contiguous blocks of 50 items and compute the average extent for each of the blocks. This is interpreted as the true target extent in this neighborhood.
3. Calculate the differences between the extents calculated in step 1 and the local averages calculated in step 2. From the differences, calculate the standard deviation for each block of 50 estimates. This estimate of the standard deviation (locally) is a measure of the stability of the method.
4. Calculate the mean and standard deviation of the local standard deviations calculated in step 3 for the entire available target data set.

The wavelet algorithm used for extracting the target extent was based on thresholding the squared modulus of the large scale component of the one-sided wavelet transform of the complex radar image. This is a method for removing noise from the target data. It has two variations depending on the order in which mathematical operations are performed:

- $|WT(\hat{z}_k)|^2$
- $WT|\hat{z}_k|^2$

where $WT()$ indicates a wavelet transform and $||^2$ the squared modulus.

The first case requires the wavelet transform of complex Fourier transform data while the second case only requires that a real wavelet transform be performed. The performance of the second method was found to be better, as well as less costly. It is described below.

The thresholding procedure is similar to the method used in the baseline method (described in appendix E) except that only one half of the number of high resolution range cells are used to compute the noise floor because the one-sided transform components are sampled at half the original rate, i.e. they are half the length of the original sequence. Two additional variations of the wavelet transform method were studied to investigate the sensitivity to scale. The one-sided wavelet transform method was recursively applied to the large scale components resulting in data which were sampled at 1/4 and 1/8 the original rate. These cases used only four and two high resolution range cells, respectively, to estimate the noise floor. The general wavelet method used to estimate target extent is the following.

1. Compute the discrete Fourier transform (DFT) \hat{z}_k of the phase history data sequence z_k .
2. Compute the squared modulus of the transformed data $|\hat{z}_k|^2$.
3. Compute the large scale component of the one-sided wavelet transform of $|\hat{z}_k|^2$.
4. Establish a threshold $T > 0$. (T became 25.)
5. Compute the average power A of the 8 (or 4 or 2) high resolution range cells furthest away from the target. Since the target is known to be located in the center of the range gate, these are the first and the last 4 (or 2 or 1) high resolution range cells.
6. Compute the indices I_1 and I_2 of the first and last entries of $|\hat{z}_k|^2$ that exceed $T \times A$.
7. Compute target extent as $2 \times (I_2 - I_1 + 1)$ [or $4 \times (I_2 - I_1 + 1)$ or $8 \times (I_2 - I_1 + 1)$].

The computational cost in real multiplies of these three filtering methods are (where K is the size of the wavelet system):

1. For the one half scale method: $\text{Cost}(N) = (K+1)(N/2) \Rightarrow O(N)$;
2. For the one quarter scale method: $\text{Cost}(N) = (K+1)(3N/4) \Rightarrow O(N)$;
3. For the one eighth scale method: $\text{Cost}(N) = (K+1)(7N/8) \Rightarrow O(N)$.

Section 2.5 contains a detailed discussion of computational complexity.

Figures 3.12 through 3.15 are plots of mean target extent deviation versus scale for a threshold value of 25. The value plotted at the 64 cell resolution position represents the baseline method. The points plotted at the 32, 16 and 8 resolution positions represent the wavelet methods at 1/2, 1/4 and 1/8 scale respectively. Note that the wavelet methods are about as stable as the baseline method with resolution (dimensionality) reduced by a factor of 4.

Mean Deviation of Target Extent, M35 Truck, Pol = LL

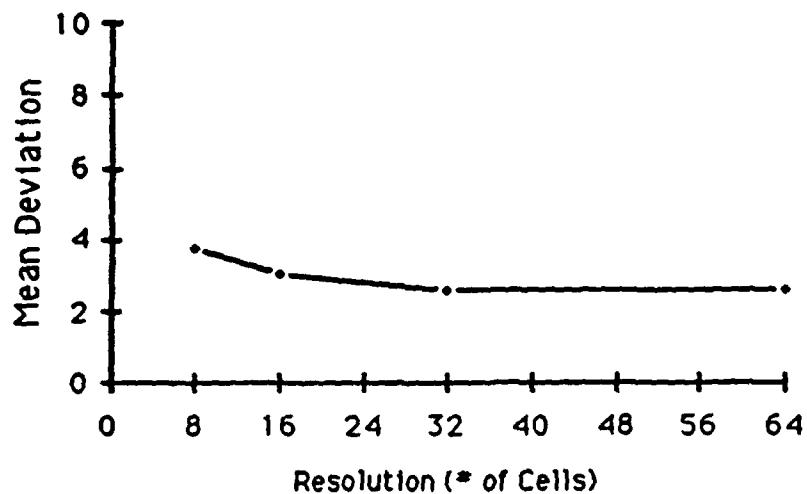


Figure 3.12: Mean Deviation of M35 Truck Target Extent - Wavelets 8,16, 32 and Baseline 64 cells - LL Polarization.

Mean Deviation of Target Extent, M35 Truck, Pol = LR

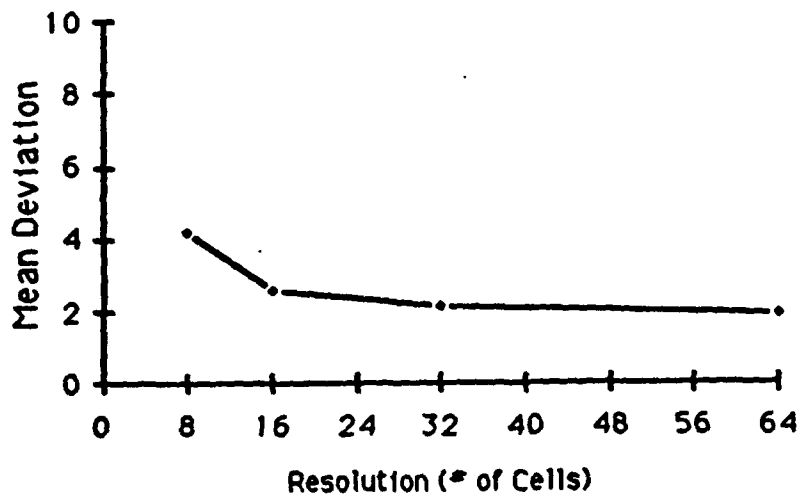


Figure 3.13: Mean Deviation of M35 Truck Target Extent - Wavelets 8,16, 32 and Baseline 64 cells - LR Polarization.

Mean Deviation of Target Extent, M60 Tank, Pol = LL

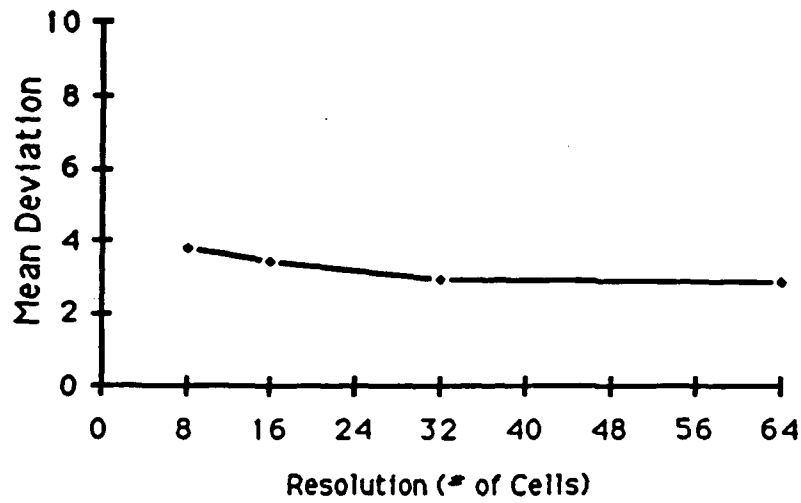


Figure 3.14: Mean Deviation of M60 Tank Target Extent - Wavelets 8,16, 32 and Baseline 64 cells - LL Polarization.

Mean Deviation of Target Extent, M60 Tank, Pol = LR

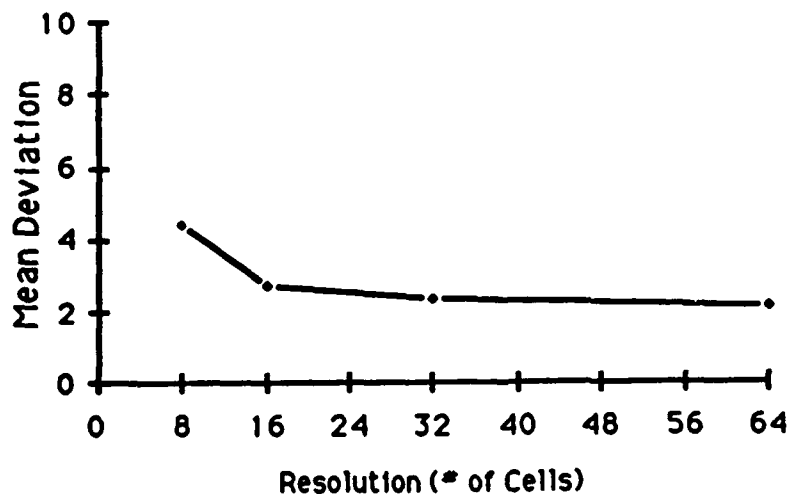


Figure 3.15: Mean Deviation of M60 Tank Target Extent - Wavelets 8,16, 32 and Baseline 64 cells - LR Polarization.

3.4 Wavelet Target Classification Results

A two class target classification experiment was conducted to see if it is feasible to improve radar target classification signal processing by wavelet methods, either by improving classifier percent correct classification (PCC) in the presence of noise (added to the very clean radar target data) or by decreasing the number of computations required by the classifier processor, or both. The classification problem examined was for two vehicles, an M60 tank and an M35 truck. The tank might be a target for a missile, but the truck might be a target-like object that one would not want to waste a missile on. Classifier overall PCC was improved in realistic signal/interference situations by up to 6 percentage points, and computations were decreased by a factor of 10.

Quadratic classifiers were used with either odd degree (1,3,5,...) aspects as the "training" set and even degree (0,2,4,...) aspects as the "test" set or the reverse. Noise was never added to the "training" set. Because this is actual radar data taken on an outdoor range with very light clutter background, the "clean" data has a signal to clutter ratio of greater than 20dB. The wavelet basis selected was the Haar or Daubechies 2 wavelet basis. The features used by the classifier were particular wavelet coefficients produced by the target HRRPs. Wavelet coefficients were selected logically but by no means optimally.

Specific results are given in Figure 3.16. These results clearly indicate that it is feasible to improve radar classifier processors by wavelet methods.

This study used one odd polarization and one even polarization. This would be the case if one transmitted only one of the two circular polarizations, but received both circular polarizations or the reverse. The starting point for this study was the target HRRPs, which contained one foot range resolution target magnitude data. It is assumed that target length (as seen by the radar) is no more than 32 feet. In reality, target length varies considerably depending on target aspect angle. For example, targets are longest when viewed from a head-on (0 degree aspect) or from a 180 degree aspect.

In Figure 3.16

S = total signal power

N = total power of noise added

S/N given is for the tank (higher for the truck)

HR64 = 32 odd & 32 even HRRP components

W64-11 = 11 coefficients from HR64 wavelet transform.

As part of the next phase, it will be important to perform a three class classifier experiment. This was not accomplished during this phase due to cost and schedule constraints.

Figure 3.16: Target Classification - Original vs. Wavelet

COMPLEXITY (number of multiplies)

HR64 = 2144
W64-11 = 205 (90% reduction)

PERCENT CORRECT CLASSIFICATION

<u>S/N</u>	<u>S/N(dB)</u>	<u>HR64</u>	<u>W64-11</u>
zero noise		92	85
6.6	8.2	77	83
2.7	4.3	69	72
0.67	-1.7	59	60

3.5 Fine Range Resolution by Wavelets

It is theoretically possible to obtain fine range resolution HRRPs by using wavelet transforms instead of FFTs if the waveform transmitted is modified to be appropriate for wavelet transforms. This possibility is important because a radar's digital signal processor (DSP) is typically one of the more costly parts of the radar due to heavy processing load requirements - primarily due to the need to perform many FFTs. Since a wavelet transform is considerably faster than an FFT, significant DSP cost, weight, and size savings will result from wavelet, rather than FFT, HRRPs.

A wavelet transform matrix W can be constructed from the product of a number of wavelet "butterfly" matrices. This is similar to computing a discrete Fourier transform (DFT) matrix as the product of FFT "butterfly" matrices. Unlike the DFT matrix, the wavelet matrix W consists of real (rather than complex) numbers, for the four wavelets of initial interest, D2 (Haar), D4, D6, and D8. The column vectors, w_1, w_2, \dots, w_n of the n -by- n matrix W are orthonormal. If y denotes the column vector of wavelet coefficients for an input column vector x , then y could be computed by (more efficiently by "butterflies")

$$y' = x' W \quad (3.2)$$

and the absolute value of the components of y will be a fine range resolution HRRP if the n transmitted waveforms correspond to the wavelets in the following ways.

1. The n sequential transmitted waveforms look like the rows of the matrix W . (The orthonormal wavelet vectors are the columns of W .)
2. The transmitted waveforms are "stretched" to twice the W -row-length, n , to allow for 2-way travel.

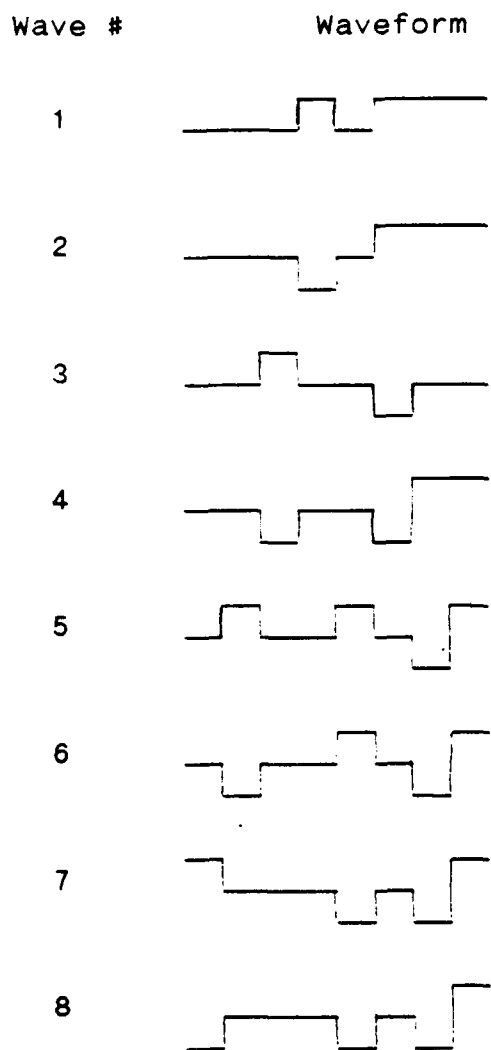
An eight dimensional example with the Haar wavelet follows in Figure 3.17. The example easily can be extended to a 32 or 64 dimensional version. The Haar wavelet is easy to describe, but due to its non-smooth nature it is probably not a good wavelet waveform for radar transmission. In Figure 17, instead of stepping frequencies from one waveform to the next, the shape of the waveform changes in a wavelet related fashion. There are 8 waveforms used to break an 8 foot long range bin into 8 one foot segments by wavelet transform (instead of FFT). The time duration of the waveforms is 16 feet divided by the speed of light.

There are two speed advantages to transmitting wavelet-related signals and processing by wavelets to get fine range profiles.

1. Wavelet transforms are $O(n)$; FFTs are $O(n \log_2(n))$.
2. D2, D4, and D6 wavelet transforms use 1-cycle real*real multiplies; FFTs of I,Q data use 6-cycle

complex*complex multiplies (4 multiplies, 1 add,
and 1 subtract)

Figure 3.17: Haar Waveforms for HRRPs



4.0 Supplemental Results

Figures 4.1 through 4.3 contain plots of partial reconstruction by D6 wavelets, of a normalized odd bounce polarization HRRP from a radar look at the calibrated trihedral corner reflector. Figures 4.4 through 4.6 contain similar plots for an even bounce polarization HRRP from a radar look at two dihedrals that are separated by about 10 feet in range. Each plot lists the number of terms used in the reconstruction and the normalized mean square error.

Figures 4.7 through 4.10 show estimated target length versus aspect angle for the M35 truck. The polarization was even (transmit left circular and receive left circular). The four plots are for FFT (Martin Marietta method) processing, wavelet reconstruction dimension reduction by a factor of 2, then 4, then 8 respectively. Similar results are given for an odd polarization (transmit right circular and receive left circular) in Figures 4.19 through 4.22. Since target length will vary with target aspect, it was decided that a good measure of length estimation stability would be the standard deviation (over blocks of 50 radar looks) of the length estimate. That is, a small standard deviation would indicate stable length estimation. These results are presented in Figures 4.11 through 4.18 for an even polarization M35 truck and in Figures 4.23 through 4.30 for an odd polarization M35 truck. Figures 4.11, 4.13, 4.15, and 4.17 contain plots of the mean of the length estimates from blocks of 50 M35 looks. Figures 4.12, 4.14, 4.16, and 4.18 contain plots of the standard deviation of the length estimates from blocks of 50 M35 looks, along with a numerical mean and standard deviation of these standard deviations. This standard deviation comparison was the figure of merit used to determine the stability of the wavelet methods.

Figures 4.31 through 4.34 show estimated target length versus aspect angle for the M60 tank. The polarization was even (transmit left circular and receive left circular). The four plots are for FFT (Martin Marietta method) processing, wavelet reconstruction dimension reduction by a factor of 2, then 4, then 8 respectively. Similar results are given for an odd polarization (transmit right circular and receive left circular) in Figures 4.43 through 4.46. Target length standard deviation versus aspect angle results for an M60 tank are presented in Figures 4.35 through 4.42 for an even polarization M60 tank and in Figures 4.47 through 4.54 for an odd polarization M60 tank. During the analysis it was discovered that a portion of the data for the M60 tank was found to be unusable. Although it was too late in the analysis to determine the problem and supply the correct data to our subcontractor, it had no significant outcome on the results.

For both trucks and tanks these results show wavelet dimension reduction by a factor of 2 or 4 looks acceptable based on a desire for small standard deviations, but when the dimension is reduced by a factor of 8 the standard deviation

becomes large and erratic. Consequently, the results show that dimension can be reduced by up to a factor of 4 but not 8, with no appreciable loss of stability in length estimation.

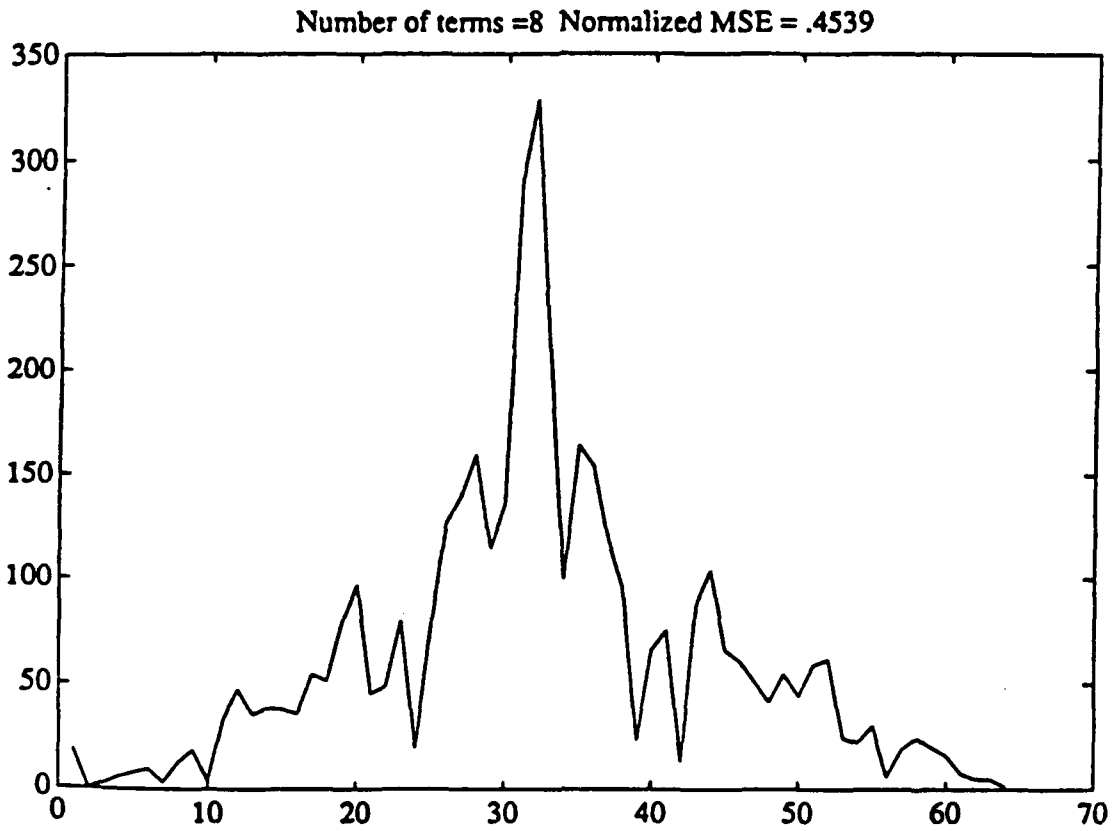


Figure 4.1: Partial Wavelet Reconstruction—Trihedral, $N=[8]$.

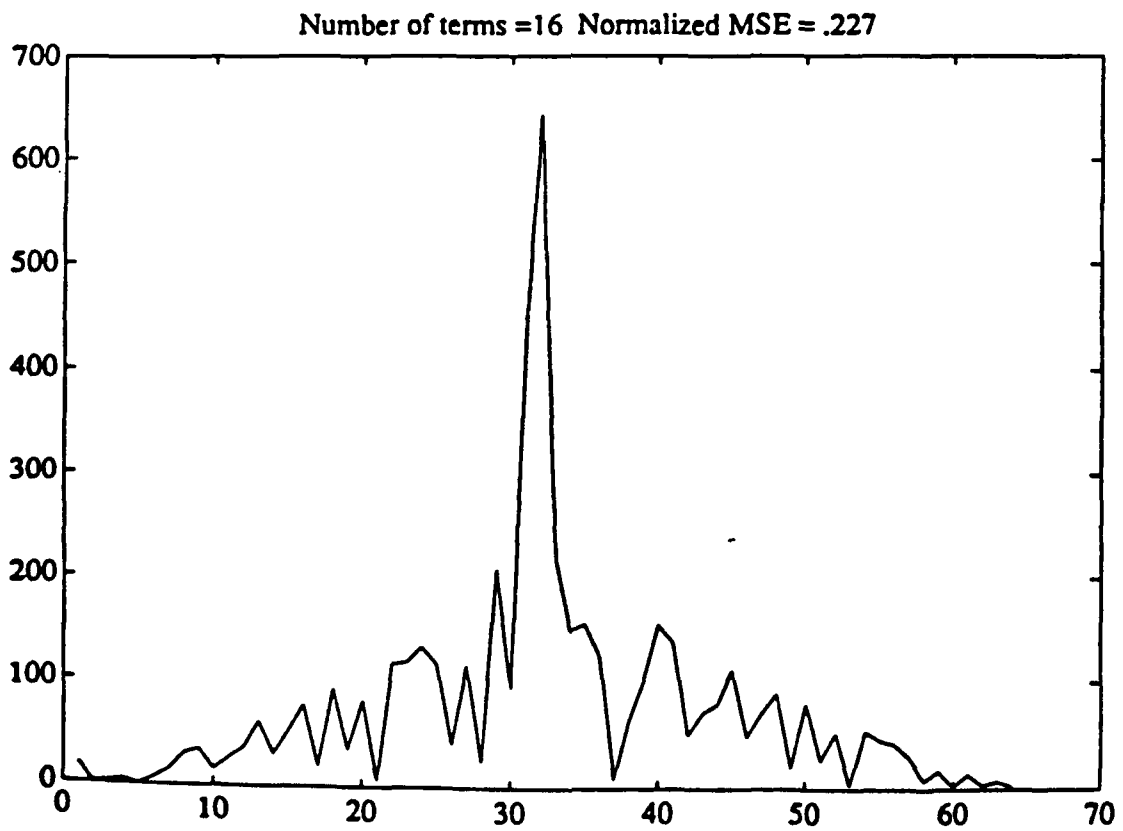


Figure 4.2: Partial Wavelet Reconstruction—Trihedral, $N=[16]$.

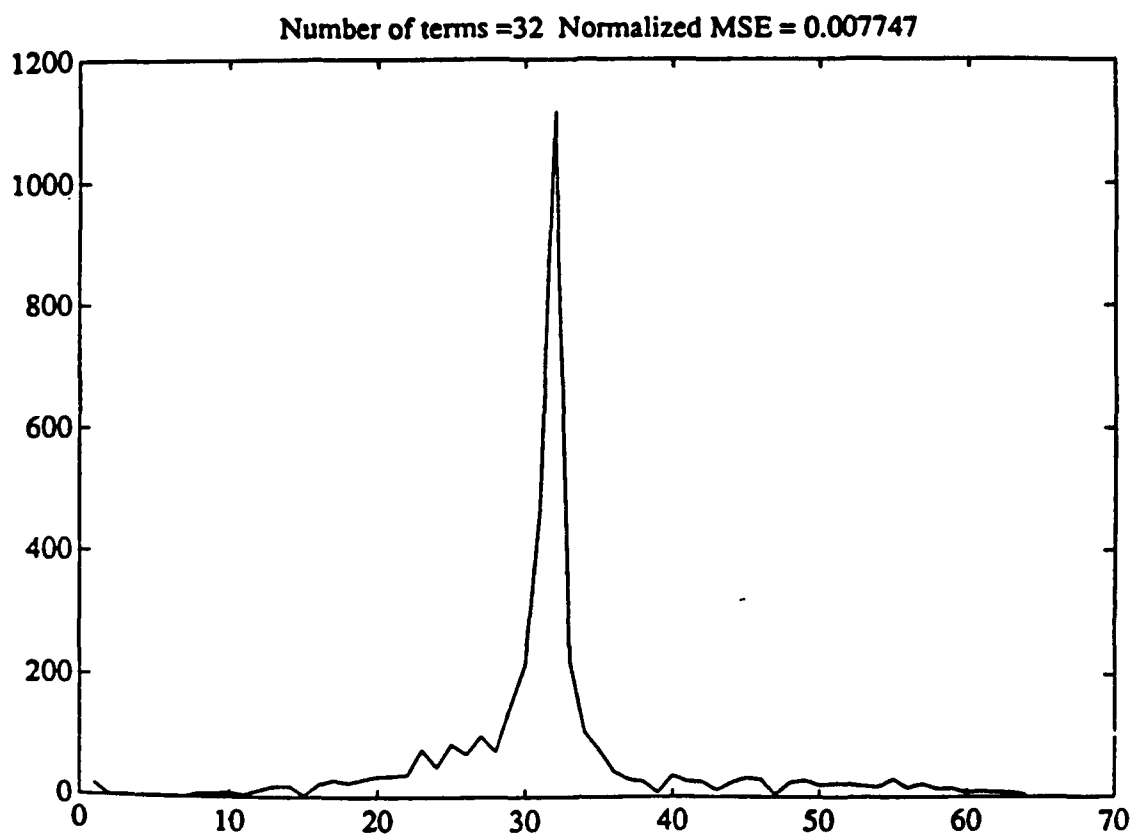


Figure 4.3: Partial Wavelet Reconstruction—Trihedral, $N=[32]$.

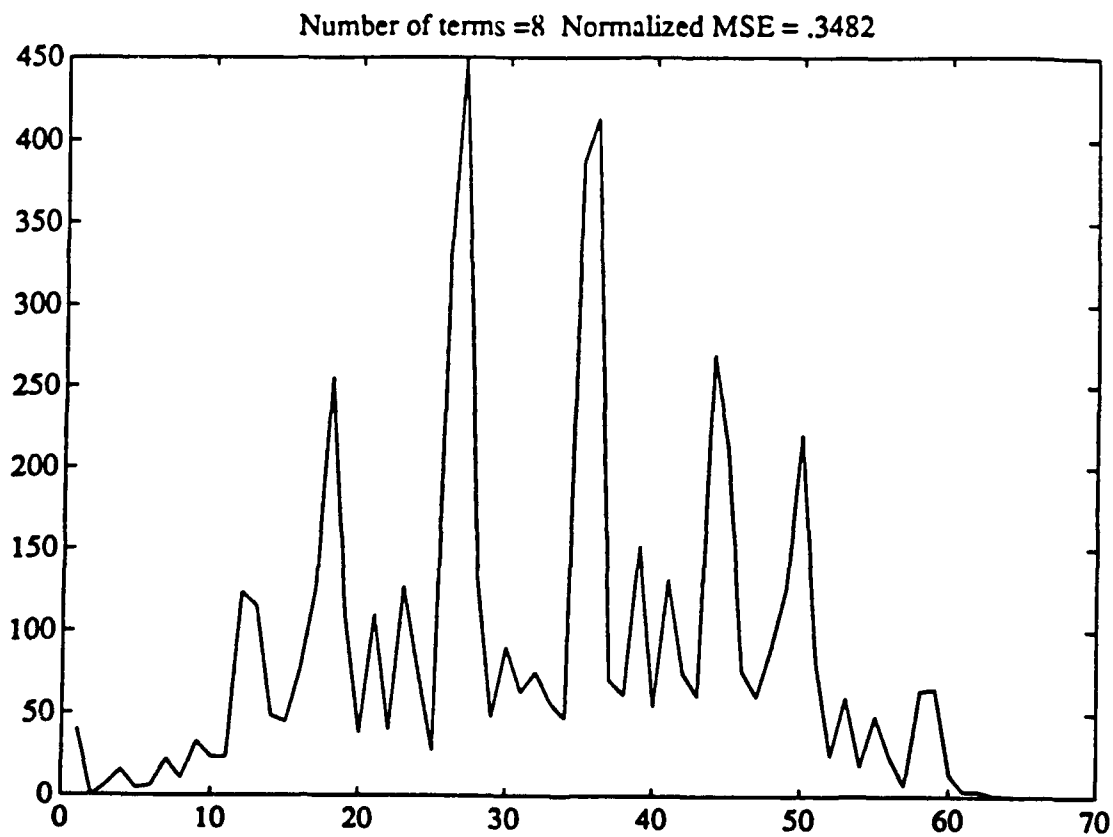


Figure 4.4: Partial Wavelet Reconstruction—Dihedral, $N=[8]$.

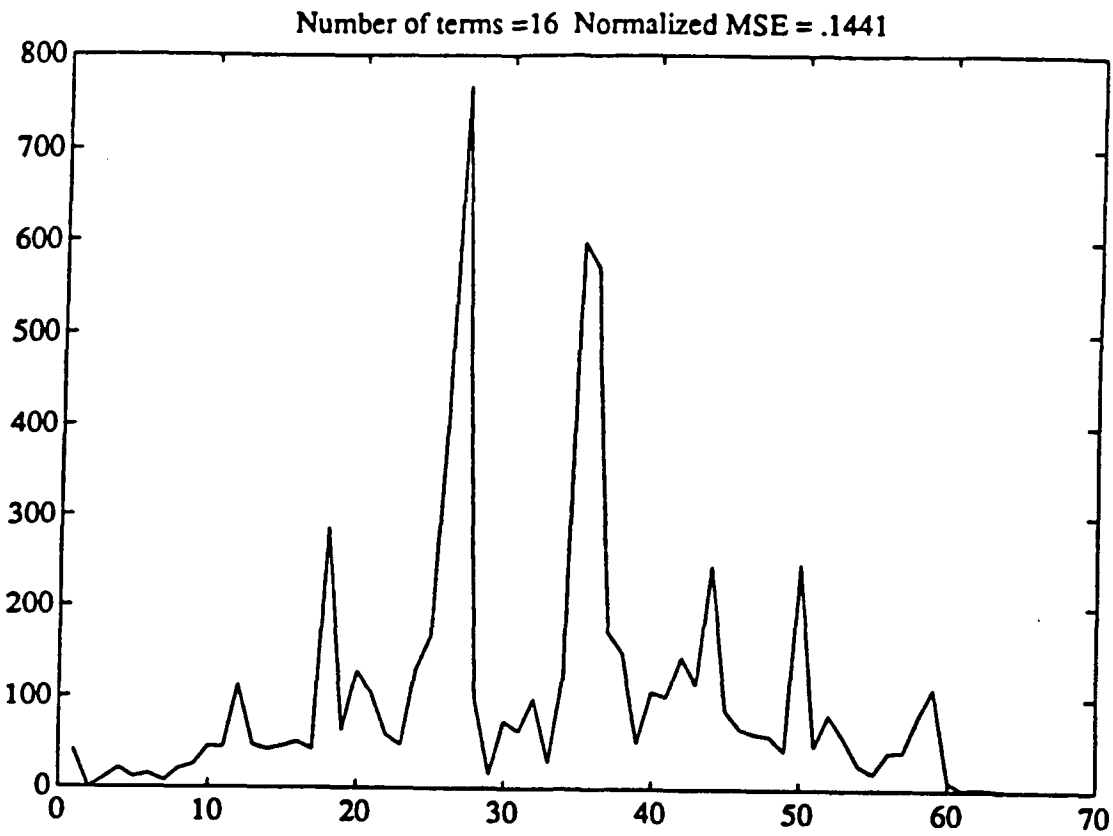


Figure 4.5: Partial Wavelet Reconstruction—Dihedral, $N=[16]$.

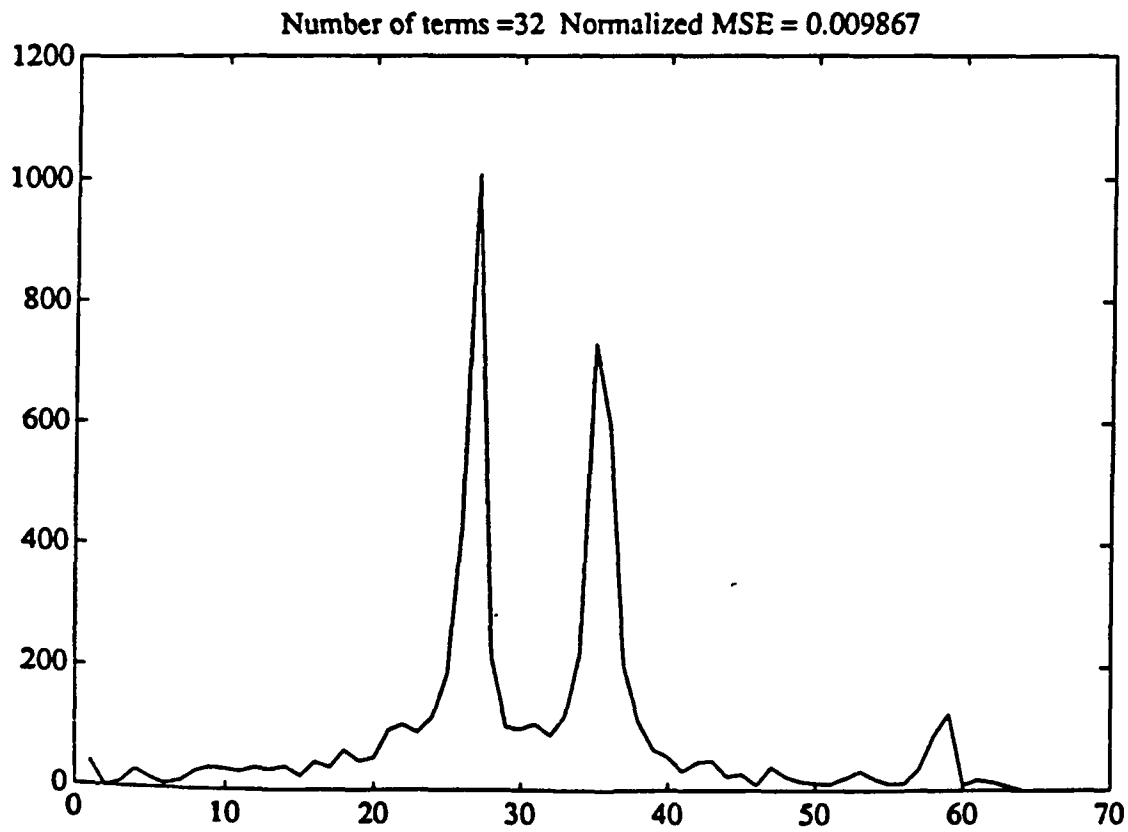


Figure 4.6: Partial Wavelet Reconstruction—Dihedral, $N=[32]$.

Figure 4.7: **Target Extent versus Aspect Angle**
Target: M35, Threshold: 25, Polarization: LL
Analysis of Real data (Martin Method)

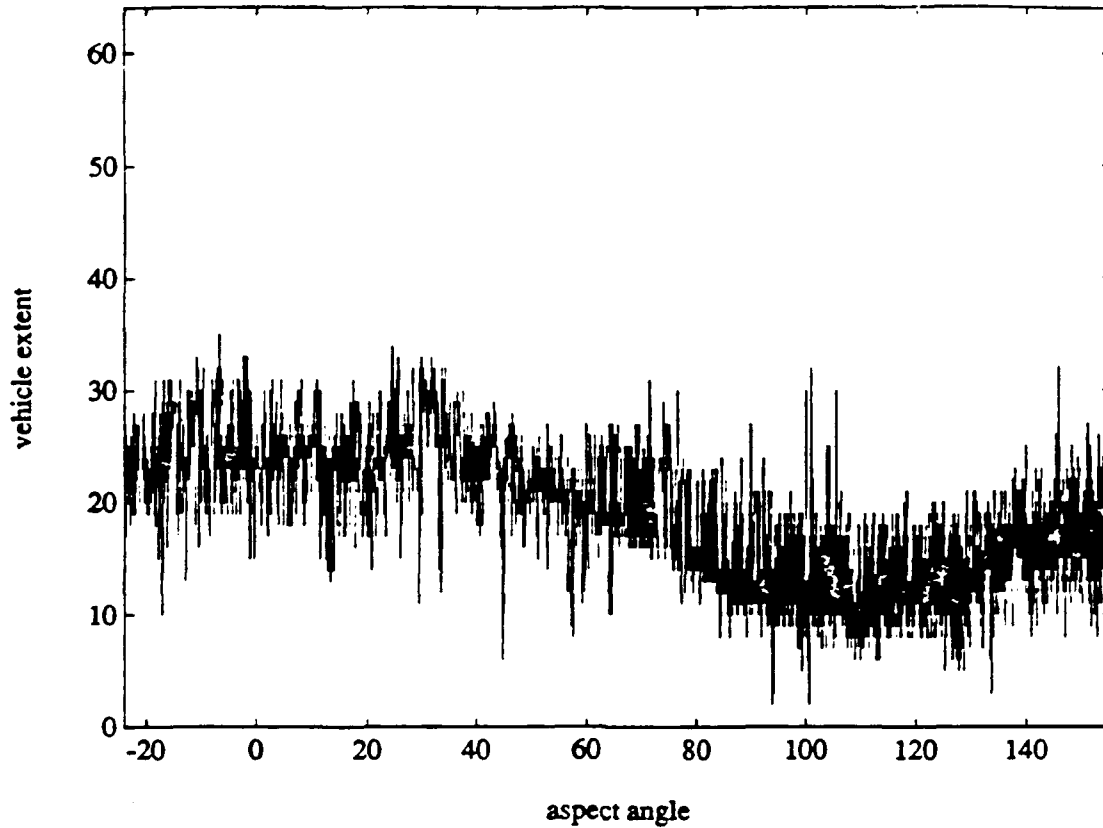


Figure 4.8: **Target Extent versus Aspect Angle**
Target: M35, Threshold: 25, Polarization: LL
Analysis of Real data (D6 Level 1)

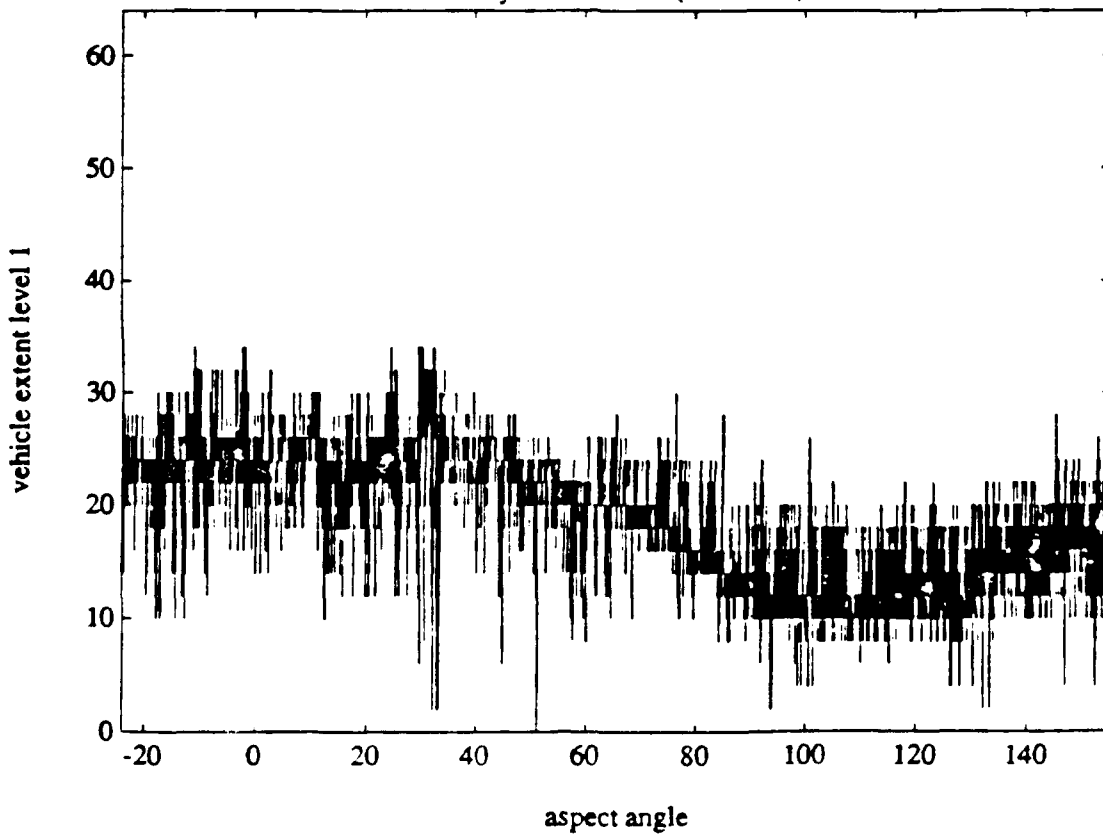


Figure 4.9:

Target Extent versus Aspect Angle
Target: M35, Threshold: 25, Polarization: LL
Analysis of Real data (D6 Level 2)

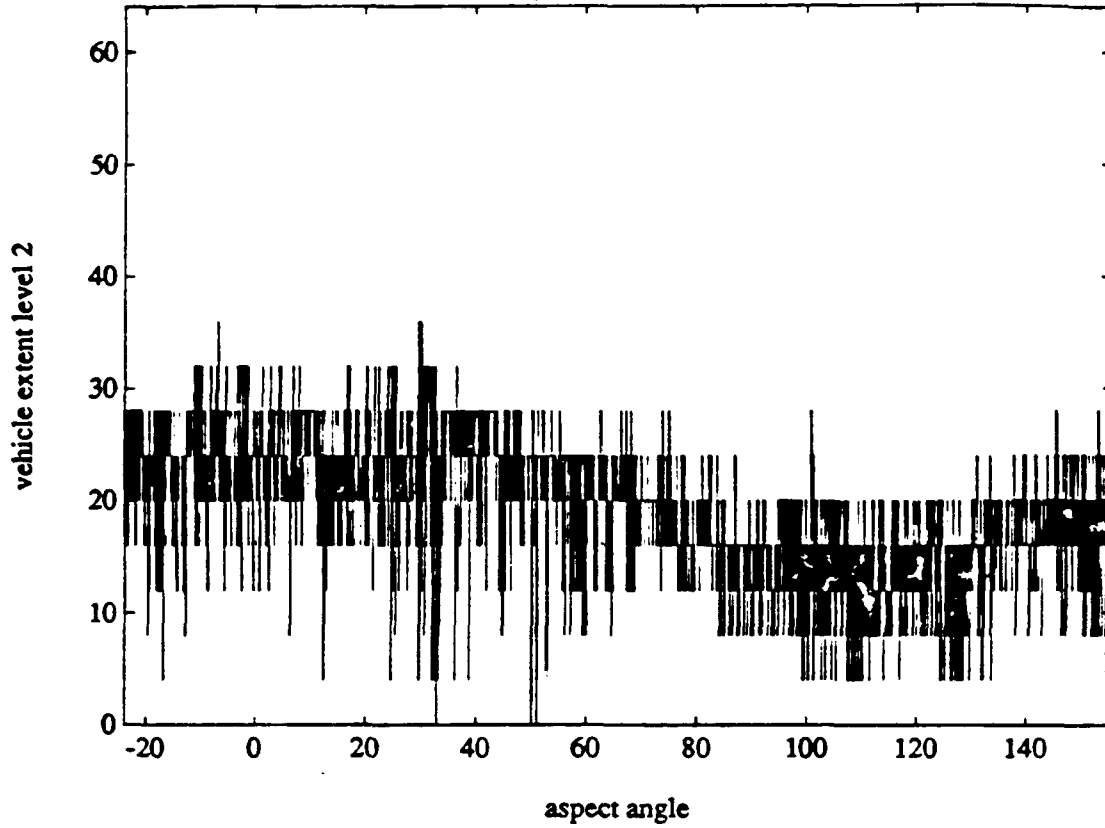


Figure 4.10:

Target Extent versus Aspect Angle
Target: M35, Threshold: 25, Polarization: LL
Analysis of Real data (D6 Level 3)

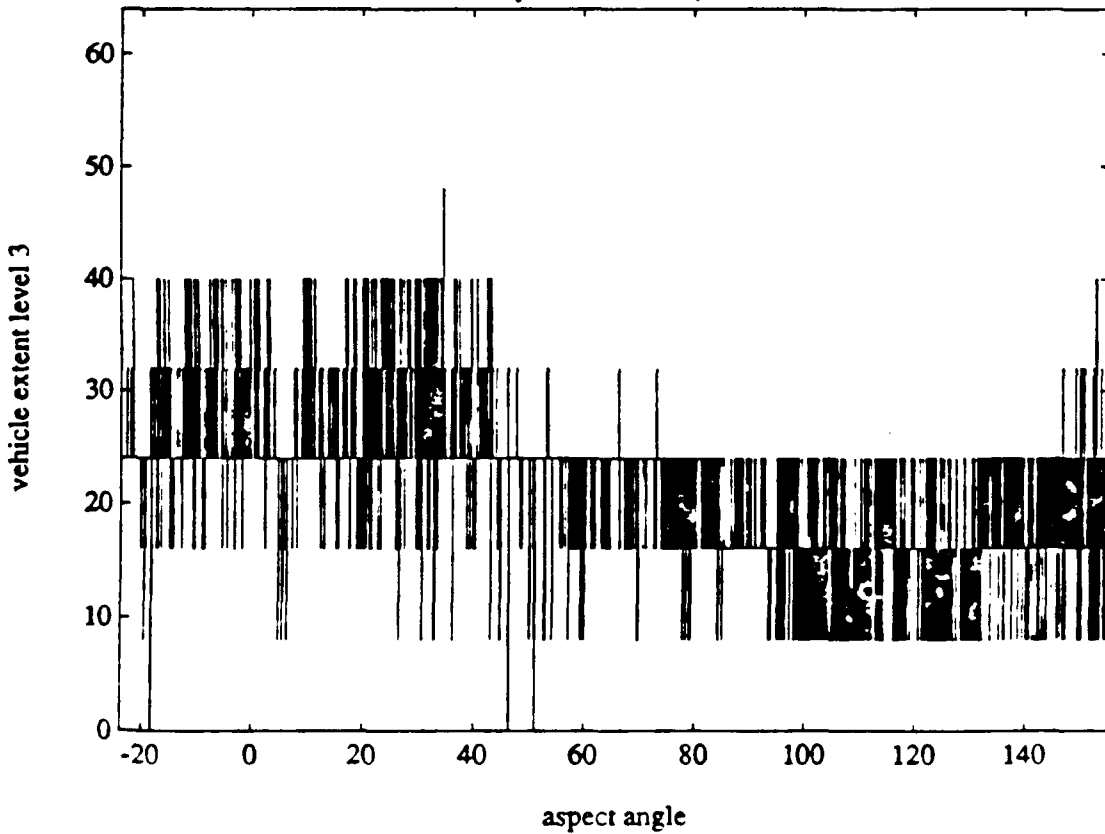


Figure 4.11: **Average Target Extent versus Aspect Angle**
Block Size: 50, Target: M35, Threshold: 25, Polarization: LL
Analysis of Real data (Martin Method)

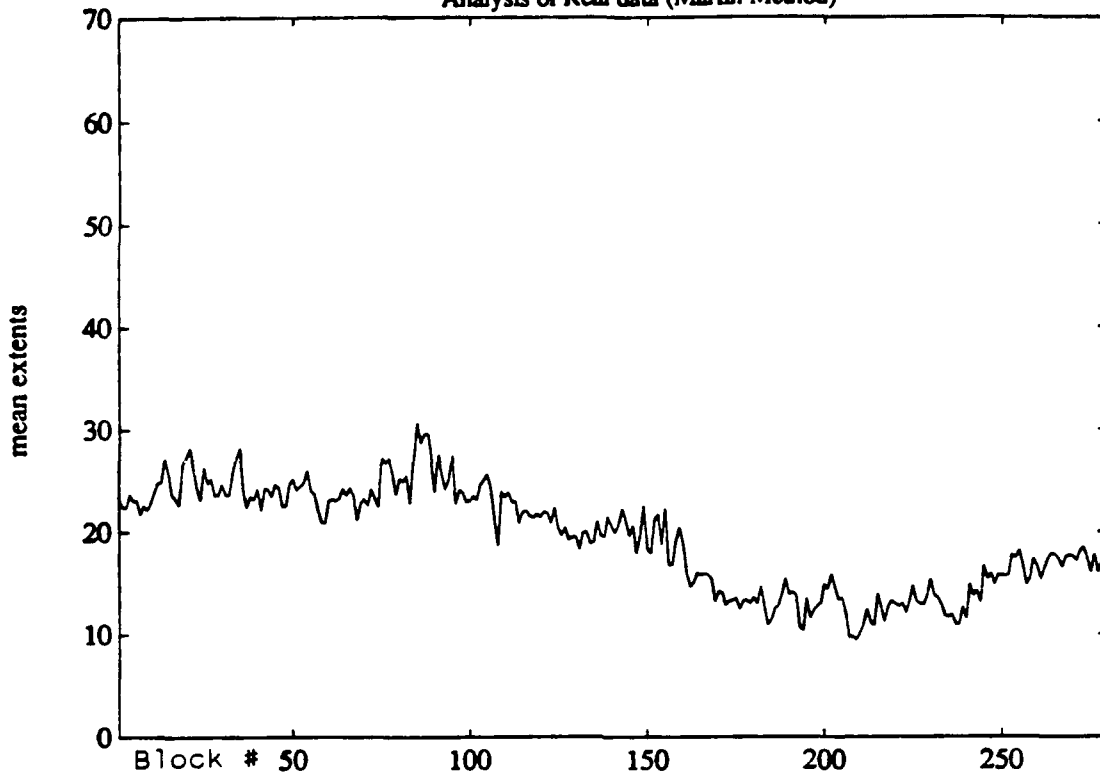


Figure 4.12: **Standard Deviation Target Extent versus Aspect Angle**
Block Size: 50, Target: M35, Threshold: 25, Polarization: LL
Analysis of Real data (Martin Method)

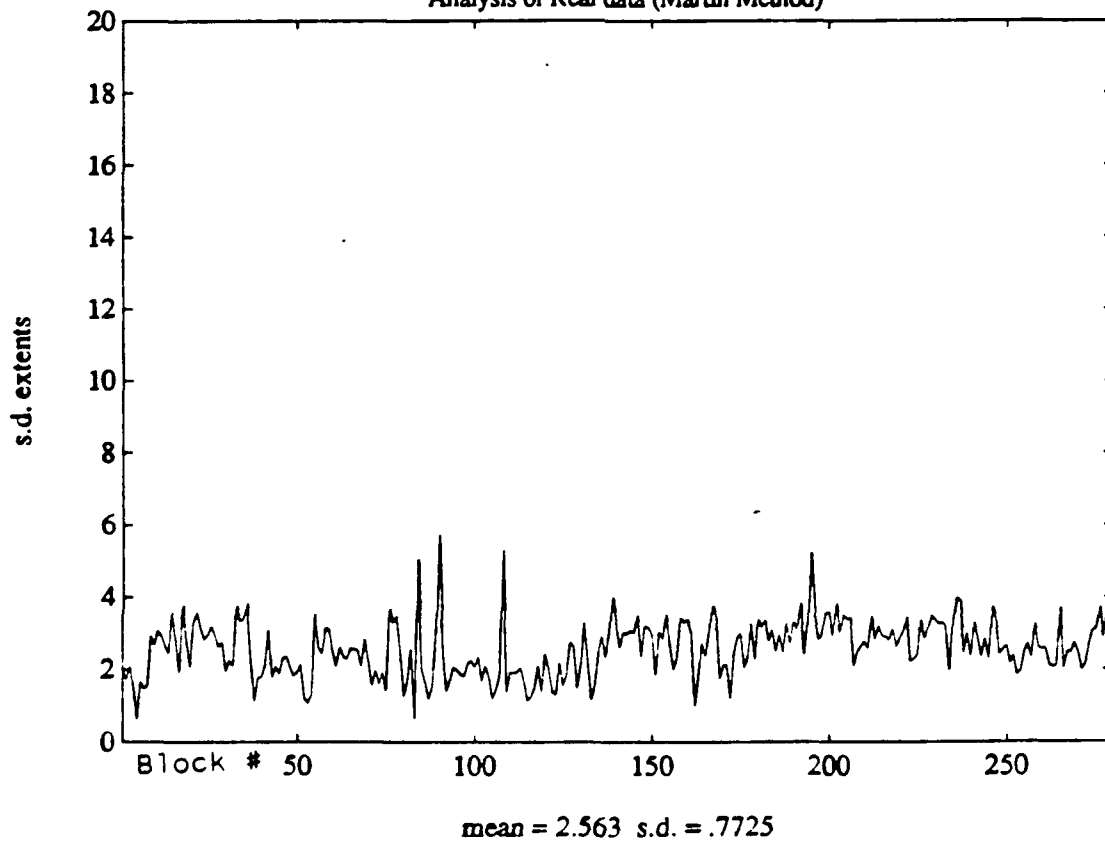


Figure 4.13: **Average Target Extent versus Aspect Angle**
Block Size: 50, Target: M35, Threshold: 25, Polarization: LL
Analysis of Real data (D6 Level 1)

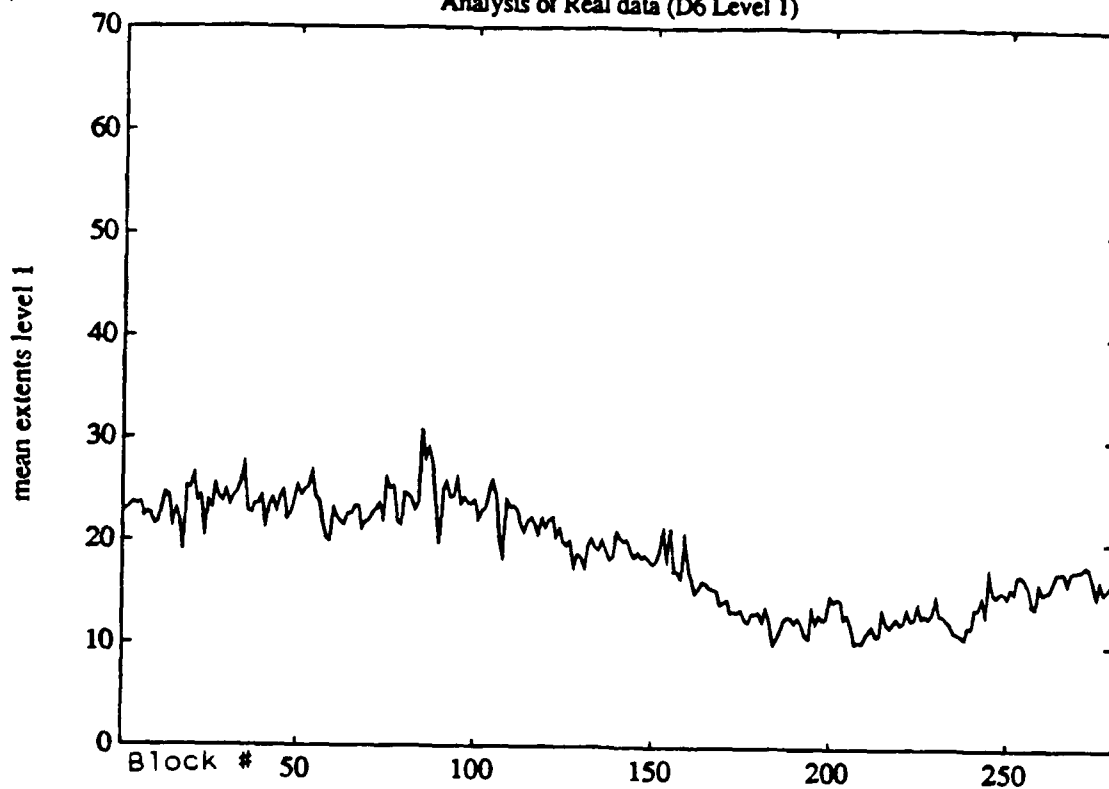
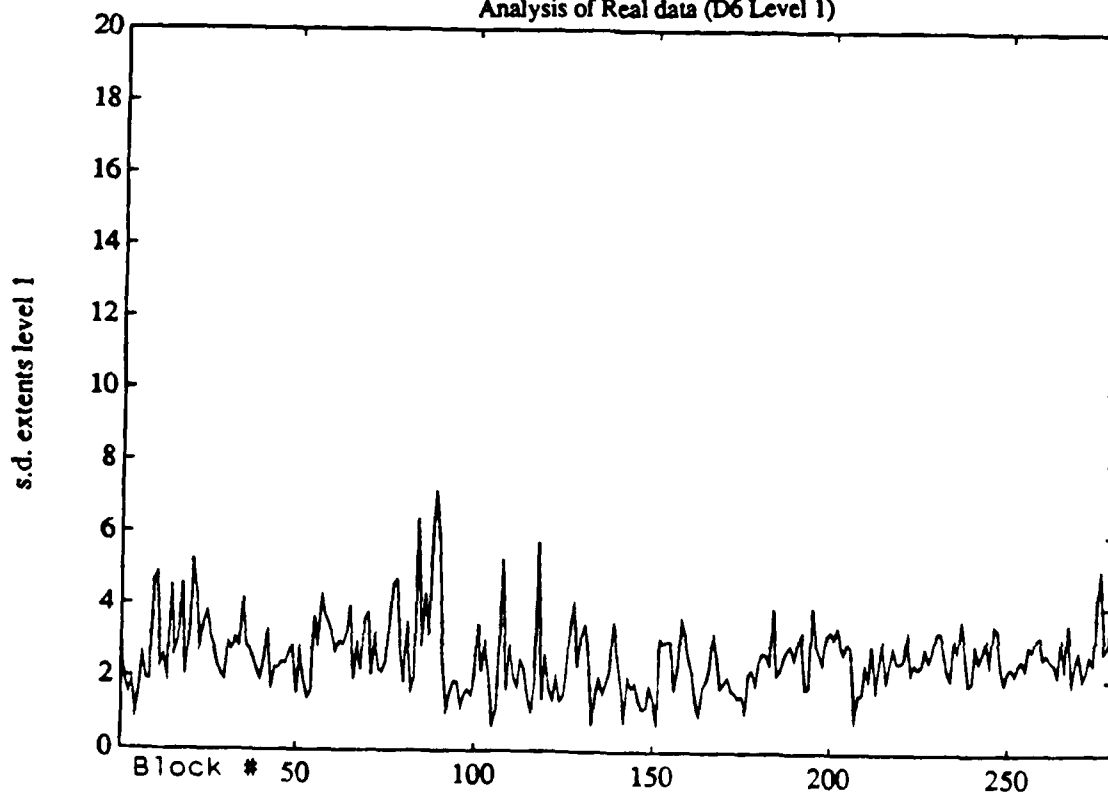


Figure 4.14: **Standard Deviation Target Extent versus Aspect Angle**
Block Size: 50, Target: M35, Threshold: 25, Polarization: LL
Analysis of Real data (D6 Level 1)



mean = 2.615 s.d. = .9637

Figure 4.15: **Average Target Extent versus Aspect Angle**
Block Size: 50, Target: M35, Threshold: 25, Polarization: LL
Analysis of Real data (D6 Level 2)

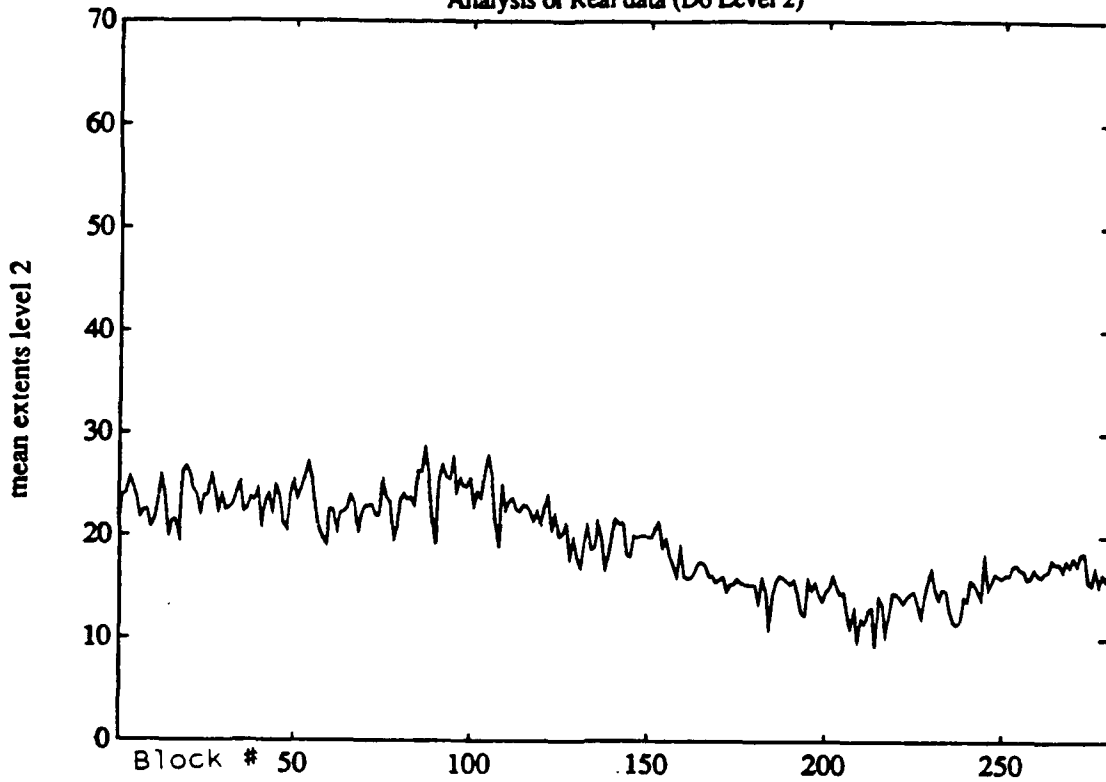
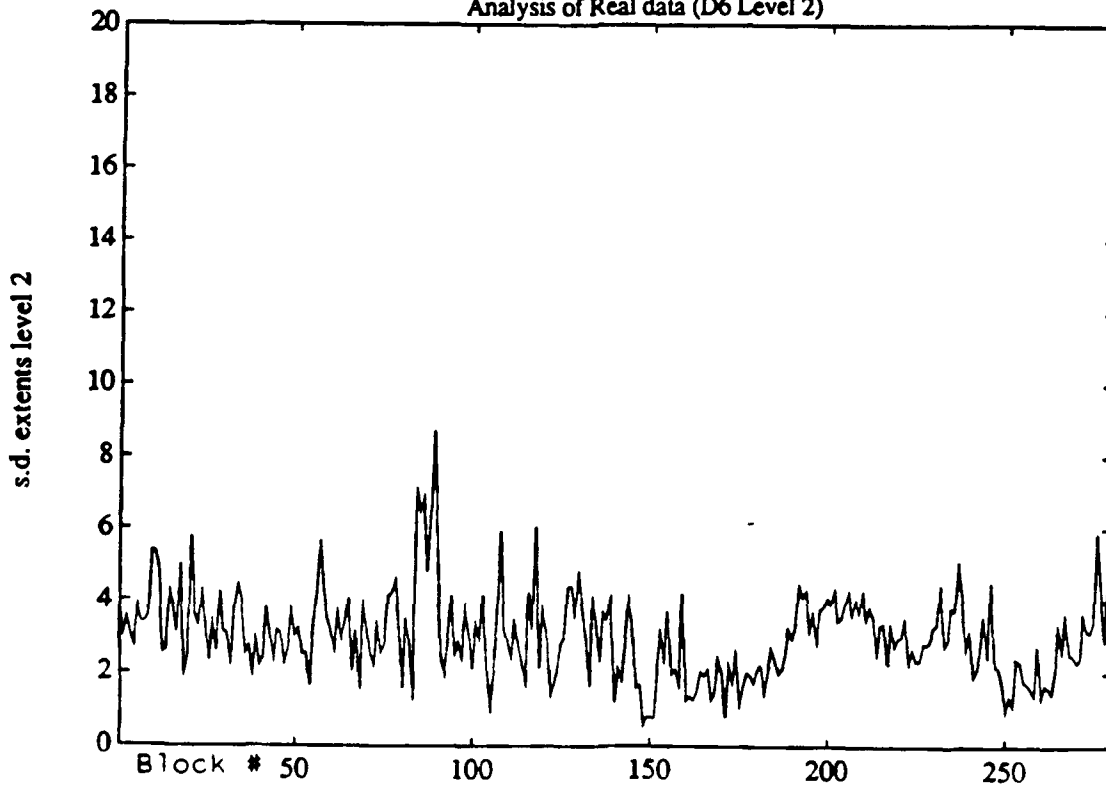


Figure 4.16: **Standard Deviation Target Extent versus Aspect Angle**
Block Size: 50, Target: M35, Threshold: 25, Polarization: LL
Analysis of Real data (D6 Level 2)



mean = 3.018 s.d. = 1.174

Figure 4.17: **Average Target Extent versus Aspect Angle**
Block Size: 50, Target: M35, Threshold: 25, Polarization: LL
Analysis of Real data (D6 Level 3)

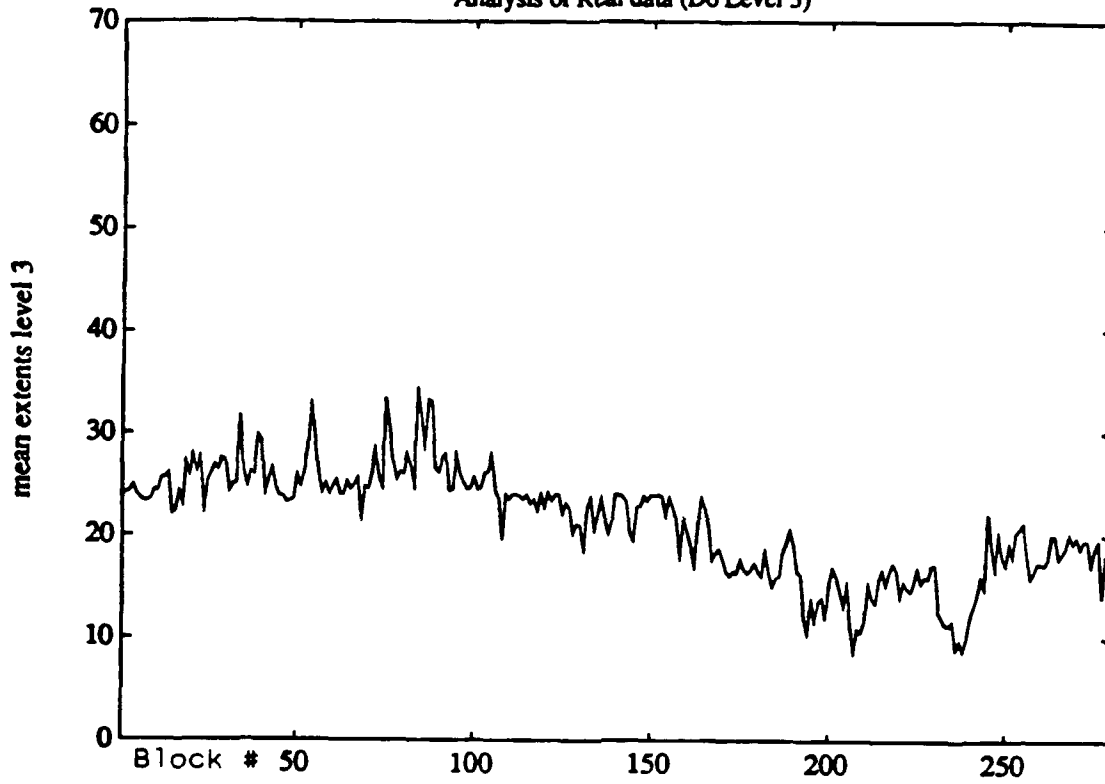


Figure 4.18: **Standard Deviation Target Extent versus Aspect Angle**
Block Size: 50, Target: M35, Threshold: 25, Polarization: LL
Analysis of Real data (D6 Level 3)

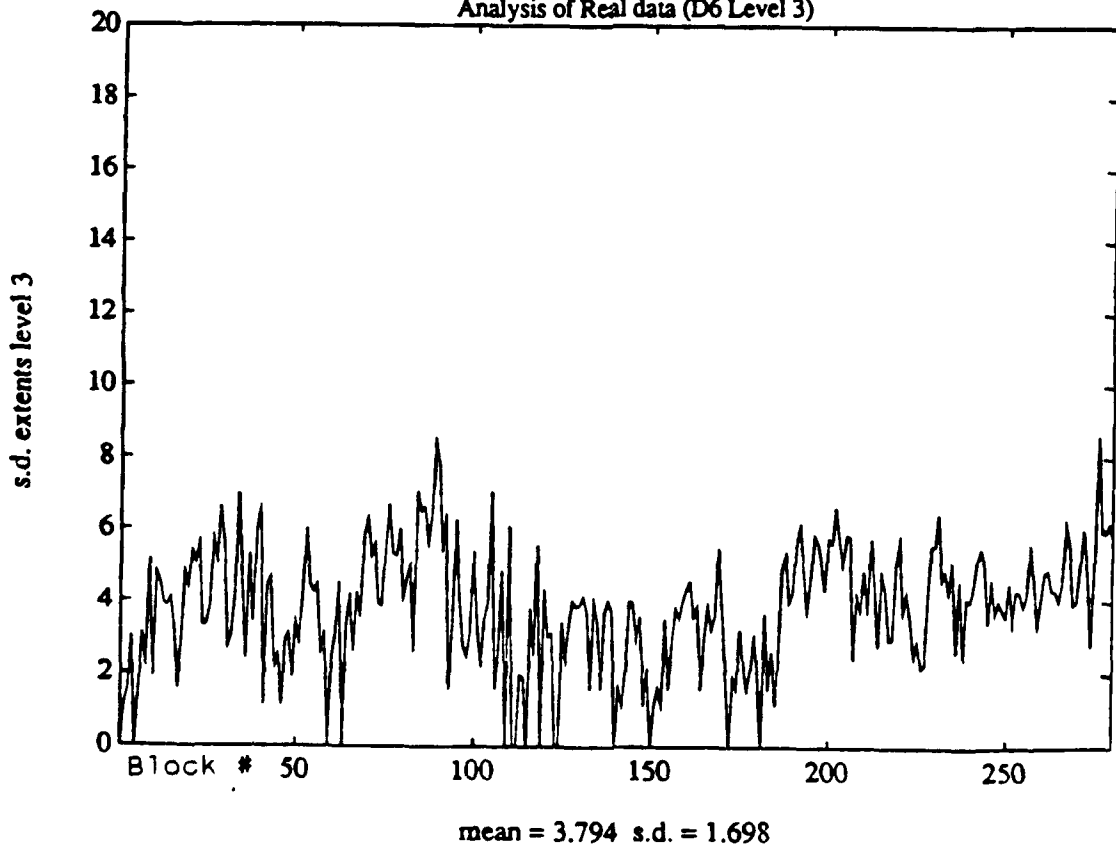


Figure 4.19: **Target Extent versus Aspect Angle**
Target: M35, Threshold: 25, Polarization: LR
Analysis of Real data (Martin Method)

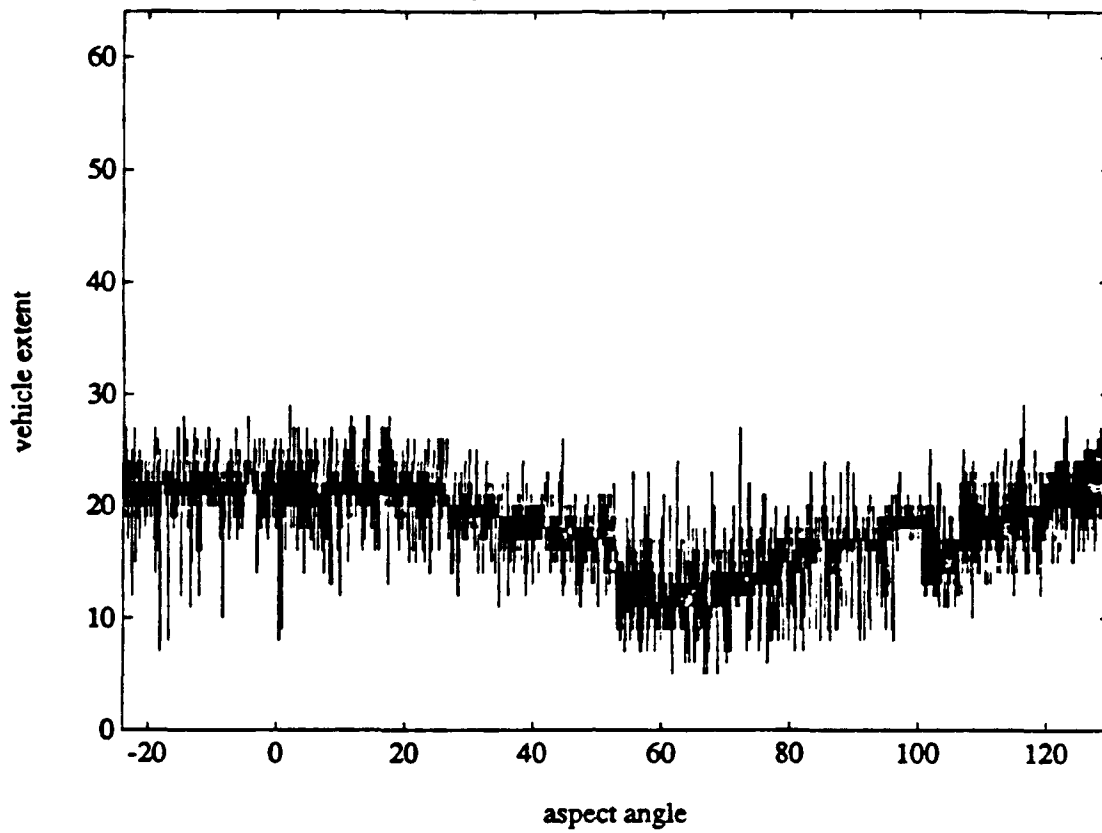


Figure 4.20: **Target Extent versus Aspect Angle**
Target: M35, Threshold: 25, Polarization: LR
Analysis of Real data (D6 Level 1)

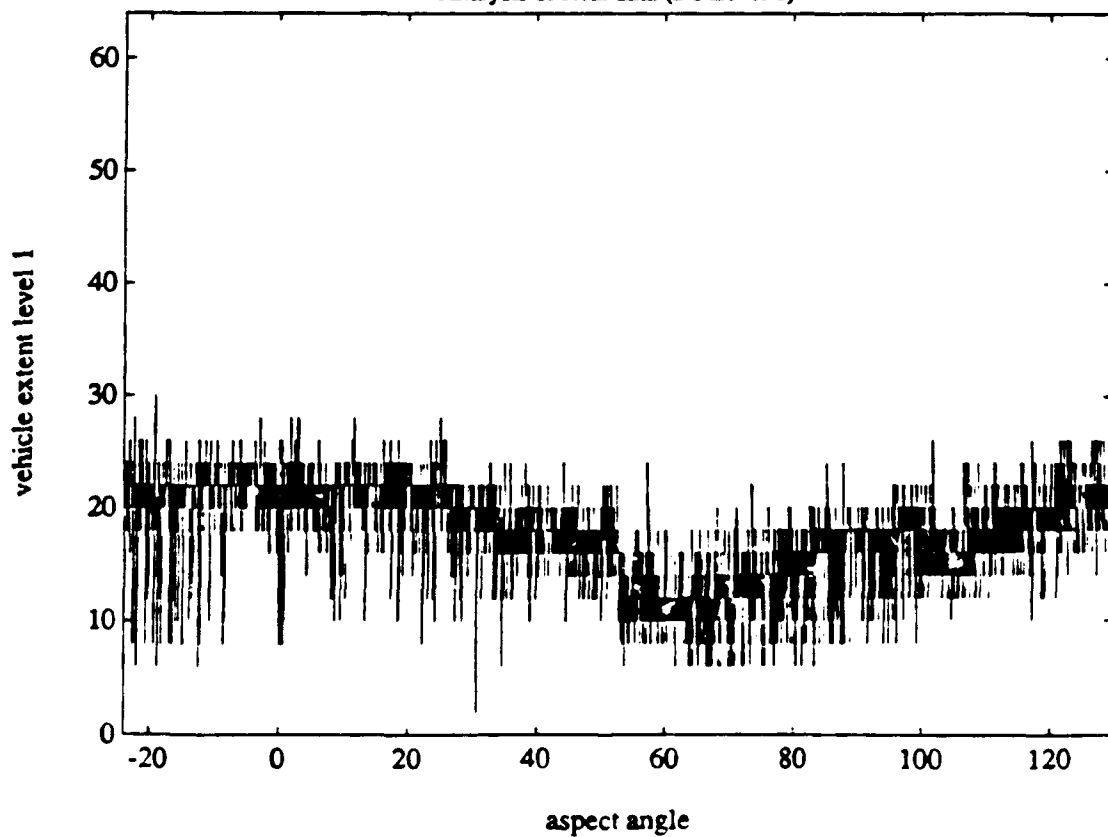


Figure 4.21: **Target Extent versus Aspect Angle**
Target: M35, Threshold: 25, Polarization: LR
Analysis of Real data (D6 Level 2)

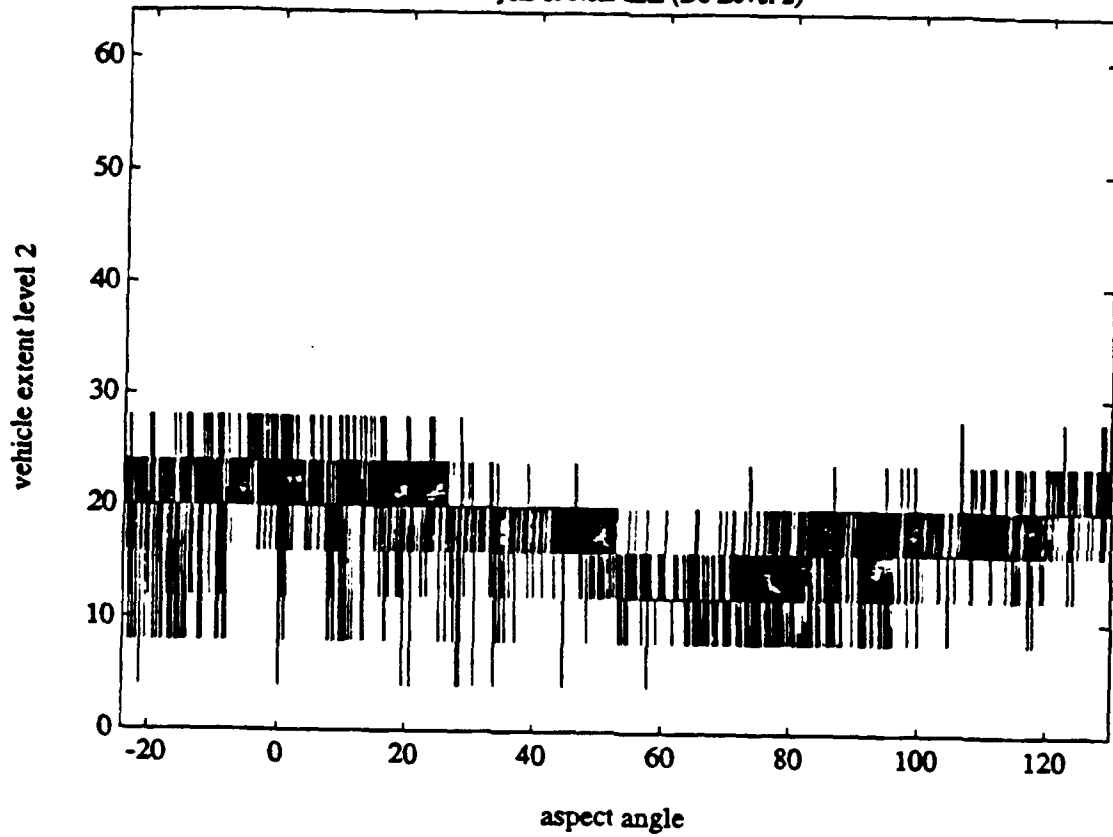


Figure 4.22: **Target Extent versus Aspect Angle**
Target: M35, Threshold: 25, Polarization: LR
Analysis of Real data (D6 Level 3)

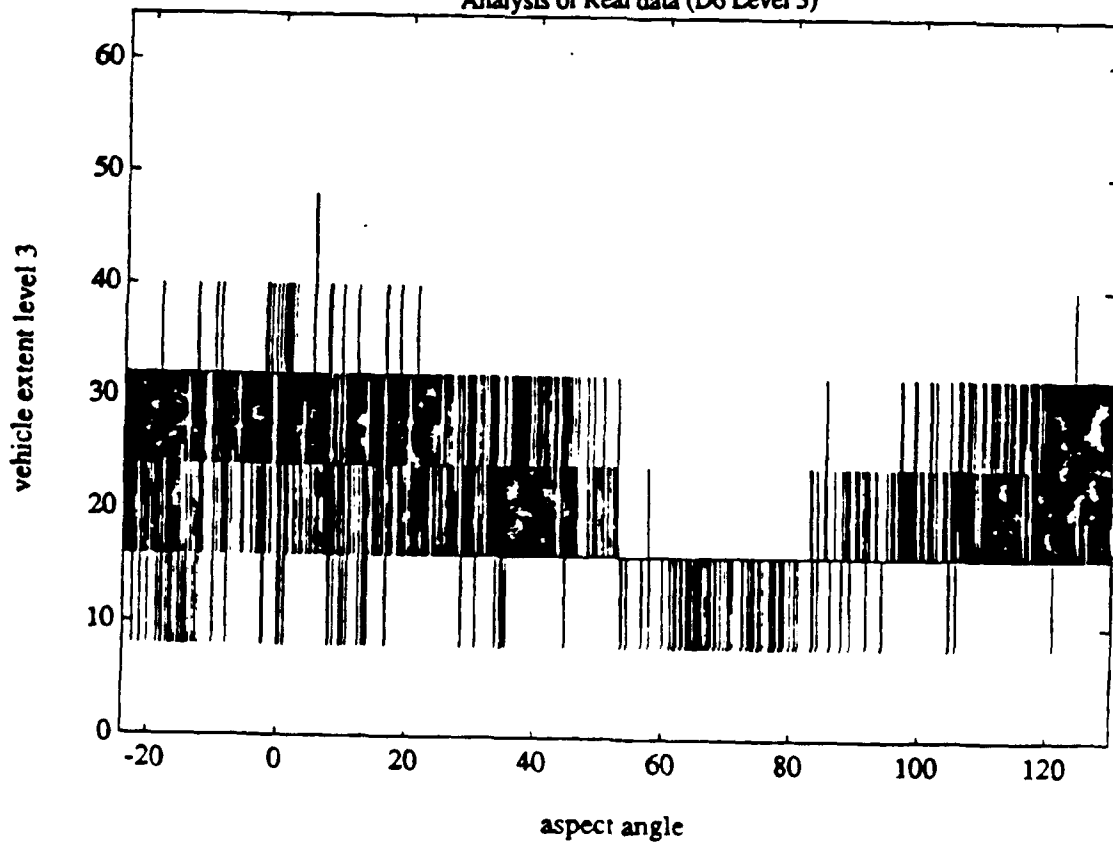


Figure 4.23: **Average Target Extent versus Aspect Angle**
Block Size: 50, Target: M35, Threshold: 25, Polarization: LR
Analysis of Real data (Martin Method)

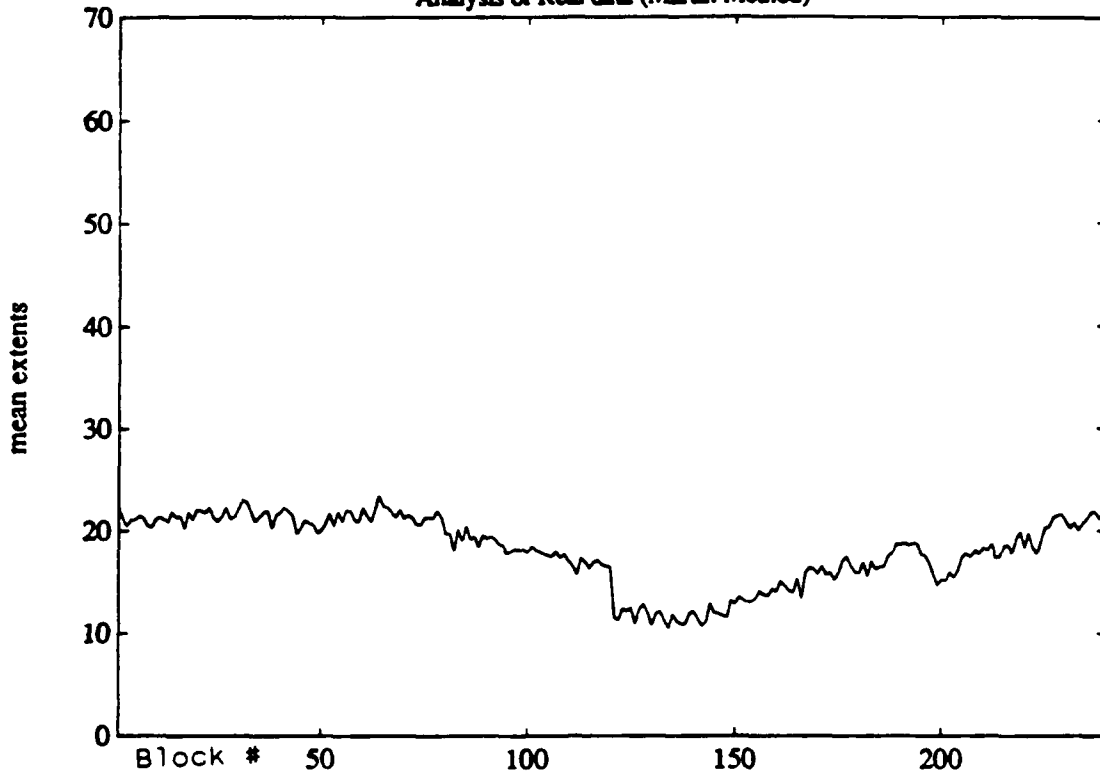


Figure 4.24: **Standard Deviation Target Extent versus Aspect Angle**
Block Size: 50, Target: M35, Threshold: 25, Polarization: LR
Analysis of Real data (Martin Method)

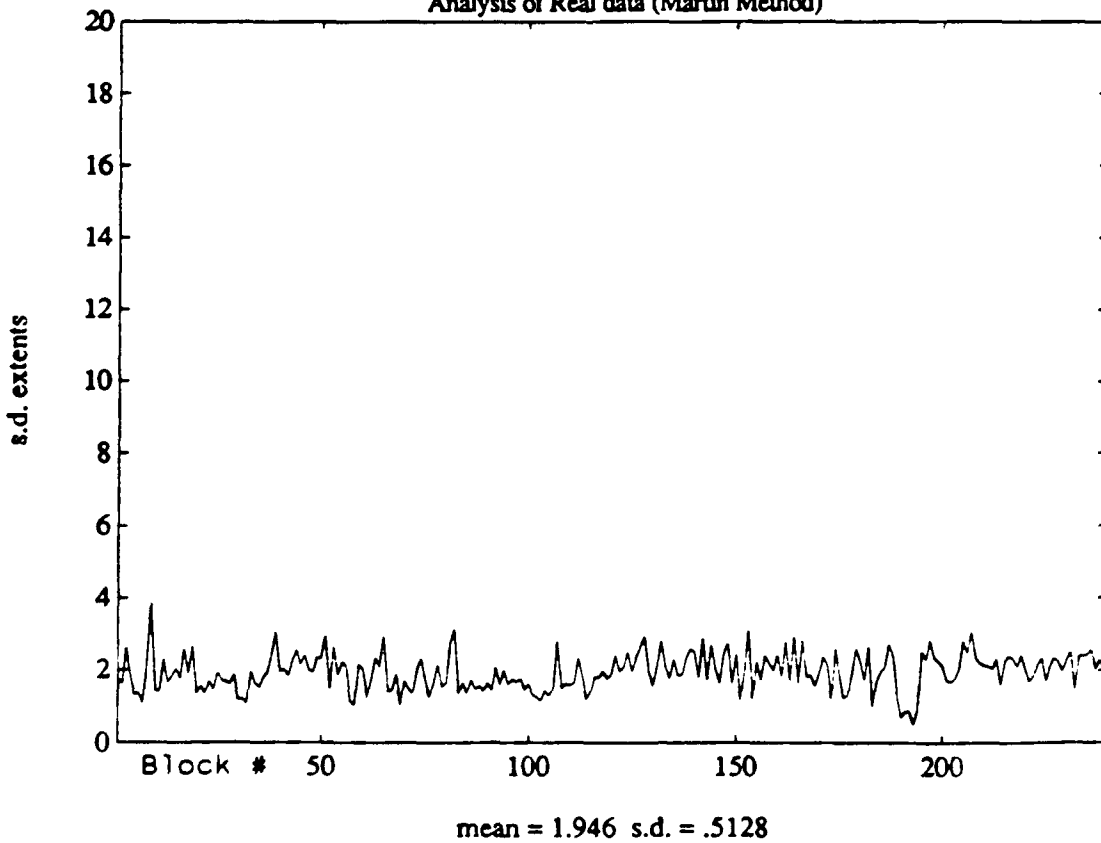


Figure 4.25: **Average Target Extent versus Aspect Angle**
 Block Size: 50, Target: M35, Threshold: 25, Polarization: LR
 Analysis of Real data (D6 Level 1)

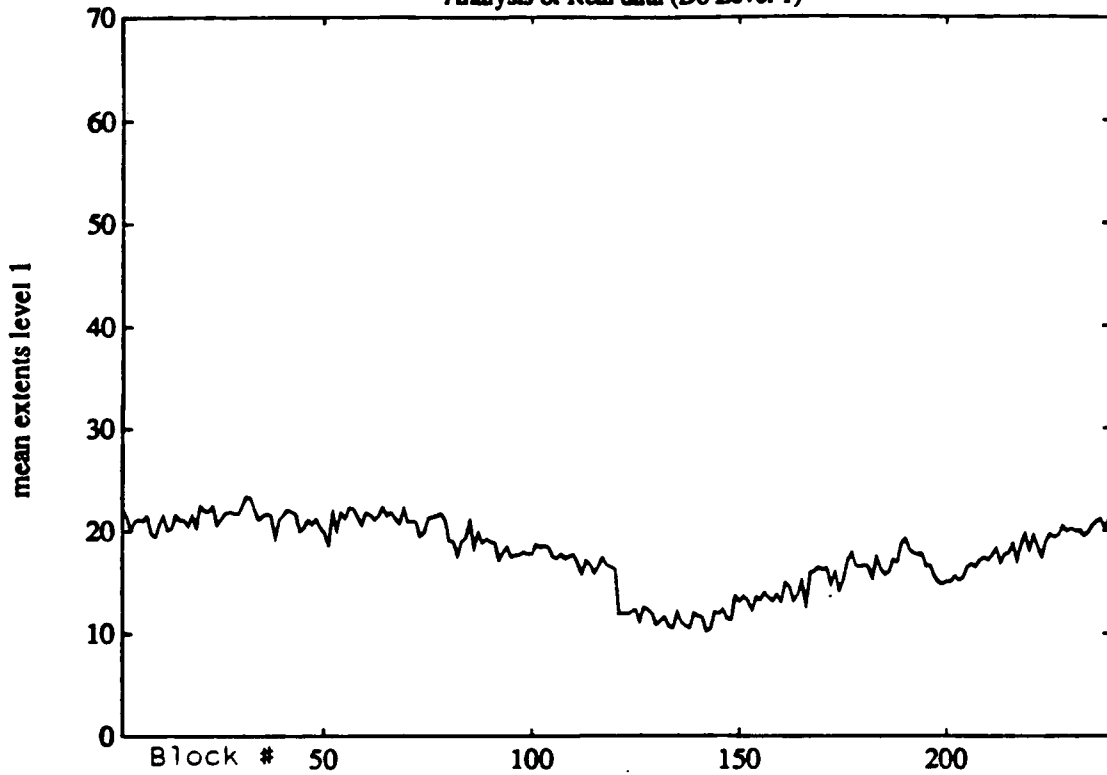


Figure 4.26: **Standard Deviation Target Extent versus Aspect Angle**
 Block Size: 50, Target: M35, Threshold: 25, Polarization: LR
 Analysis of Real data (D6 Level 1)

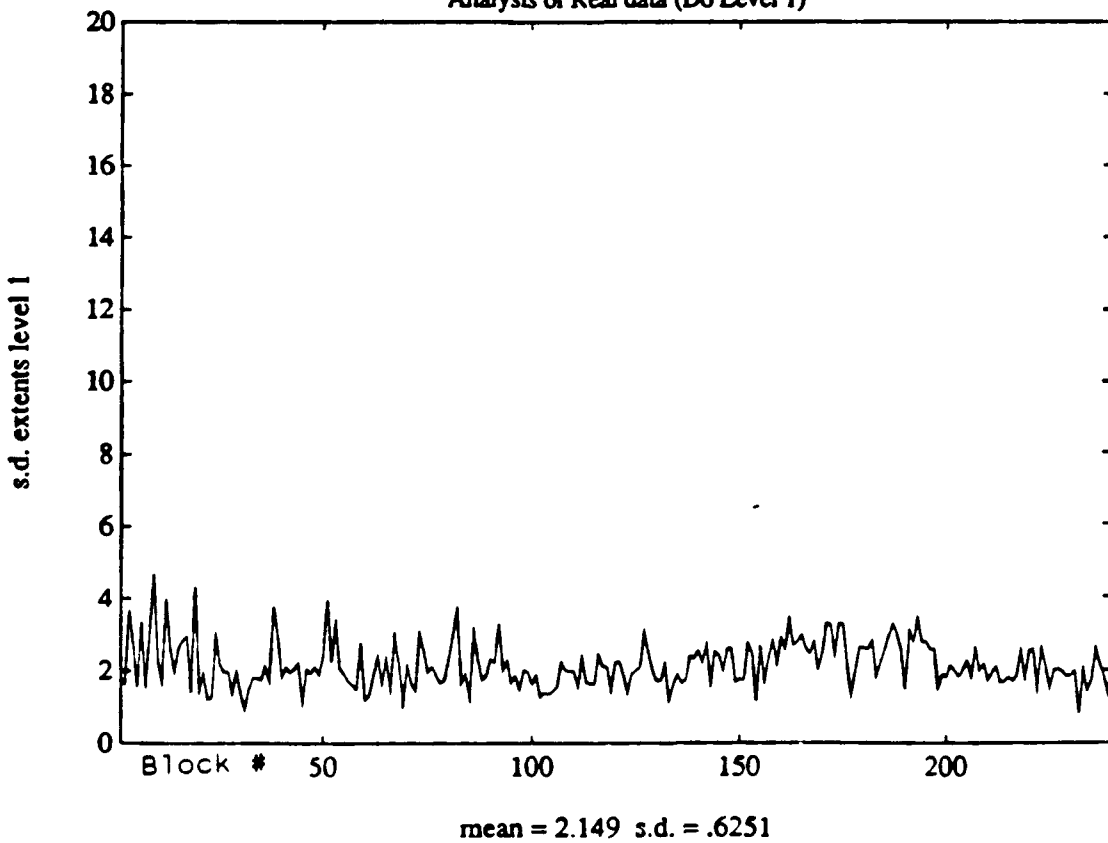


Figure 4.27: **Average Target Extent versus Aspect Angle**
Block Size: 50, Target: M35, Threshold: 25, Polarization: LR
Analysis of Real data (D6 Level 2)

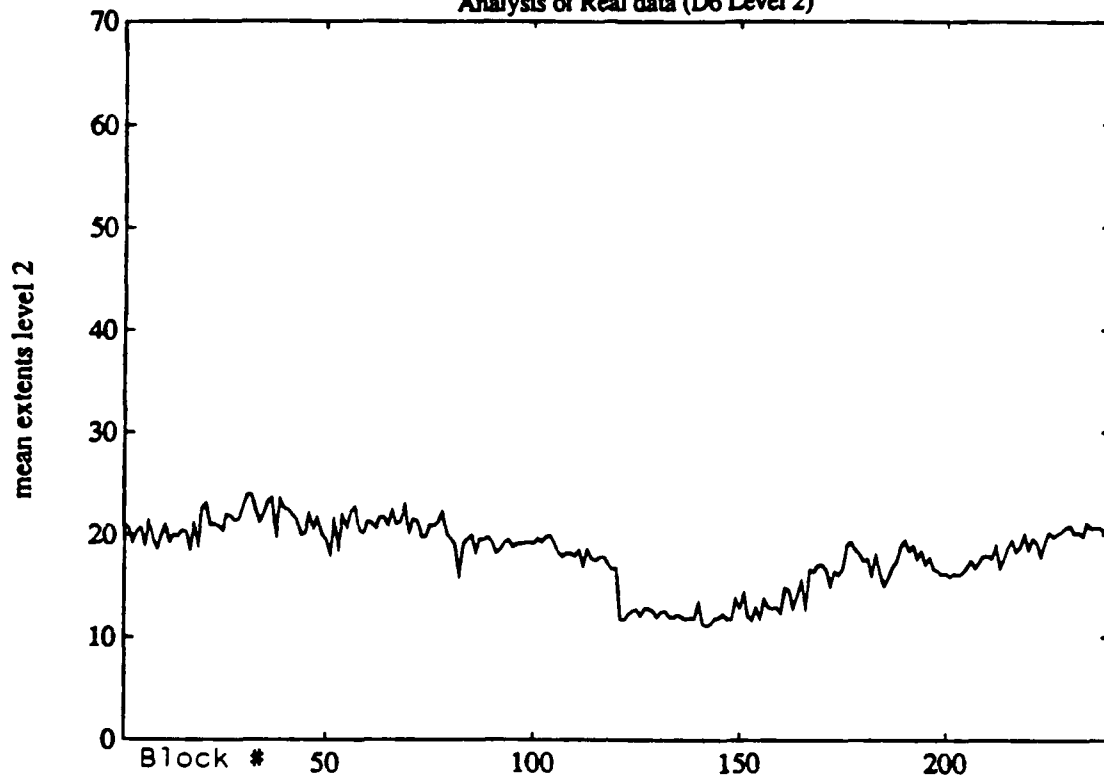
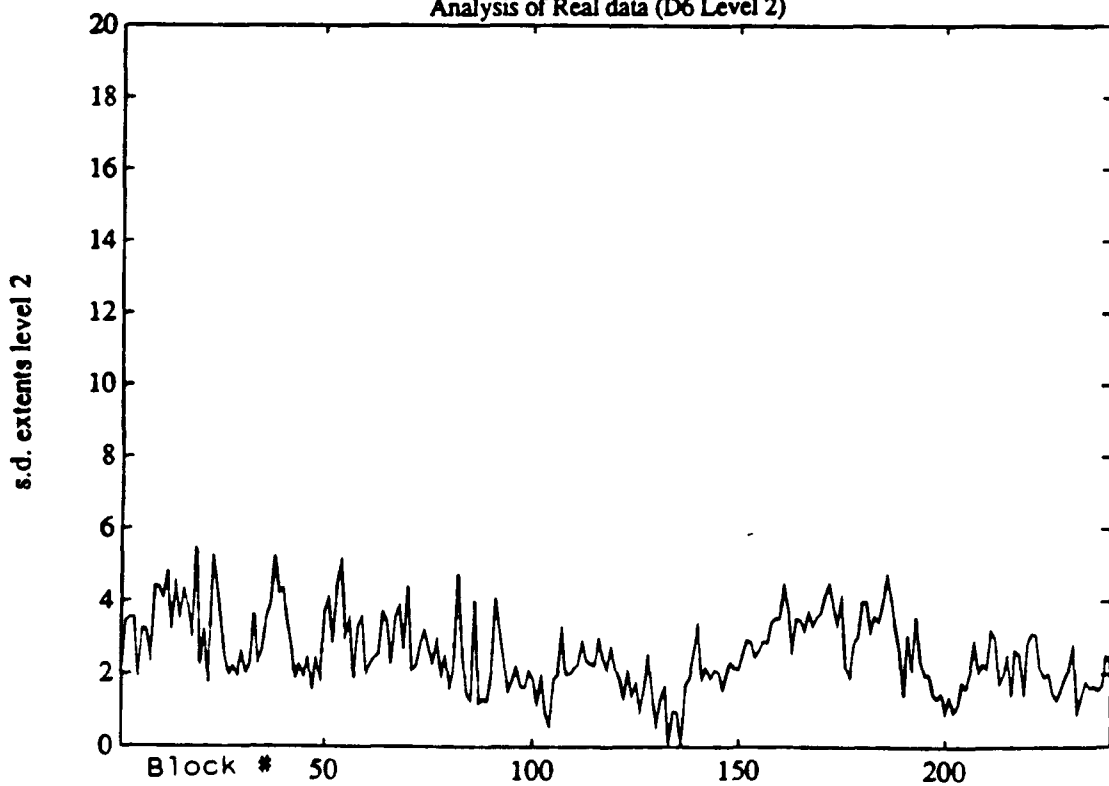


Figure 4.28: **Standard Deviation Target Extent versus Aspect Angle**
Block Size: 50, Target: M35, Threshold: 25, Polarization: LR
Analysis of Real data (D6 Level 2)



mean = 2.578 s.d. = 1.023

Figure 4.29: **Average Target Extent versus Aspect Angle**
Block Size: 50, Target: M35, Threshold: 25, Polarization: LR
Analysis of Real data (D6 Level 3)

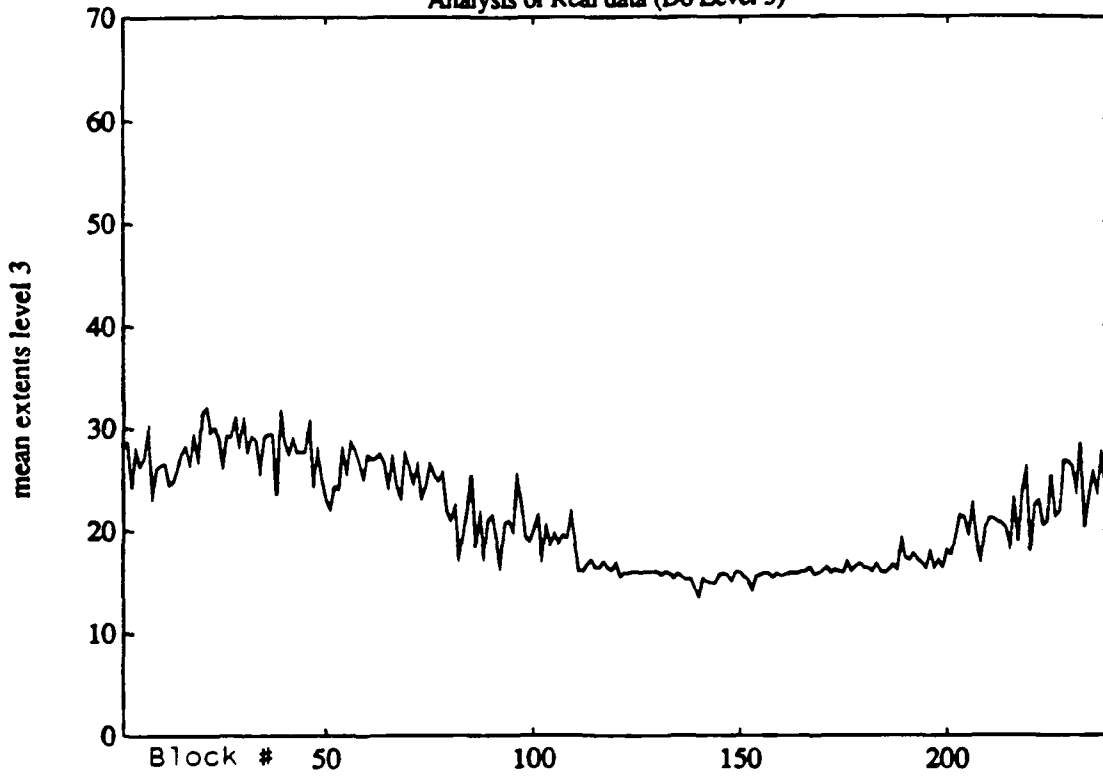


Figure 4.30: **Standard Deviation Target Extent versus Aspect Angle**
Block Size: 50, Target: M35, Threshold: 25, Polarization: LR
Analysis of Real data (D6 Level 3)

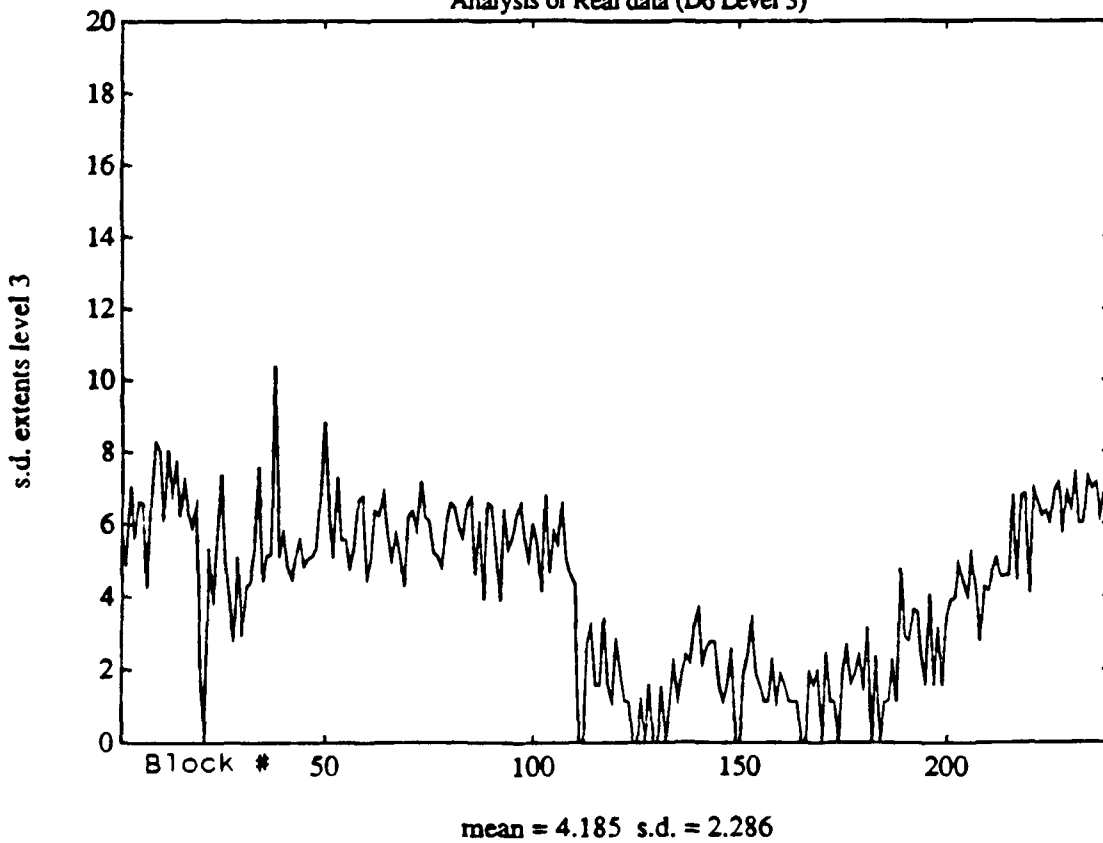


Figure 4.31: **Target Extent versus Aspect Angle**
Target: M60, Threshold: 25, Polarization: LL
Analysis of Real data (Martin Method)

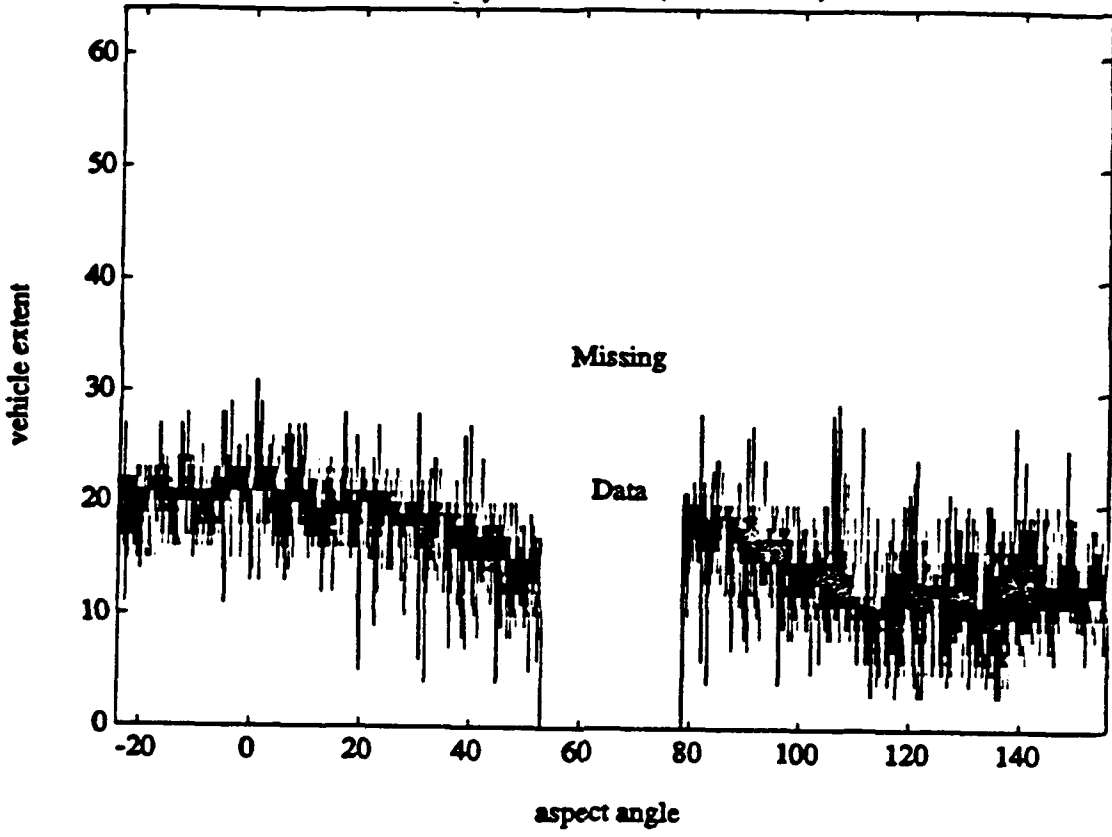


Figure 4.32: **Target Extent versus Aspect Angle**
Target: M60, Threshold: 25, Polarization: LL
Analysis of Real data (D6 Level 1)

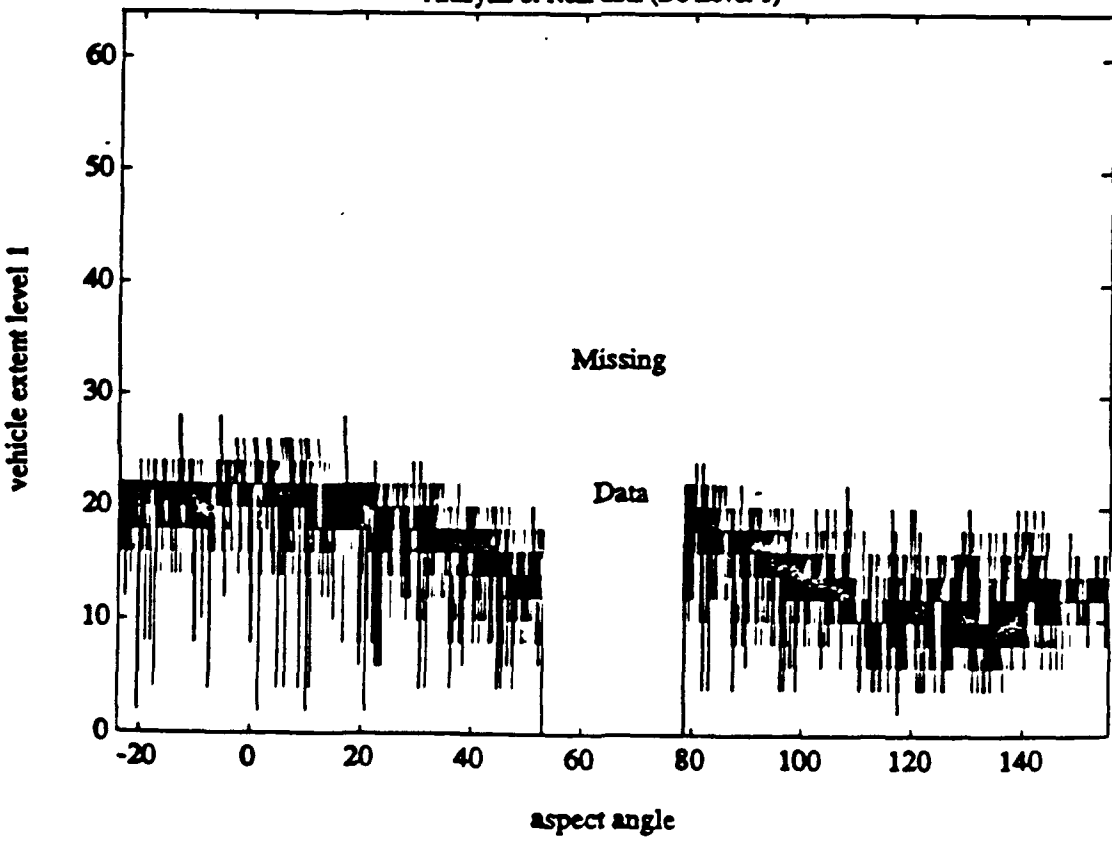


Figure 4.33: Target Extent versus Aspect Angle
Target: M60, Threshold: 25, Polarization: LL
Analysis of Real data (D6 Level 2)

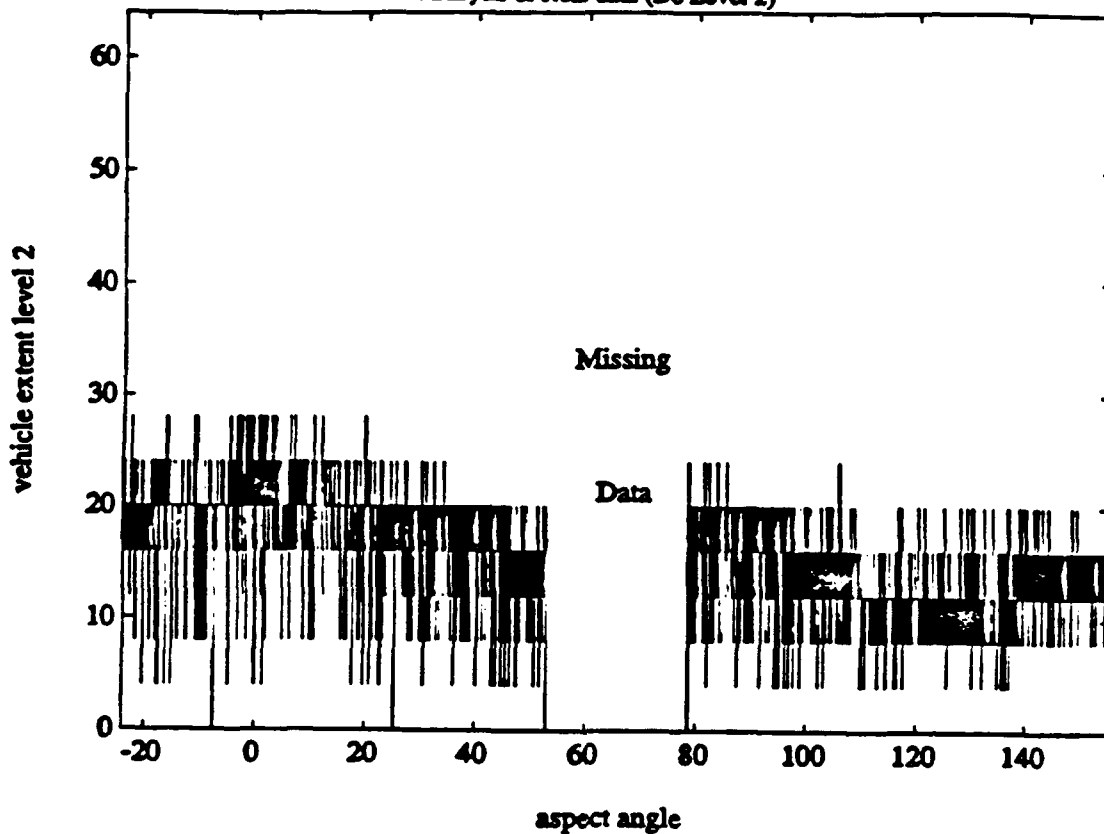


Figure 4.34: Target Extent versus Aspect Angle
Target: M60, Threshold: 25, Polarization: LL
Analysis of Real data (D6 Level 3)

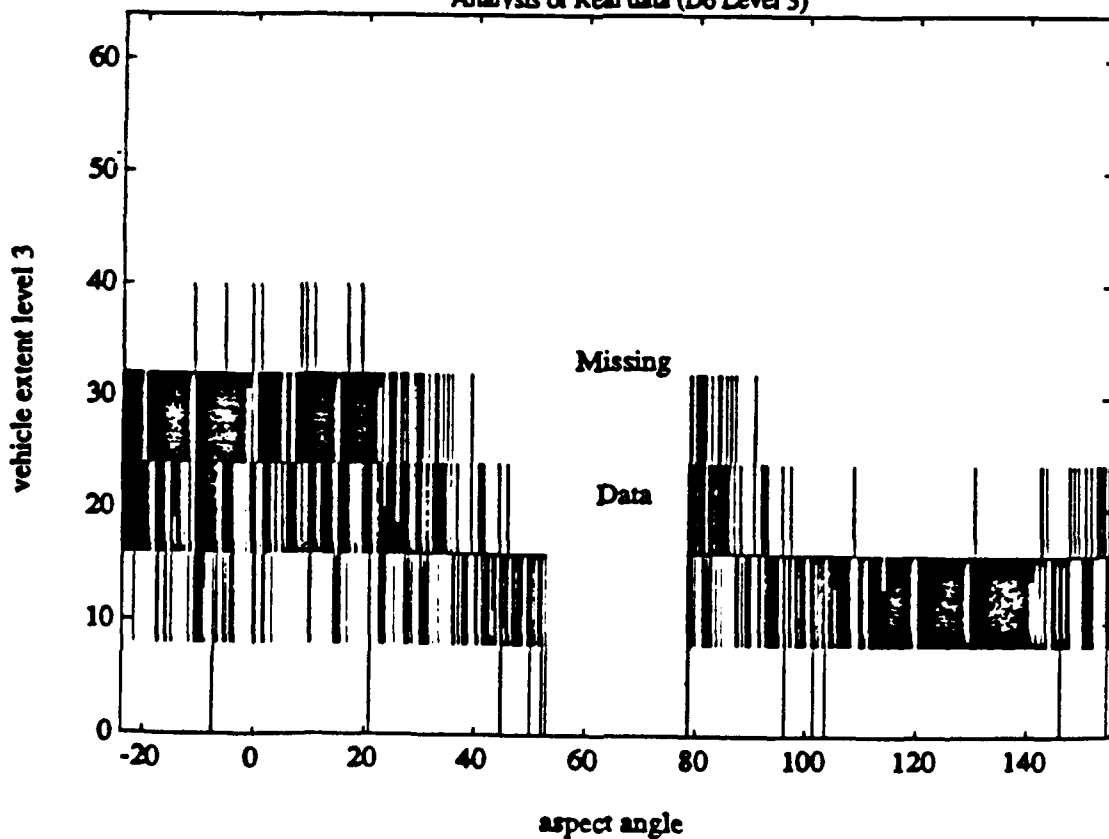


Figure 4.35: **Average Target Extent versus Aspect Angle**
Block Size: 50, Target: M60, Threshold: 25, Polarization: LL
Analysis of Real data (Martin Method)

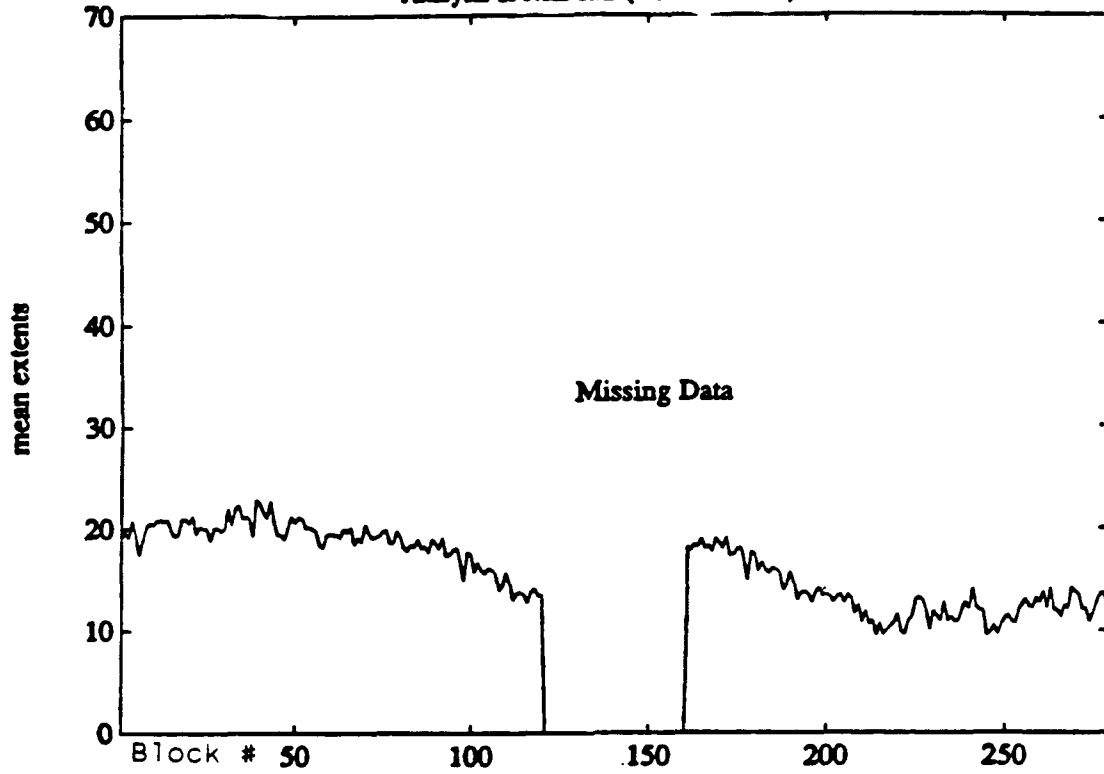


Figure 4.36: **Standard Deviation Target Extent versus Aspect Angle**
Block Size: 50, Target: M60, Threshold: 25, Polarization: LL
Analysis of Real data (Martin Method)

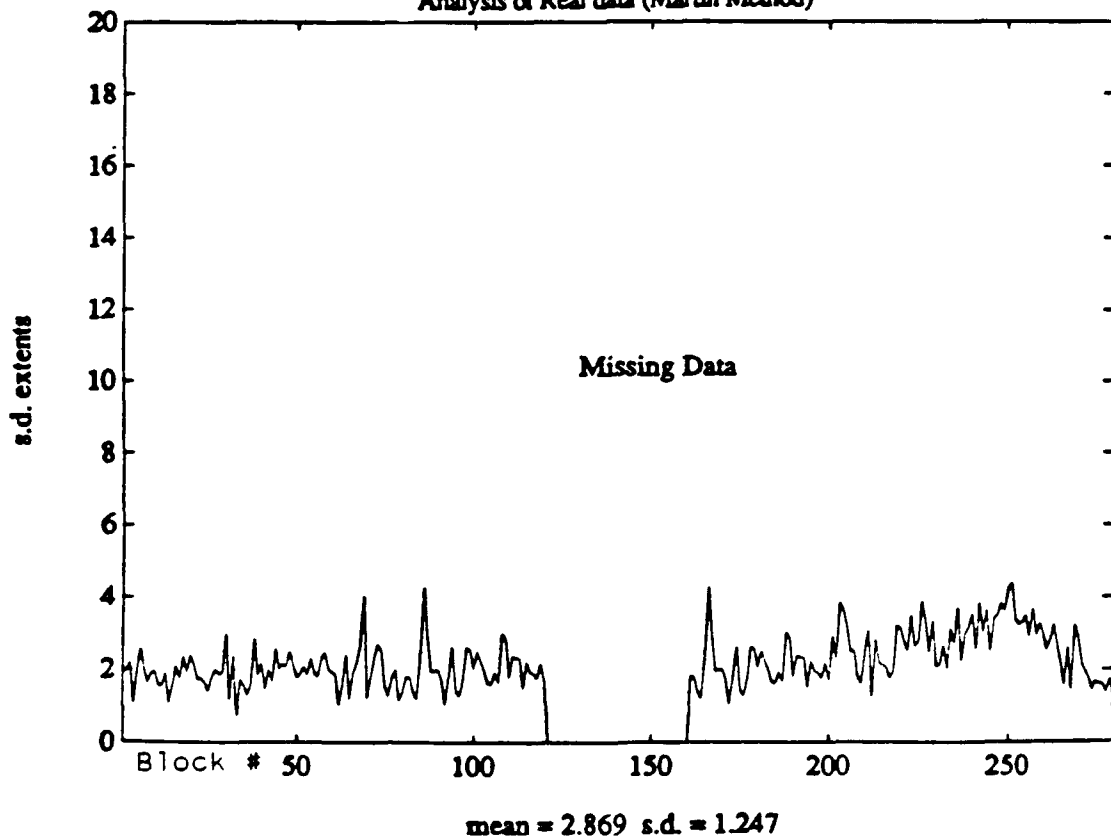


Figure 4.37: **Average Target Extent versus Aspect Angle**
 Block Size: 50, Target: M60, Threshold: 25, Polarization: LL
 Analysis of Real data (D6 Level 1)

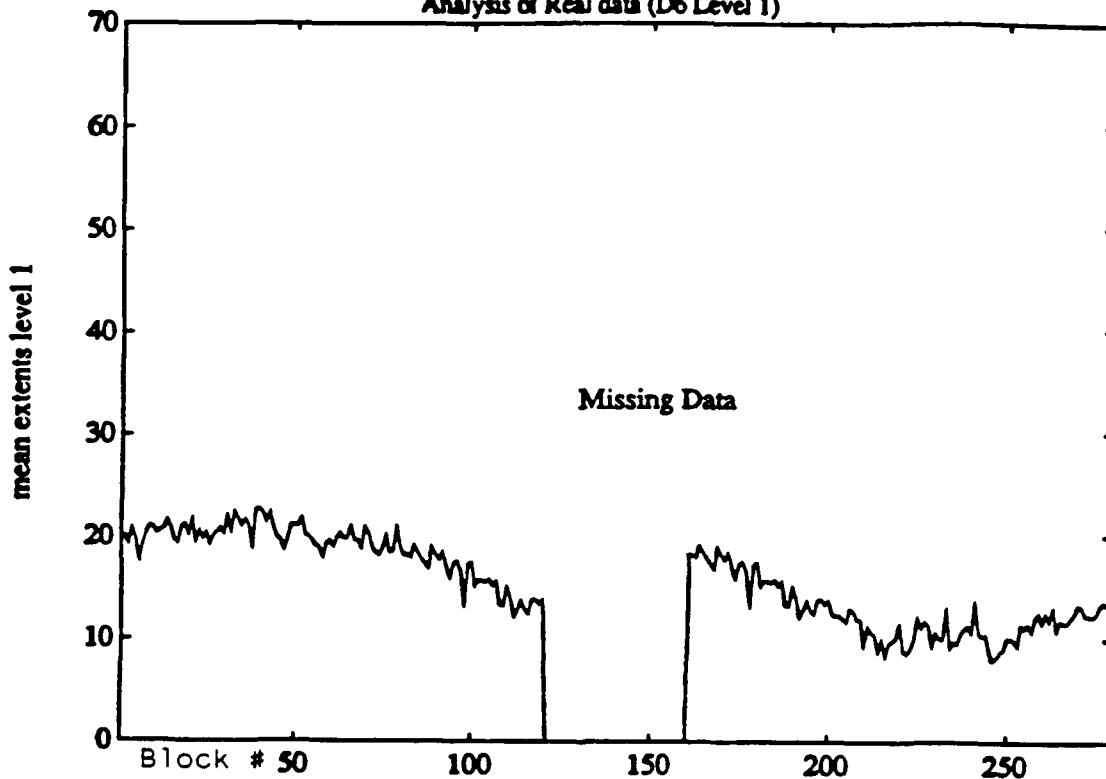


Figure 4.38: **Standard Deviation Target Extent versus Aspect Angle**
 Block Size: 50, Target: M60, Threshold: 25, Polarization: LL
 Analysis of Real data (D6 Level 1)

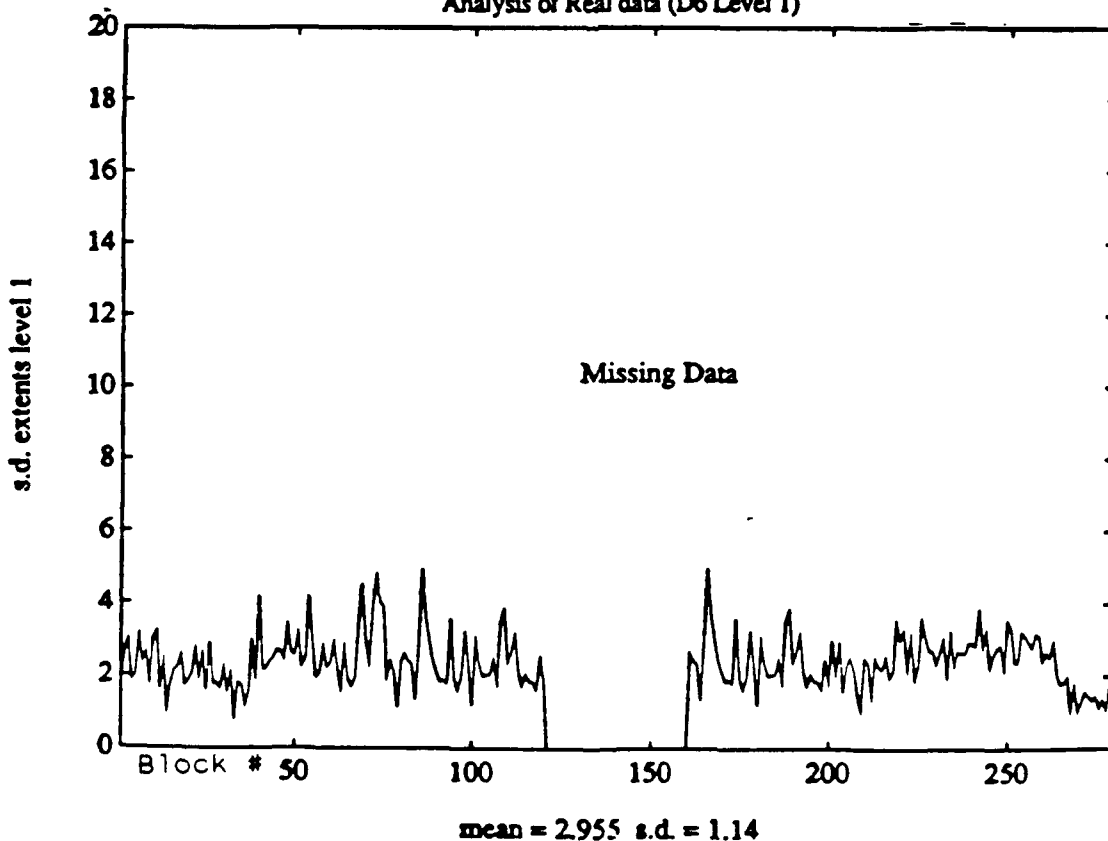


Figure 4.39: **Average Target Extent versus Aspect Angle**
 Block Size: 50, Target: M60, Threshold: 25, Polarization: LL
 Analysis of Real data (D6 Level 2)

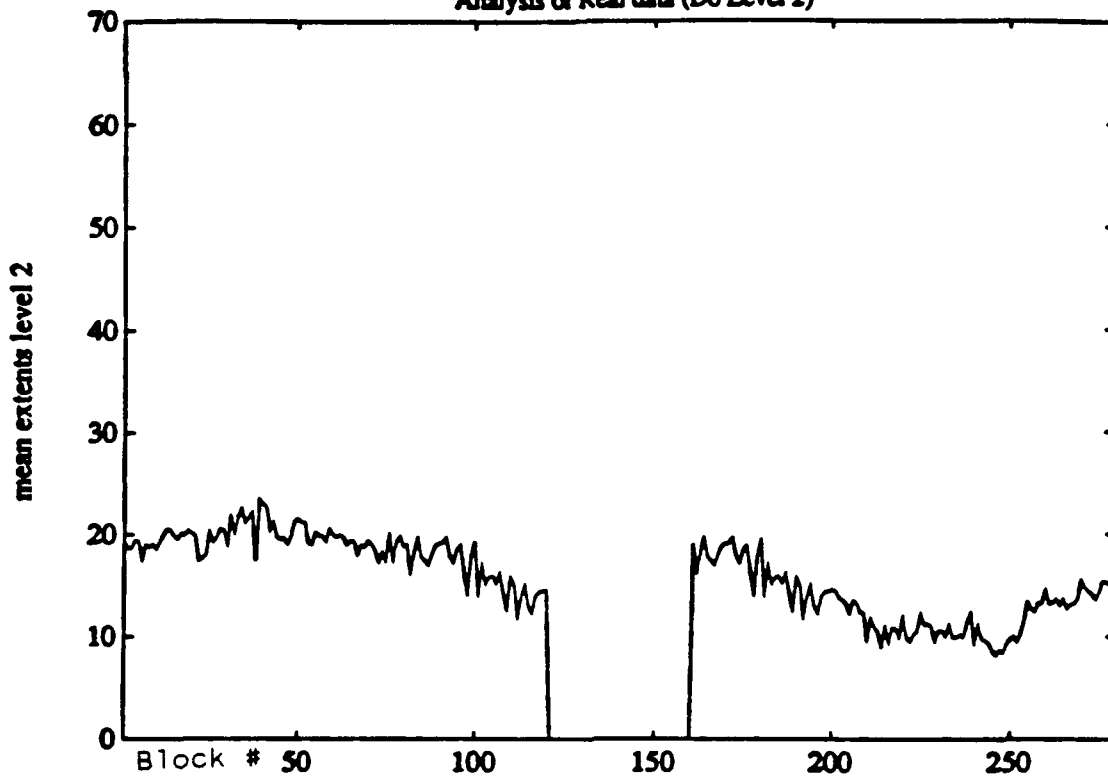


Figure 4.40: **Standard Deviation Target Extent versus Aspect Angle**
 Block Size: 50, Target: M60, Threshold: 25, Polarization: LL
 Analysis of Real data (D6 Level 2)

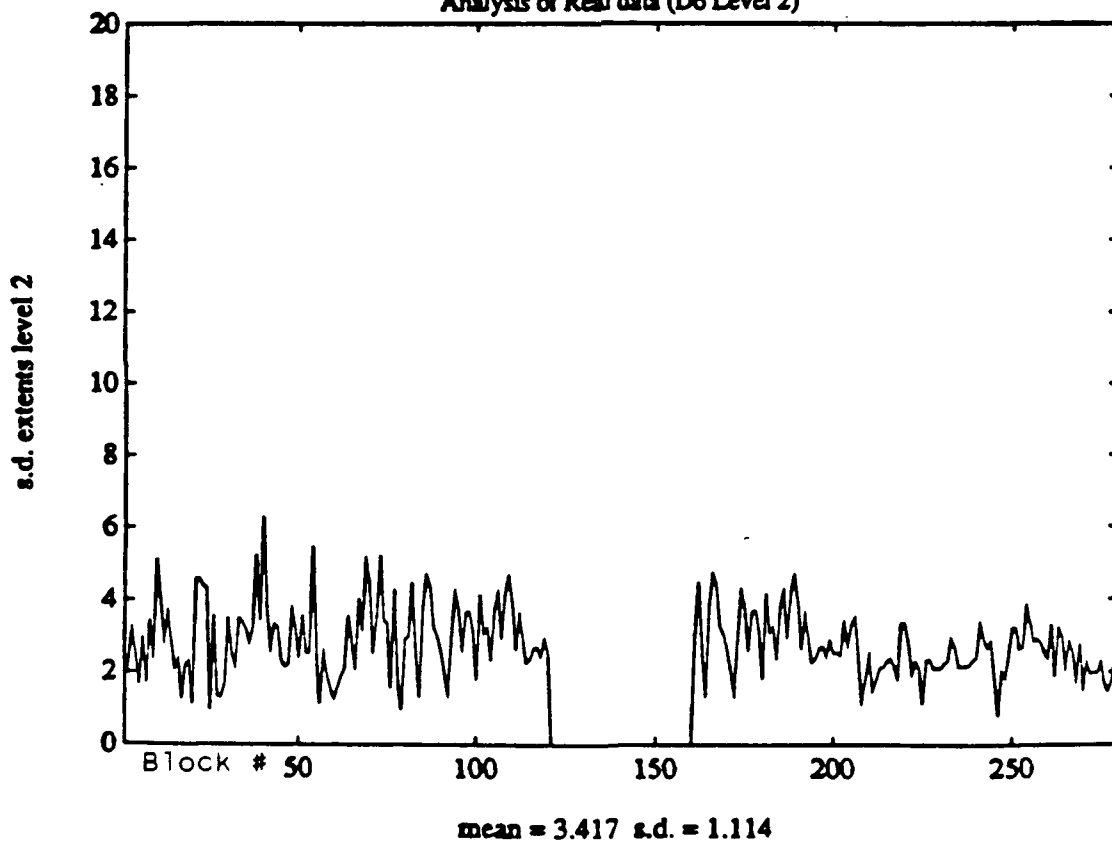


Figure 4.41: **Average Target Extent versus Aspect Angle**
 Block Size: 50, Target: M60, Threshold: 25, Polarization: LL
 Analysis of Real data (D6 Level 3)

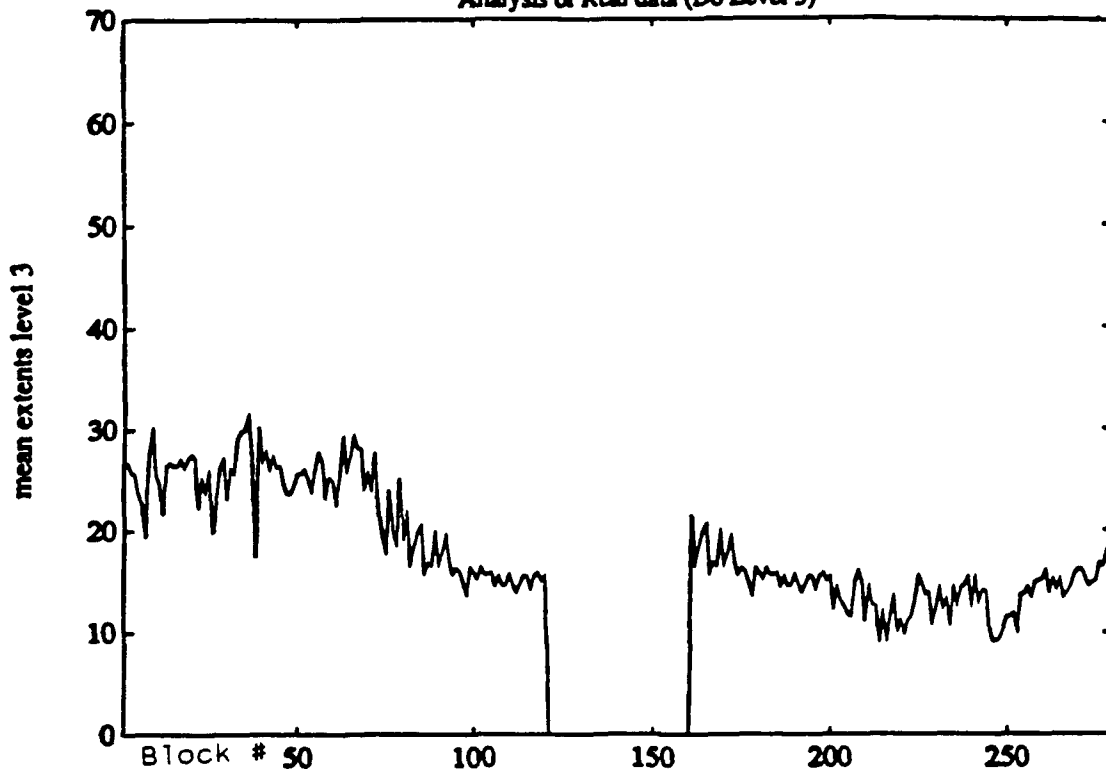


Figure 4.42: **Standard Deviation Target Extent versus Aspect Angle**
 Block Size: 50, Target: M60, Threshold: 25, Polarization: LL
 Analysis of Real data (D6 Level 3)

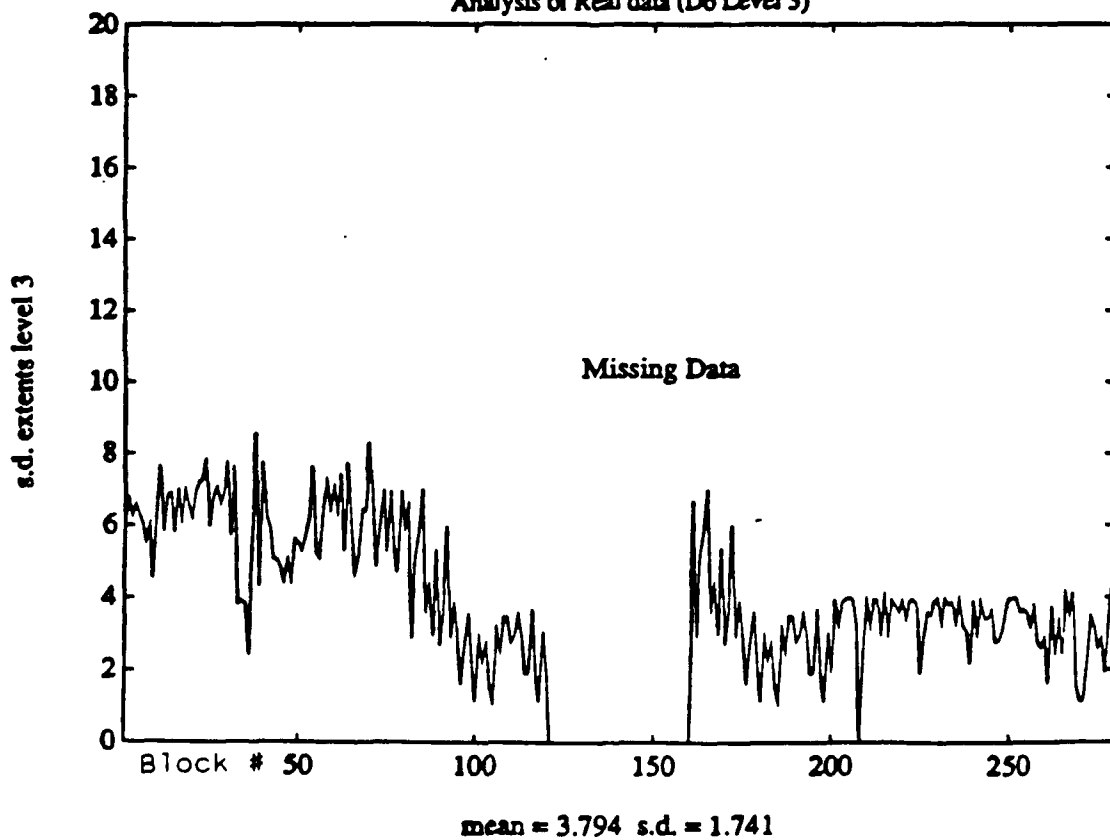


Figure 4.43: **Target Extent versus Aspect Angle**
Target: M60, Threshold: 25, Polarization: LR
Analysis of Real data (Martin Method)

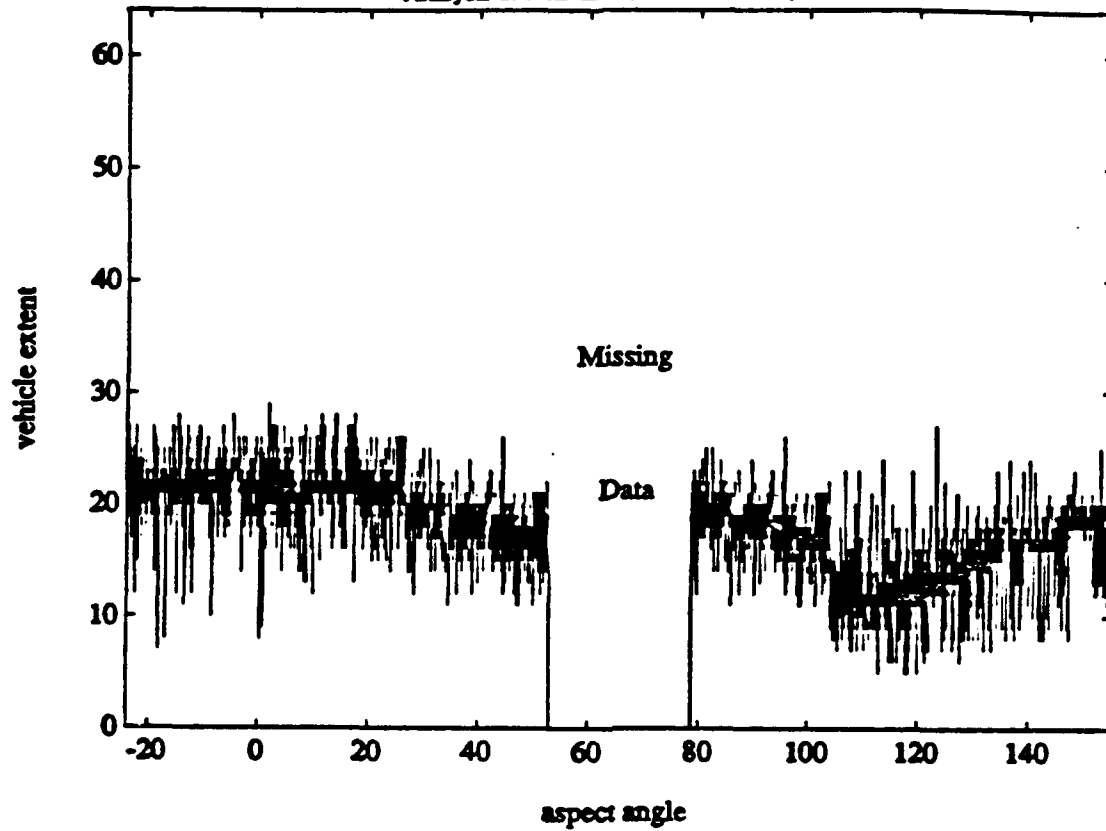


Figure 4.44: **Target Extent versus Aspect Angle**
Target: M60, Threshold: 25, Polarization: LR
Analysis of Real data (D6 Level 1)

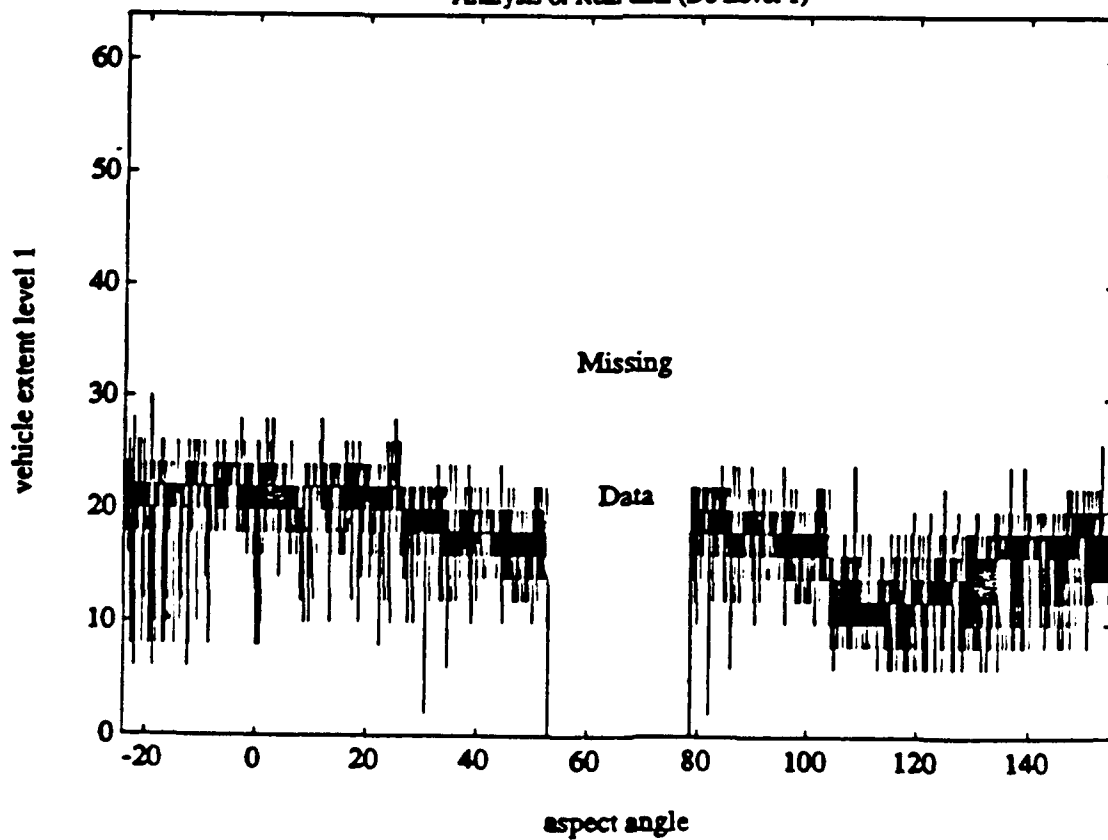


Figure 4.45: **Target Extent versus Aspect Angle**
Target: M60, Threshold: 25, Polarization: LR
Analysis of Real data (D6 Level 2)

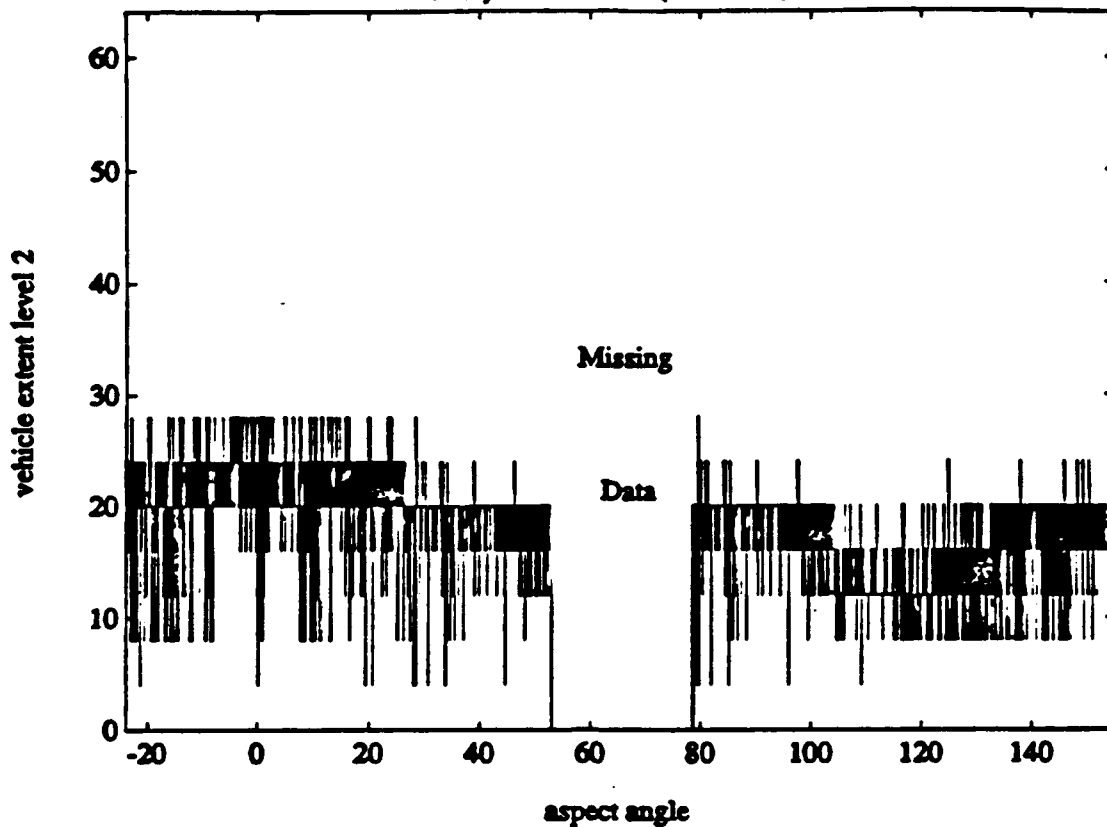


Figure 4.46: **Target Extent versus Aspect Angle**
Target: M60, Threshold: 25, Polarization: LR
Analysis of Real data (D6 Level 3)

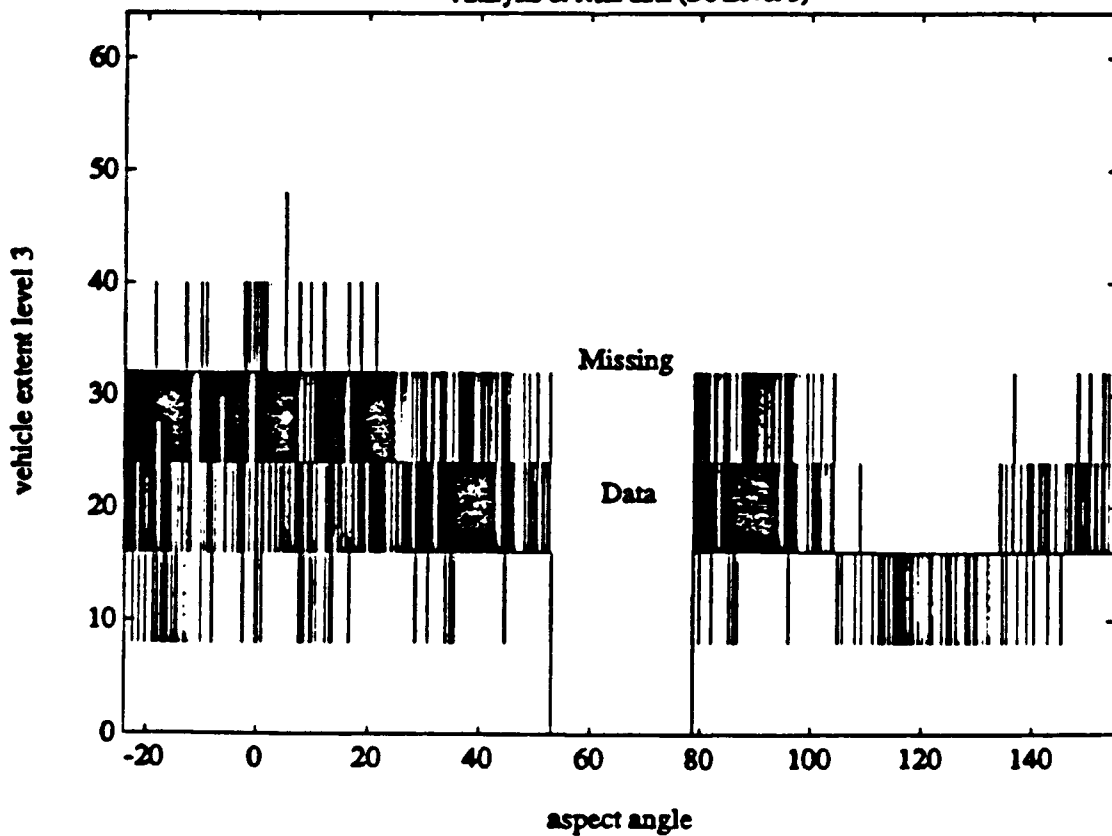


Figure 4.47: **Average Target Extent versus Aspect Angle**
 Block Size: 50, Target: M60, Threshold: 25, Polarization: LR
 Analysis of Real data (Martin Method)

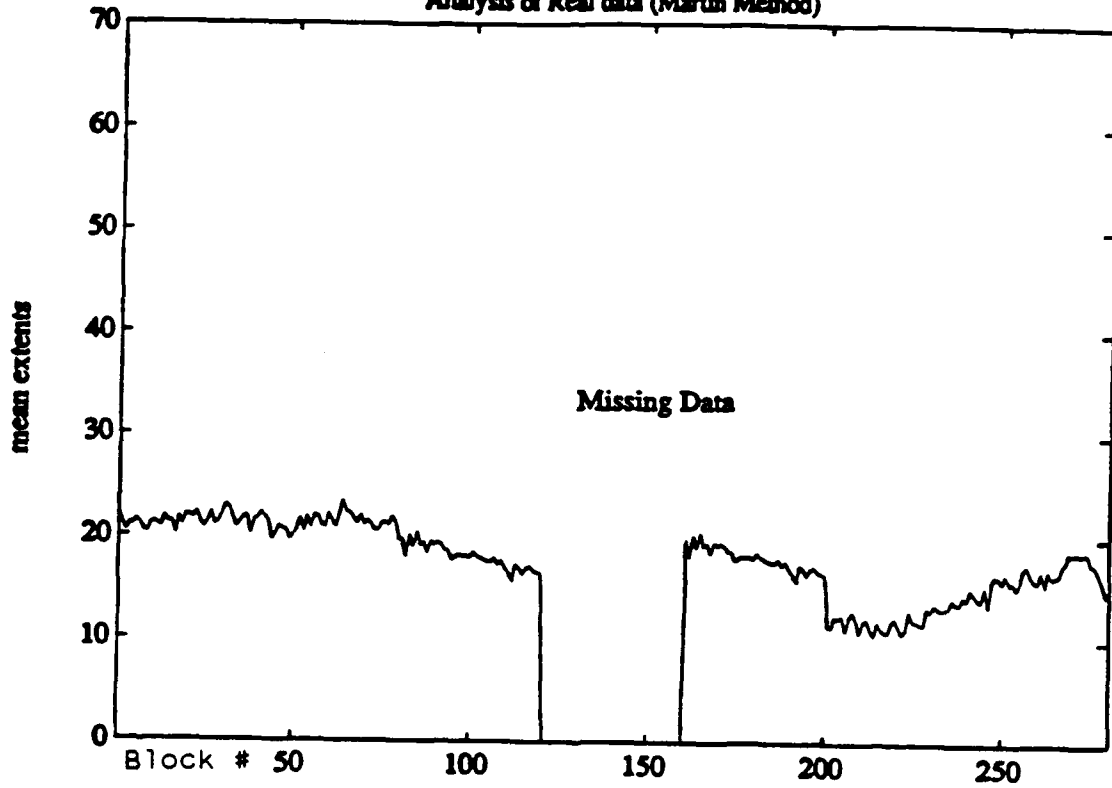


Figure 4.48: **Standard Deviation Target Extent versus Aspect Angle**
 Block Size: 50, Target: M60, Threshold: 25, Polarization: LR
 Analysis of Real data (Martin Method)

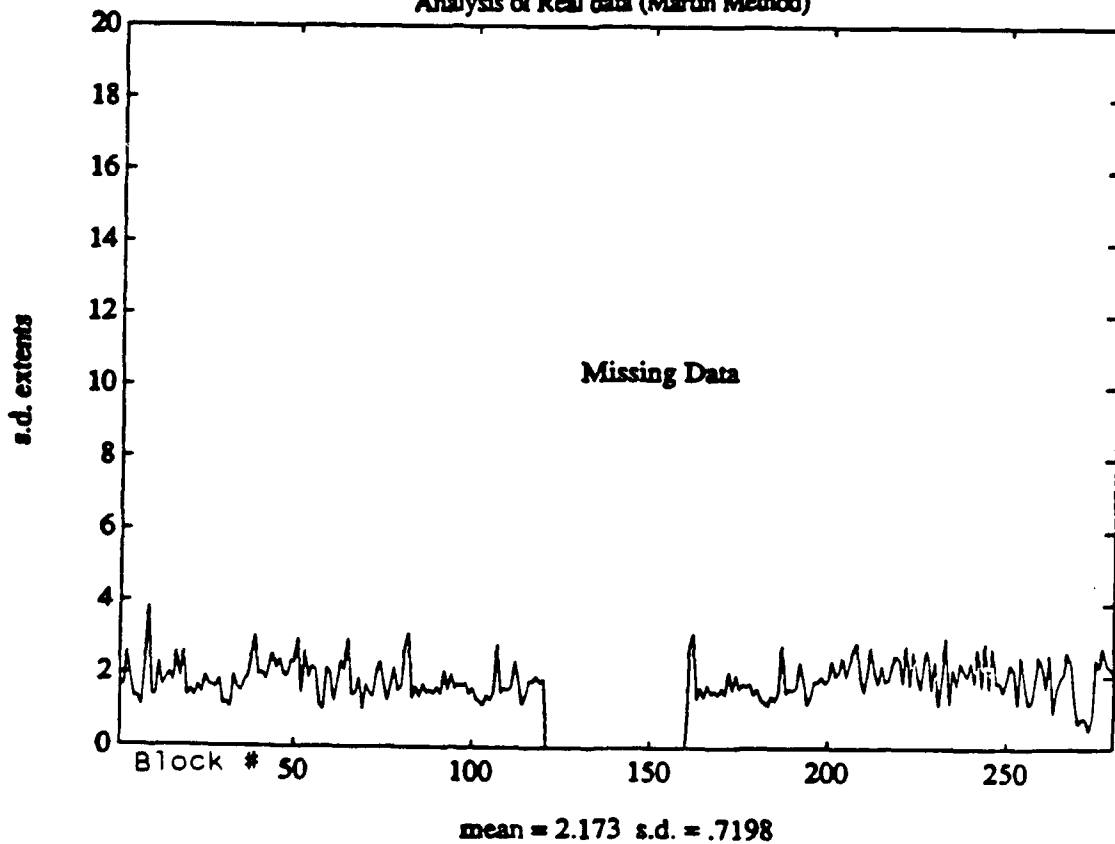


Figure 4.49: **Average Target Extent versus Aspect Angle**
 Block Size: 50, Target: M60, Threshold: 25, Polarization: LR
 Analysis of Real data (D6 Level 1)

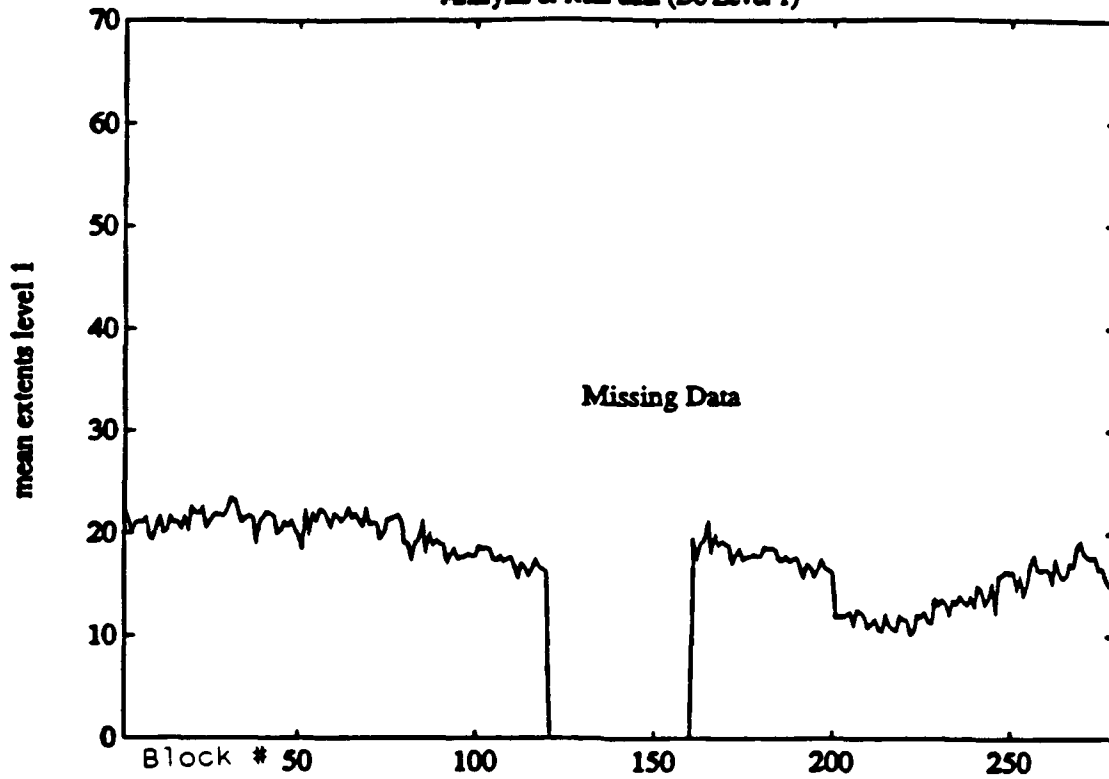


Figure 4.50: **Standard Deviation Target Extent versus Aspect Angle**
 Block Size: 50, Target: M60, Threshold: 25, Polarization: LR
 Analysis of Real data (D6 Level 1)

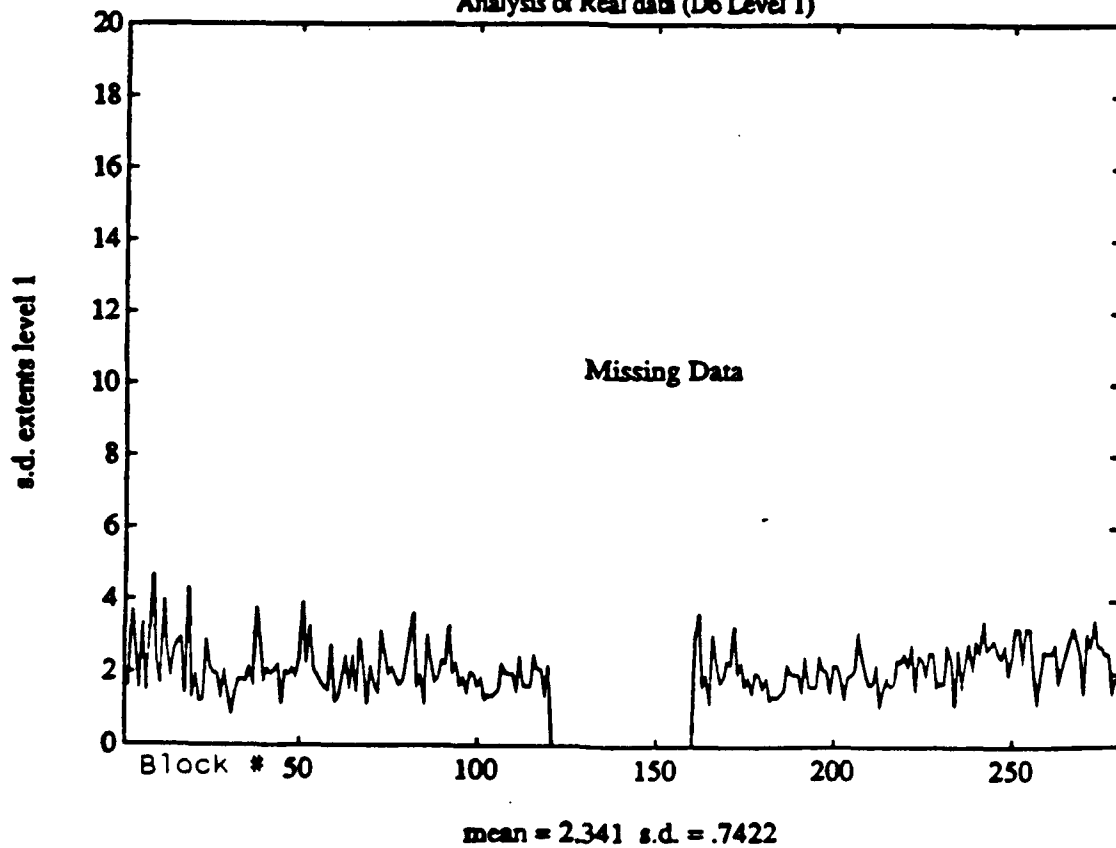


Figure 4.51: **Average Target Extent versus Aspect Angle**
 Block Size: 50, Target: M60, Threshold: 25, Polarization: LR
 Analysis of Real data (D6 Level 2)

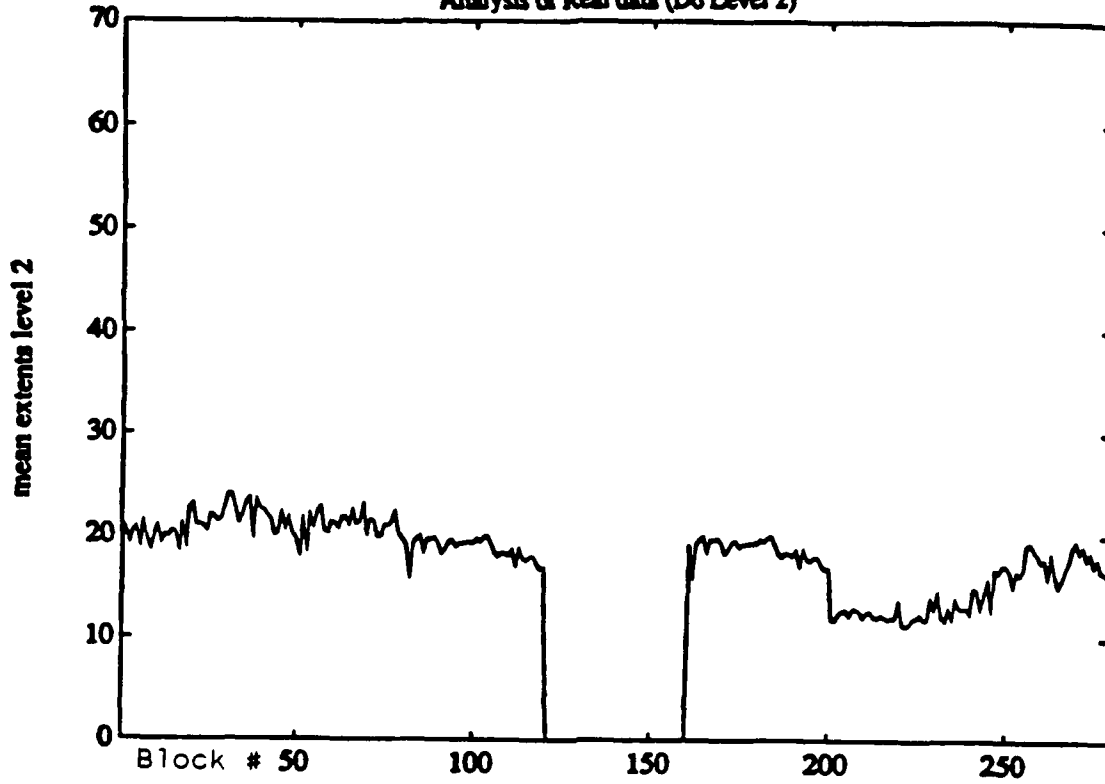


Figure 4.52: **Standard Deviation Target Extent versus Aspect Angle**
 Block Size: 50, Target: M60, Threshold: 25, Polarization: LR
 Analysis of Real data (D6 Level 2)

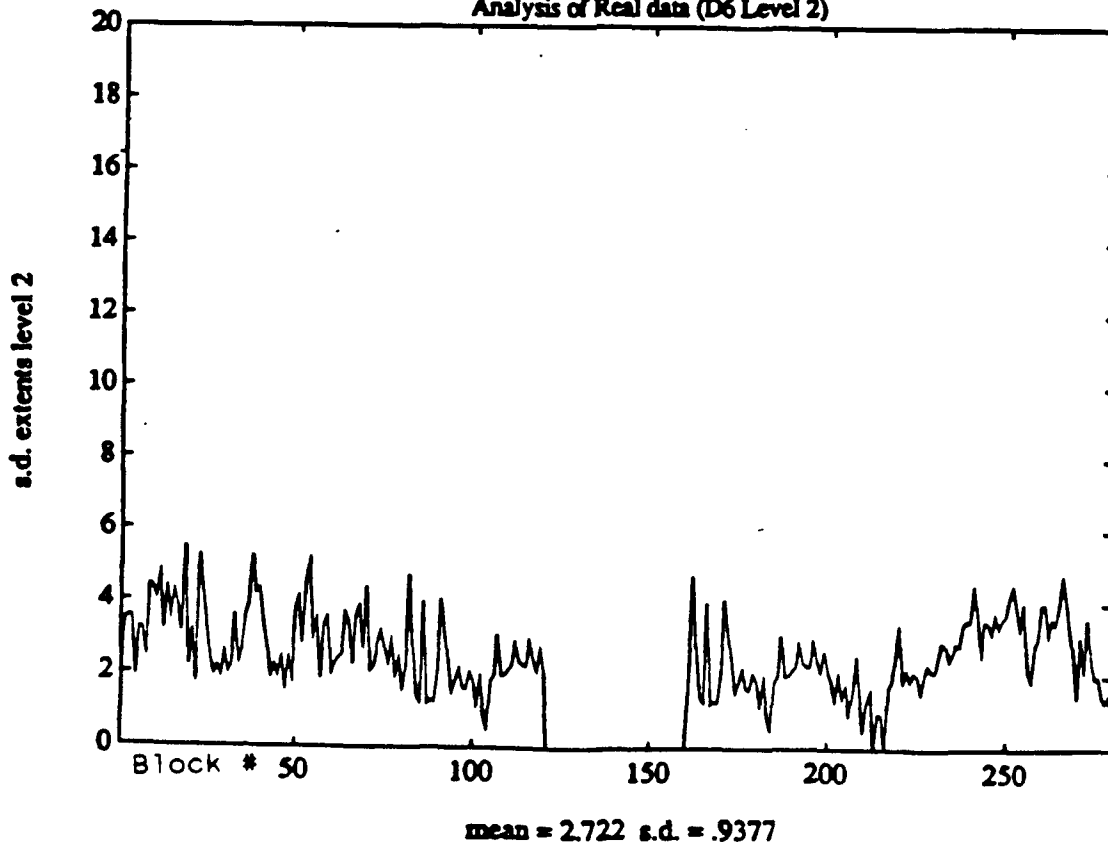


Figure 4.53: **Average Target Extent versus Aspect Angle**
 Block Size: 50, Target: M60, Threshold: 25, Polarization: LR
 Analysis of Real data (D6 Level 3)

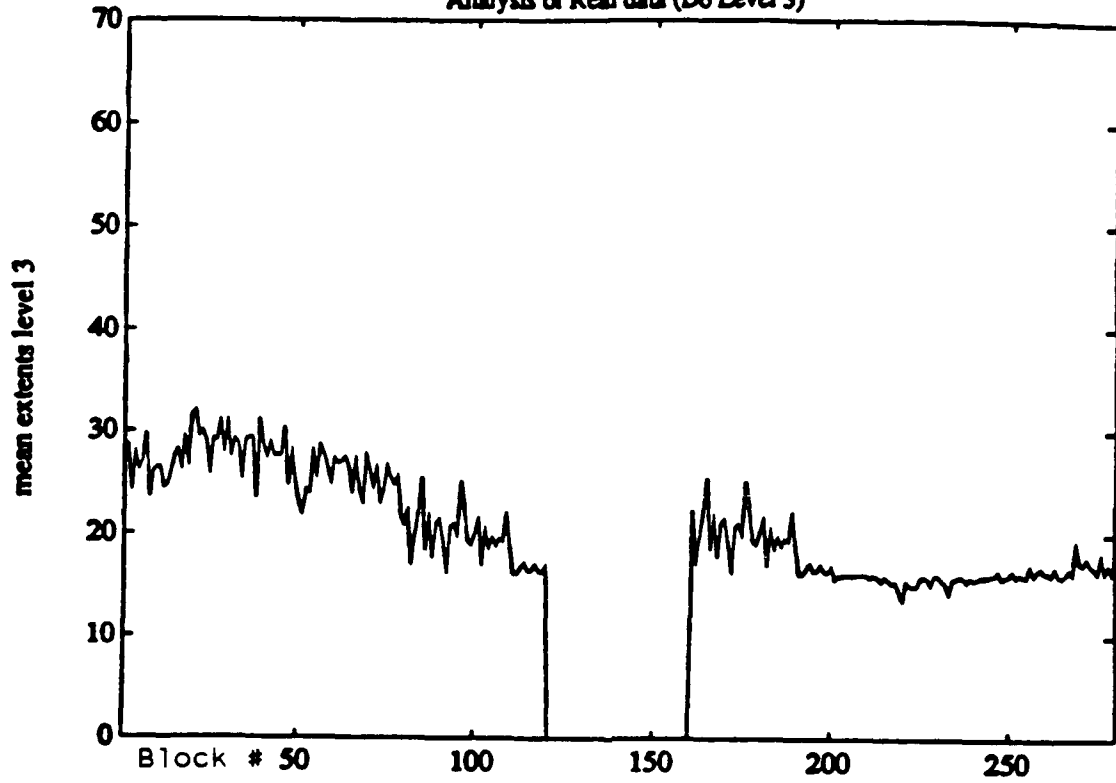
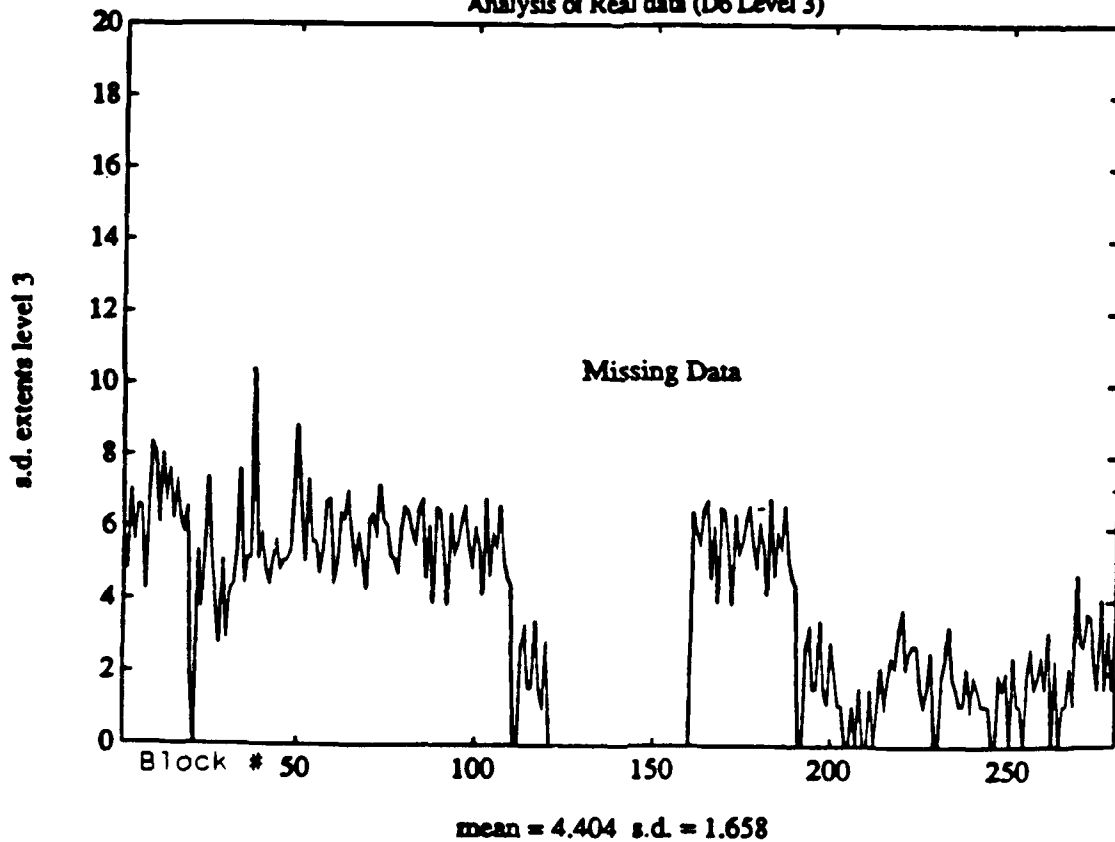


Figure 4.54: **Standard Deviation Target Extent versus Aspect Angle**
 Block Size: 50, Target: M60, Threshold: 25, Polarization: LR
 Analysis of Real data (D6 Level 3)



Appendix A

List of Symbols

D := Ring of dyadic rational numbers
:= $\{x : x = m/2^n, m, n \in \mathbf{Z}, n \geq 0\}$

R := Field of real numbers.

Z := Ring of rational integers.

μ := Multiplier for wavelet system. $\mu \in \mathbf{Z}$ and $\mu \geq 2$.

[a] := Wavelet Coefficient Matrix ("WCM").
:= $\begin{pmatrix} a_0^0 & a_1^0 & \cdots & a_{N-1}^0 \\ a_0^{\mu-1} & a_1^0 & \cdots & a_{N-1}^{\mu-1} \end{pmatrix}$

where N is an integer multiple of the multiplier μ .

If $\mu = 2$ then we write:

[a] := Wavelet Coefficient Matrix ("WCM").
:= $\begin{pmatrix} a_0 & a_1 & \cdots & a_{N-1} \\ b_0 & b_1 & \cdots & b_{N-1} \end{pmatrix}$

N := Number of columns in a WCM. N is an integer multiple of μ .
If $\mu = 2$ then N is even.

Appendix B

Wavelet Transform Theory

B.1 Wavelets and Wavelet Transforms

Most signals in science and engineering are modeled as mathematical functions for purposes of analysis. In order to separate or examine certain important features or characteristics of the signal, the function is often expanded in terms of basis functions that span the space or a subspace that the signals of interest reside in. The most common example of this is the Fourier transform where a signal that originates in the time domain is reformulated in the frequency domain by expanding the function in terms of trigonometric or complex exponential basis functions. This basis is most appropriate when the signals have periodic components or are produced by systems that are modeled by constant coefficient differential or difference equations.

Consider a periodic, possibly complex-valued, signal $g(t)$ that is square integrable over the range $\{0 \leq t \leq 1\}$ and with period one so that

$$g(t) = g(t + 1). \quad (\text{B.1})$$

This function can be expanded in a Fourier series of the form

$$g(t) = \sum_{n=-\infty}^{\infty} b_n e^{i2\pi nt} \quad (\text{B.2})$$

with the coefficients given by

$$b_n = \int_0^1 g(t) e^{-i2\pi nt} dt \quad (\text{B.3})$$

which is an inner product of $g(t)$ with the basis functions. Similarly, one defines the wavelet transform with respect to a basis of wavelet functions.

The wavelet basis is generated by a $\mu \times N$ matrix $[a]$, where μ and N are positive integers and N is a multiple of μ . The matrix

$$[a] := \begin{pmatrix} a_0^0 & \dots & a_{N-1}^0 \\ \vdots & a_j^i & \vdots \\ a_0^{\mu-1} & \dots & a_{N-1}^{\mu-1} \end{pmatrix} \quad (\text{B.4})$$

is a *wavelet coefficient matrix* ("WCM") if it satisfies the *scaling conditions*

$$\sum_{k=0}^{N-1} \bar{a}_k^i a_{k+\mu l}^j = \mu \delta_{i,j} \delta_{0,l} \quad (\text{B.5})$$

$$\sum_k a_k^i = \mu \delta_{0,i} \quad (\text{B.6})$$

where $\delta_{i,j}$ equals 1 if $i = j$ and 0 otherwise. The overbar denotes complex conjugation and l is an integer. The sums over k are finite sums since only finitely many of the numbers a_k^i are different from zero.

The positive integer μ is called the *multiplier* of the wavelet system and N is called its *length*;

This matrix of numbers provides coefficients for the vector of recursions

$$\varphi^i[a](x) = \sum_{k=0}^{N-1} a_k^i \varphi^0[a](2x - k) \quad (\text{B.7})$$

which implicitly define the *wavelet scaling function* $\varphi^0[a]$ and explicitly define the *basic wavelet functions* $\varphi^i[a](x)$, $1 \leq i < \mu$. Observe that only $\varphi^0[a]$ appears on the right hand side. The functions $\varphi^i[a](x)$ are defined for all real numbers $x \in \mathbb{R}$.

The fundamental fact about systems of compactly supported wavelets is that the collection of functions

$$\text{Basis}[a] := \{ \mu^{j/2} \varphi^i[a](\mu^j x - k) : \\ 0 \leq i < \mu, \quad j, k \in \mathbb{Z} \}$$

form a basis for L^2 spaces, in particular for $L^2(\mathbb{R})$.

We now focus on the case of $\mu = 2$ and will use the following simplified notation for the scaling function $\varphi(t) \equiv \varphi^0[a](t)$ and the wavelet function $\psi(t) \equiv \varphi^1[a](t)$ where $t \in \mathbb{R}$. It can be shown that if the coefficients of this equation satisfy the wavelet conditions, stated above, the solution $\varphi(t)$ will be orthogonal to integer translates of itself and can be normalized such that

$$\langle \varphi(t), \varphi(t - k) \rangle \triangleq \int \varphi(t) \varphi(t - k) dt = \delta_{0,k} \quad (\text{B.8})$$

This means the set of basis functions

$$\varphi_l(t) = \varphi(t - l) \quad (\text{B.9})$$

spans a subspace \mathcal{V}_0 in L^2 and the coefficients of an expansion within this subspace can be calculated as simple inner products. The feature of scaling functions that makes them attractive for signal processing is their ability to model signal properties that are related to the independent variable t . One can increase the size of the subspace spanned by the scaling functions by using $\varphi_{j,k}(t) := 2^{j/2} \varphi(2^j t - k)$ which spans a subspace \mathcal{V}_j . One can show that $\mathcal{V}_0 \subset \mathcal{V}_1 \subset \mathcal{V}_2 \subset \dots$.

The features of a signal can often be better described by defining a slightly different set of orthogonal basis functions that span the *differences* between the spaces spanned by the various scales of the scaling function. These new functions are the wavelets. The *basic wavelet* is defined in terms of the scaling function by

$$\psi(t) = \sum_k (-1)^k a_{N-k-1} \varphi(2t - k). \quad (\text{B.10})$$

It is the prototype of a class of orthonormal basis functions of the form

$$\psi_{j,k}(t) = 2^{j/2} \psi(2^j t - k) \quad (\text{B.11})$$

where 2^j is the scaling of t , $2^{-j}k$ is the translation in t , and $2^{j/2}$ maintains the unity norm of the wavelet. We shall say that j is the base-2 logarithm of the scale. If \mathcal{W}_j is the subspace of $L^2 = L^2(\mathbb{R})$ spanned by the integer translates of the wavelet $2^{j/2} \psi(2^j t)$, additional disjoint subspaces are spanned by integer translates of the wavelets for each different scale index j , that is, by the functions $\psi_{j,k}(t)$. The relationship of the various subspaces can be seen from the following expressions:

$$\mathcal{V}_0 \subset \mathcal{V}_1 \subset \mathcal{V}_2 \subset \dots \subset L^2 = L^2(\mathbb{R}), \quad (\text{B.12})$$

$$\mathcal{V}_0 \oplus \mathcal{W}_0 = \mathcal{V}_1, \quad (\text{B.13})$$

$$\mathcal{V}_{j-1} \oplus \mathcal{W}_{j-1} = \mathcal{V}_j, \quad (\text{B.14})$$

$$L^2 = \mathcal{V}_0 \oplus \mathcal{W}_0 \oplus \mathcal{W}_1 \oplus \dots \quad (\text{B.15})$$

and indeed, if we allow j to run over *all* integers, then

$$L^2 = \dots \mathcal{W}_{-2} \oplus \mathcal{W}_{-1} \oplus \mathcal{W}_0 \oplus \mathcal{W}_1 \dots \mathcal{W}_j \dots \quad (\text{B.16})$$

This states that the set of basis functions formed from $\varphi_l(t)$ and $\psi_{j,k}(t)$ span all of L^2 and, therefore, any function in L^2 can be written

$$g(t) = \sum_{l=-\infty}^{\infty} c_l \varphi_l(t) + \sum_{j=0}^{\infty} \sum_{k=-\infty}^{\infty} d_{j,k} \psi_{j,k}(t) \quad (\text{B.17})$$

with the coefficients expressed by

$$c_l = \int g(t) \varphi_l(t) dt \quad (\text{B.18})$$

and

$$d_{j,k} = \int g(t) \psi_{j,k}(t) dt. \quad (\text{B.19})$$

The basis functions $\varphi_l(t)$ and $\psi_{j,k}(t)$ are numerical valued functions of numerical variables; they have no physical dimension. In the expansion formula (B.17) the argument $2^j t - k$ of ψ is a pure number so, writing

$$2^j t - k = 2^j \left(t - \frac{k}{2^j} \right)$$

the quantity 2^j has the dimension t^{-1} , i.e. frequency, and $k/2^j$ has the dimension time.

These wavelet coefficients completely and uniquely describe the original signal and can be used to represent it in a way similar to Fourier coefficients. Because of the orthonormality of the basis functions, there is a version of Parseval's theorem that relates the energy of the signal $g(t)$ to the energy in each of the wavelet expansion components and their wavelet coefficients by the formula

$$\|g\|^2 = \sum_l |c_l|^2 + \sum_{j \geq 0} \sum_{k=-\infty}^{\infty} |d_{j,k}|^2. \quad (\text{B.20})$$

This is one reason why the orthonormality is so important. Daubechies [2] showed that the translates of the scaling function and the translated dilations of the wavelets are orthonormal, and all of these functions have compact support (i.e. are non-zero only over a finite region) if there are only a finite number of non-zero coefficients a_k in the recursive scaling equation (B.7). This provides the time localization that is particularly desirable for analyzing both the time and the frequency behavior of transient signals.

Note that there is an infinite set of scaling functions and wavelets that can be obtained by choosing different coefficients a_k in (B.7).

B.2 Wavelet Approximation to the Fourier Transform

In this chapter we state the relationships between the wavelet transform and the Fourier transform as derived by Resnikoff and Burrus [5].

In this section we restrict attention to periodic functions $g(t)$. Let $g(t+1) = g(t)$. Then the scaling function and wavelet coefficients in (B.18) and (B.19) are also periodic. The scaling function coefficients c_l calculated from (B.18) and using (B.1) are

$$c_l = \int_{-\infty}^{\infty} \varphi(t-l) g(t) dt = \int_{-\infty}^{\infty} \varphi(\tau) g(\tau+l) d\tau = \int_{-\infty}^{\infty} \varphi(\tau) g(\tau) d\tau = c_0. \quad (\text{B.21})$$

Using the "partition of unity" property of scaling functions which states

$$\sum_{l=-\infty}^{\infty} \varphi(t-l) = 1 \quad (\text{B.22})$$

we can write (B.21) as

$$c_0 = \sum_{l=-\infty}^{\infty} \int_0^1 \varphi(\tau-l) g(\tau) d\tau = \int_0^1 g(\tau) \sum_l \varphi(\tau-l) d\tau = \int_0^1 g(\tau) d\tau = c. \quad (\text{B.23})$$

Therefore, c_l is a constant and not a function of l . Note the interesting property of $\varphi(t)$ which causes the scaling function coefficient of a periodic

function to be equal to the DC Fourier series coefficient for any scaling function satisfying (B.7);

$$\int_{-\infty}^{\infty} \varphi(t) g(t) dt = \int_0^1 g(t) dt. \quad (\text{B.24})$$

Using the partition of unity property (B.22) again shows the scaling function term of the expansion in (B.17) is a constant.

$$\sum_l c_l \varphi_l(t) = c \sum_l \varphi(t-l) = c. \quad (\text{B.25})$$

In a like manner, using (B.19) we calculate the wavelet coefficients in the expansion (B.17) by

$$d_{j,k+K} = 2^{j/2} \int \psi(2^j t - k - K) g(t) dt = 2^{j/2} \int \psi(2^j(t - 2^{-j}K) - k) g(t) dt \quad (\text{B.26})$$

which, after the change of variables $\tau = t - 2^j K$ and $l = 2^{-j} K$ or $K = 2^j l$, becomes

$$d_{j,k+K} = 2^{j/2} \int \psi(2^j \tau - k) g(\tau + 2^{-j} K) d\tau = d_{j,k}. \quad (\text{B.27})$$

This states

$$d_{j,k} = d_{j,k+2^j l} \quad (\text{B.28})$$

or, the wavelet coefficients $d_{j,k}$ are periodic in k with period 2^j . We now use these properties with the basic definition of the Fourier series coefficients from (B.3).

$$b_n = \int_0^1 g(t) e^{-i2\pi n t} dt \quad (\text{B.29})$$

Substituting the wavelet expansion from (B.17) for $g(t)$ into (B.29) gives

$$b_n = \begin{cases} c & \text{if } n = 0; \\ \sum_{j=0}^{\infty} \sum_{k=0}^{2^j-1} d_{j,k} \hat{\psi}_{j,k}(n) & \text{in } n \neq 0 \end{cases}. \quad (\text{B.30})$$

where $\hat{\psi}(f)$ is the Fourier transform of $\psi(t)$ defined by

$$\hat{\psi}(f) = \int_{-\infty}^{\infty} \psi(t) e^{-i2\pi f t} dt \quad (\text{B.31})$$

with an inverse given by

$$\psi(t) = \int_{-\infty}^{\infty} \hat{\psi}(f) e^{i2\pi ft} df. \quad (\text{B.32})$$

An alternative form, which uses the Fourier transform of the basic wavelet $\psi(t)$ rather than $\psi_{j,k}(t)$, is [5]:

$$b_n = \begin{cases} c & \text{if } n = 0; \\ \sum_{j=0}^{\infty} 2^{-j/2} \hat{d}_j(n) \hat{\psi}\left(\frac{n}{2^j}\right) & \text{if } n \neq 0 \end{cases}. \quad (\text{B.33})$$

where $\hat{d}_j(f)$ is the discrete Fourier transform (DFT) of $d_{j,k}$ for various scales j and is defined by [1]

$$\hat{d}_j(m) = \sum_{k=0}^{N-1} d_{k,j} e^{-i2\pi mk/N} \quad (\text{B.34})$$

with an inverse given by

$$d_{j,k} = \frac{1}{N} \sum_{m=0}^{N-1} \hat{d}_j(m) e^{i2\pi mk/N}. \quad (\text{B.35})$$

The formula for expressing the wavelet coefficients in terms of the Fourier coefficients is easily obtained. From (B.19) we have

$$d_{j,k} = \int_{-\infty}^{\infty} g(t) \psi_{j,k}(t) dt.$$

which, after using (B.2) and reordering, gives

$$d_{j,k} = \sum_{n=-\infty}^{\infty} b_n \int_{-\infty}^{\infty} e^{i2\pi nt} \psi_{j,k}(t) dt \quad (\text{B.36})$$

$$d_{j,k} = \sum_{n=-\infty}^{\infty} b_n \hat{\psi}_{j,k}(-n) \quad (\text{B.37})$$

and, from (B.24), the scaling function coefficient is given by

$$c_k = b_0 = c. \quad (\text{B.38})$$

An alternative derivation of (B.37) is

$$d_{j,k} = \text{DTFT} \left\{ b_n \hat{\psi} \left(\frac{n}{2^j} \right) \right\}_{f=k/2^j} \quad (\text{B.39})$$

where the discrete-time Fourier transform is defined by

$$\text{DTFT}\{x_n\} = \hat{x}(f) = \sum_{n=-\infty}^{\infty} x_n e^{-i2\pi n f} \quad (\text{B.40})$$

and the inverse is

$$x_n = \int_0^1 \hat{x}(f) e^{i2\pi n f} df. \quad (\text{B.41})$$

These are the basic relationships between the Fourier transform and wavelet transform. Equation (B.33) relates the Fourier series expansion coefficients of $g(t)$ to the Fourier transform of the fundamental wavelet and the DFT of the wavelet expansion coefficients of $g(t)$. Equation (B.39) expresses the wavelet expansion coefficients of $g(t)$ in terms of samples of the DTFT of the product of samples of the Fourier transform of the basic wavelet and the Fourier series coefficients.

In practice, a band limited signal sampled at the appropriate rate implies a finite sum in (B.33) that corresponds to the finest scale of $j = J$ and the Fourier series is likewise finite. The independent variable f is frequency in Hertz or cycles per second, $\hat{d}(m)$ is periodic with period $N = 2^j$, and $\hat{x}(f)$ is periodic with period one. Clearly, the DFT or its inverse can be calculated with the FFT [1].

Energy and Parseval's Theorem

Orthonormal basis systems allow direct calculation and interpretation of the energy in a signal partitioned in both the time and the expansion domains. Parseval's theorem for the Fourier series (B.2) states

$$\int_0^1 |g(t)|^2 dt = \sum_{n=-\infty}^{\infty} |b_n|^2. \quad (\text{B.42})$$

The "power" in a signal is proportional to the square of the signal (e.g. voltage, current, force, or velocity) and, therefore, the energy is given by the integral of the square of the signal magnitude. Parseval's theorem states

how the total energy is partitioned in the frequency domain in terms of the partition provided by the orthonormal basis functions. For the general wavelet expansion of (B.17), Parseval's theorem is

$$\int_0^1 |g(t)|^2 dt = \sum_{l=-\infty}^{\infty} |c_l|^2 + \sum_{j=0}^{\infty} \sum_{k=-\infty}^{\infty} |d_{j,k}|^2 \quad (\text{B.43})$$

with the energy in the expansion domain partitioned in time by l and k and in scale by j . For the case of periodic functions, the relationship reduces to

$$\int_0^1 |g(t)|^2 dt = |c_l|^2 + \sum_{j=0}^{\infty} \sum_{k=1}^{2^j} |d_{j,k}|^2. \quad (\text{B.44})$$

One can show that $|\hat{\psi}(f)| \rightarrow 0$ as $f \rightarrow 0$ and also as $f \rightarrow \infty$. Therefore, there will be a band of frequencies where most of the energy in $\hat{\psi}(f)$ is concentrated. Likewise, for many signals, the energy will be concentrated in a region of the (j, k) plane. Because of this concentration and using (B.33), the energy of the signal $g(t)$ at frequency n and at scale j and time k is approximately measured by

$$2^{-j} \left| \hat{\psi} \left(\frac{n}{2^j} \right) \right|^2 |d_{j,k}|^2 \quad (\text{B.45})$$

If most of the energy in $\hat{\psi}(f)$ occurs around frequency f_0 , then $f_0 = n/2^j$ relates the dominant Fourier frequency f_0 to the dominant wavelet scale j . Scale and frequency are independent primitive concepts, but the selection of a wavelet basis establishes a connection between them, and the results of this chapter allow one to move between the two descriptions, using the one most appropriate for a particular problem. The simple partitioning of the energy content of a signal among frequencies has been generalized to include the parameters of time and scale. In addition, we have at our disposal the choice of wavelet systems, which is controlled by the choice of a_k in (B.7), and determines the detailed nature of the relationship between frequency and scale.

B.3 Computational Complexity of the Wavelet Approximation to the Fourier Transform

This section is concerned with the computational efficiency of wavelet-based approximations to the Fourier Transform. The computational cost for several wavelet approximations of the Fourier transform are presented and comparisons are made with the computational complexity of the FFT.

In the most applications, the size of the data set is the determining factor. We will refer to a technique's asymptotic complexity as representative of *how quickly* the number of computations grows as the problem size, N , increases. Comparisons with the FFT are natural here, since the FFT is a commonly used and well understood algorithm. We consider wavelet transforms which resolve to sub-band frequency components in part or perhaps all of the signal bandwidth. No attempt will be made to assign a value to a particular scheme, since the level of approximation appropriate for a given application can only be determined by extensive experiments. The quality of the approximation varies from approach to approach, and many simple and consistent optimizations can be made, but usually require specialization to a particular set of circumstances.

The simplest, and also least accurate technique for estimating the DFT of a signal is a direct, balanced tree approach with filters optimized for sharp out-of-band rejection. Typically the Daubechies wavelets are used for this approach, although slight improvements in the quality of the results are possible with other choices.¹ The computational complexity of pure wavelet methods are analyzed in section 2.5.

Additional improvements in the quality of the results and the speed of computation is possible when full frequency resolution within a limited sub-

¹Real wavelet filters have spectral characteristics which are conjugate-symmetric, and these would combine large and small frequencies in the same band. To avoid this aliasing, a modification was made to the analysis and synthesis filters. Simply put, the filter characteristics were "rotated" so that, for a full bandwidth complex signal, whose Fourier transform has the full $2N$ degrees of freedom, the low-pass side of a single analysis stage captures the lower half of the spectrum and the high pass the upper. In the real case, the Fourier transform is conjugate-symmetric, the "full" bandwidth amounts to only $f_s/2$, half the sample rate, and "low-frequency" is then interpreted as being $f_s/4$.

band is the desired result. This is accomplished by using the wavelet transform to separate sub-bands, and then using an FFT on the data within the band to reconstruct a "local" approximation to the "full" Fourier transform. This can be done either (1) solely within that band, or (2) throughout the entire bandwidth. If the sub-bands used in such a reconstruction capture a significant fraction of the total energy contained in the signal, excellent approximations can be constructed quite cheaply. Notably, the locations of peaks within bands are properly located and reconstruction away from edges of sub-bands is quite accurate. The complexity of such a technique is:

$$OPS = \alpha(K)N(1 - R) + NR(3 + \log(NR)) + RN \quad (\text{B.46})$$

where

- N = the number of data points;
- K = the size of the wavelet filter (assumed to be constant throughout the procedure);
- R = the portion of the bandwidth of the signal which is resolved (assumed to be $1/2^L$ for some L).

For this estimate we assume that the reconstruction is done purely in-band, and only a single band is used (i.e., we *don't* expand further than necessary to locate the energy, since that is wasted work if we truly want the DFT).

Figure B.2 shows the results of this calculation superimposed on the results for a straight wavelet approach. The tightly clustered lines represent the hybrid case, and clearly show a usable advantage (i.e., reasonable length filters are justified) over both the FFT and the straight wavelet methods for problem sizes starting around 64 data points.

In addition to the results stated there we note that significant improvements may be made by combining these methods with phase-unwrapping in order to move the "mass" of the return to the region of best filter performance, namely zero frequency for real filters and $f = f_s/4$ for the "rotated" filters.

The approach of relocating the center of the "target" frequency band is the essence of the phase unwrapping technique, where the centroid is moved to the center of the DC or zero frequency band. Real Daubechies wavelets

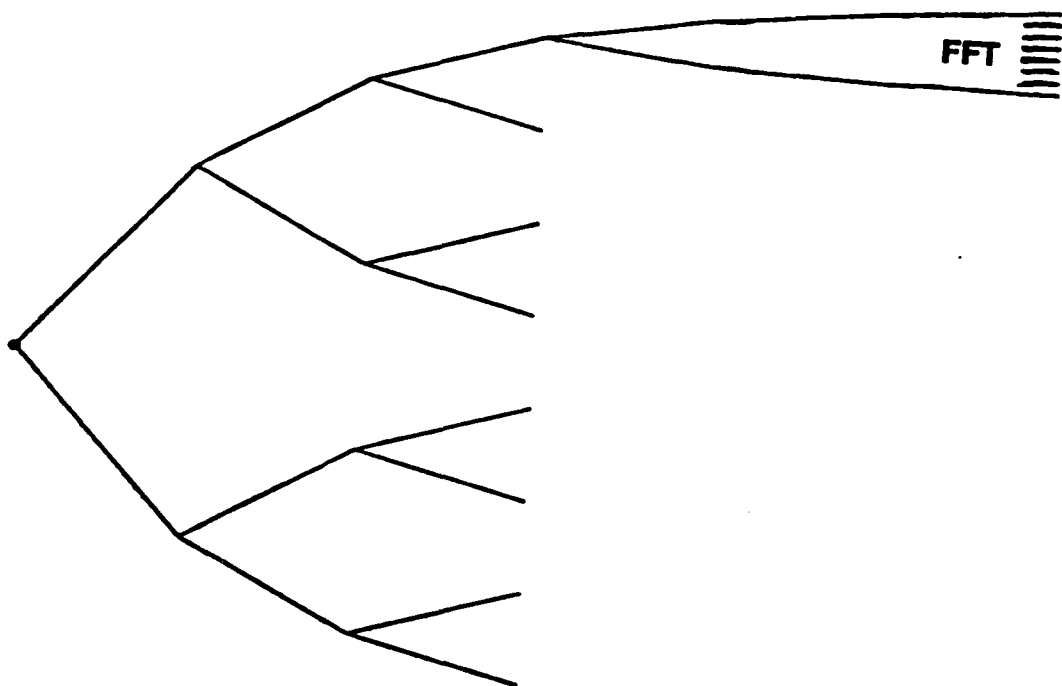


Figure B.1: Tree Structure for the Hybrid Wavelet-Fourier Transform Method.

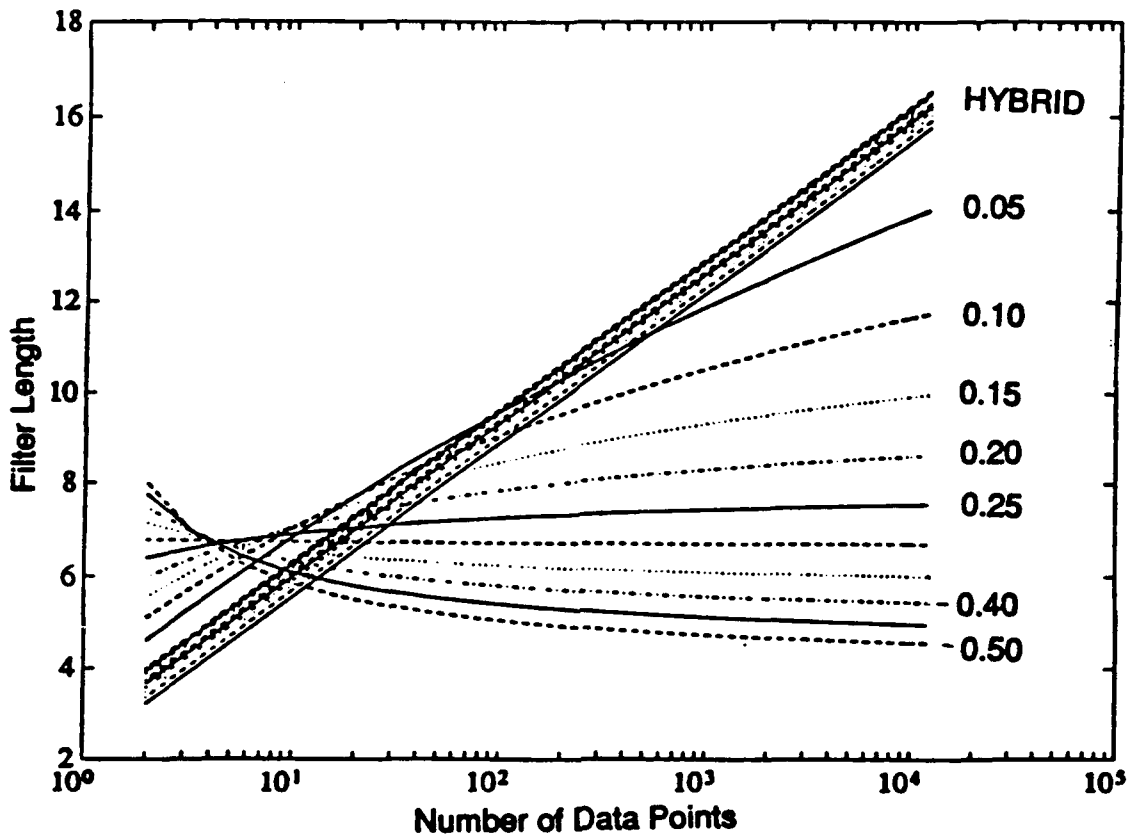


Figure B.2: Computational Complexity of the Wavelet Transform vs. the FFT: Filter Length vs. N for equivalent complexity for various fractions of the total bandwidth (R) with the addition of the case when the FFT is used to perform the final frequency analysis in a subband

have optimal performance at D.C and minimum aliasing. Phase unwrapping carries an overhead of N complex multiplies per N input points. In addition, calculation of the FFT for in-band components takes R additional operations while calculation of the entire FFT from inband components takes approximately N additional computations. Neither of these has a significant contribution to the total computation for large problem sizes, since both are overwhelmed by the $O(n \log_2(n))$ behavior of the DFT's. The number of operations is then:

$$OPS = N + RN + \alpha N(1 - R) + NR(3 + \log(NR)) \quad (B.47)$$

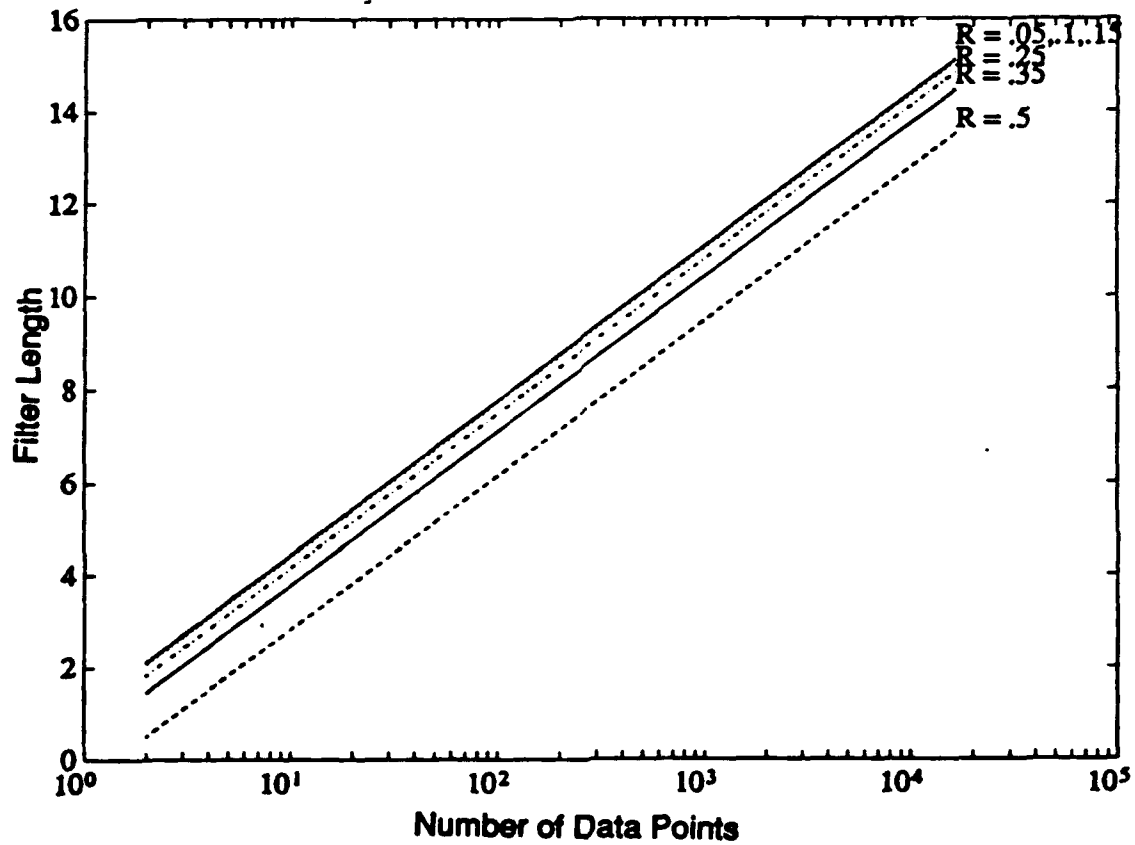


Figure B.3: Computational Complexity of the Wavelet Transform with Phase Unwrapping vs. the FFT: Filter Length vs. N for equivalent complexity for various values of R for the case of using phase unwrapping and the FFT to perform the final frequency analysis in a subband

Figure B.3 shows the trade-off between this method and an FFT on the full problem, reflected in the allowable filter size for equivalent quantities of computations.

Appendix C

Phase Unwrapping

In this section we describe a method for preprocessing MMW radar data to concentrate the target energy into the largest scale wavelet coefficients. It is called *phase unwrapping*. It can be used to process radar fine range data from phase history data sequences whose bandwidth is less than one half the sampling rate.

This section has the following objectives:

- to describe the phase unwrapping algorithm
- to describe a method of radar imaging based on combining phase unwrapping with the one-sided "Mallat" algorithm
- to present numerical examples using actual radar phase history data

The phase unwrapping algorithm is based on the topological concept of winding number. Let $z : [a, b] \rightarrow C$ be a differentiable complex valued function. Define the *winding number* of z over the interval $[a, b]$ by

$$W(z, a, b) = \int_{t=a}^{t=b} \text{Real}(w(t)/z(t))dt, w = dz/idt. \quad (C.1)$$

Hence $W(z, a, b)$ represents the amount of angular winding about 0 (in the counterclockwise direction) of the point $z(t)$ as t moves from a to b . If $z(t)$ represents (interpolated) phase history data formed from a rough reflector (several scatterers per resolution cell) then it is generally understood that $z(t)$ may be approximately modelled by a complex Gaussian random process

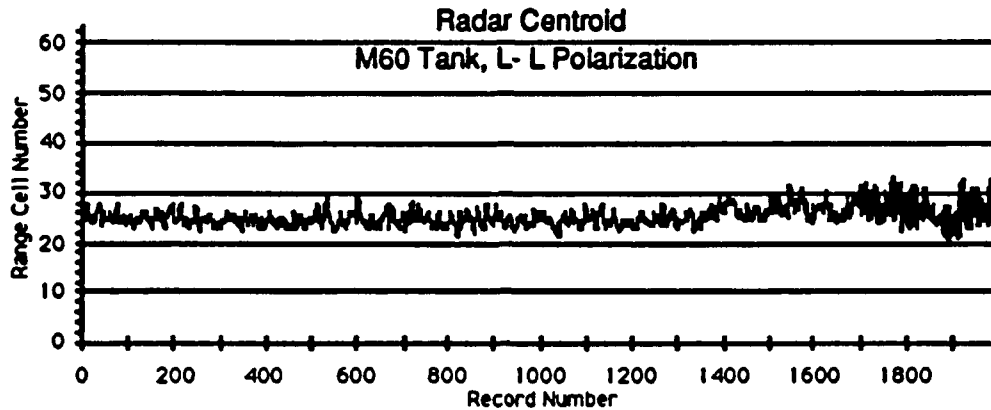


Figure C.1: Radar Centroids for M60 Tank Target

having power spectral density function $I(y)$. Furthermore, I represents the expected value of $|\hat{z}(y)|^2$ where \hat{z} denotes the Fourier transform of z .

The expected value $E(W)$ of $W(z, a, b)$ equals $2\pi(b-a)$ times the *centroid* of I , thus

$$E(W) = 2\pi(b-a) \int I(x)x dx / \int I(x) dx. \quad (C.2)$$

The factor 2π arises because of its appearance in the definition of the Fourier transform.

The radar centroids and phase centers were calculated for 2000 different aspect angles of the M60 tank target to evaluate the stability of the phase unwrapping algorithm. Figure C.1 plots the results of the centroid calculations and figure C.2 plots the results of the phase unwrapping method. Statistical analysis of these two sets of data reveals that the mean difference is 0.33 range cells and the standard deviation of the difference is 1.32 indicating a slight bias but otherwise very consistent results. The correlation coefficient r between the two sets of data is 0.9986 indicating that the phase unwrapping method is a near perfect predictor of the true radar centroid.

The phase unwrapping algorithm consists of two parts:

1. estimate the total phase winding of a phase history function $z(t)$ from its sample values z_k ,
2. remove this phase winding by multiplying z_k by an appropriate complex sinusoidal sequence.

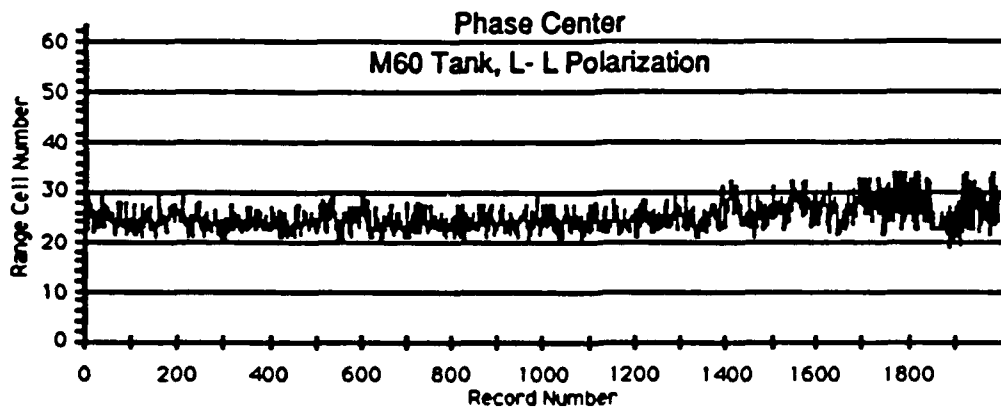


Figure C.2: Phase Centers Calculated by Unwrapping Method for M60 Tank Target

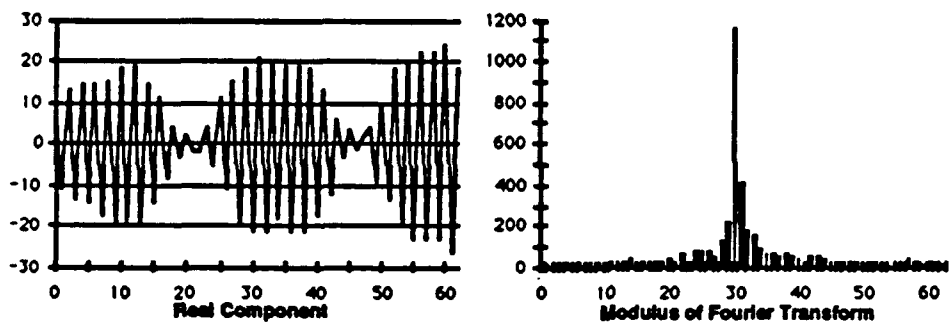


Figure C.3: Raw Range Data and DFT for Trihedral Target

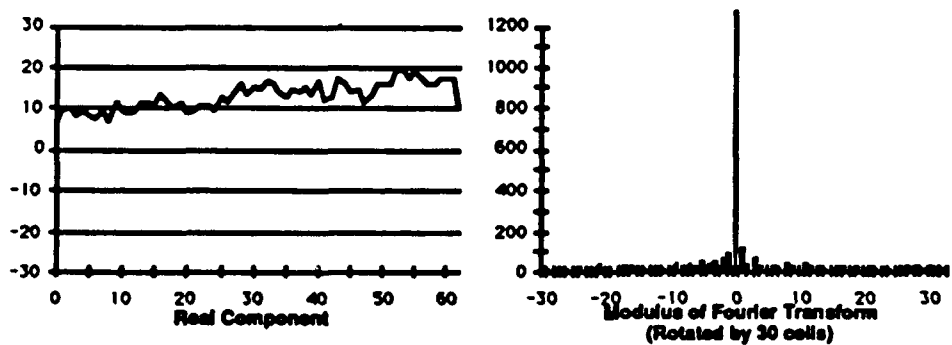


Figure C.4: Phase Unwrapped Data and DFT for Trihedral Target

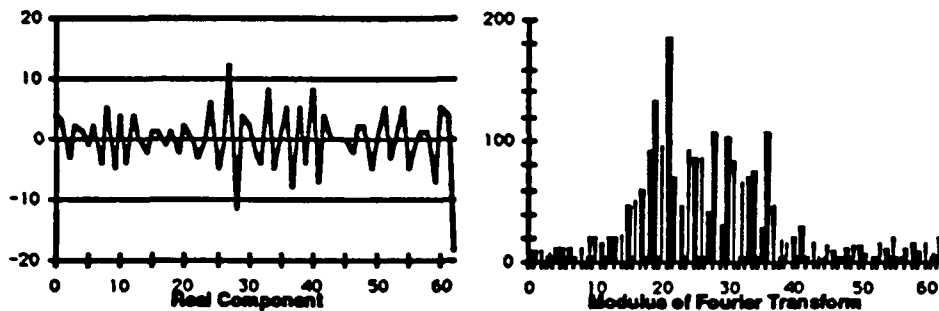


Figure C.5: Raw Range Data and DFT for M60 Tank Target

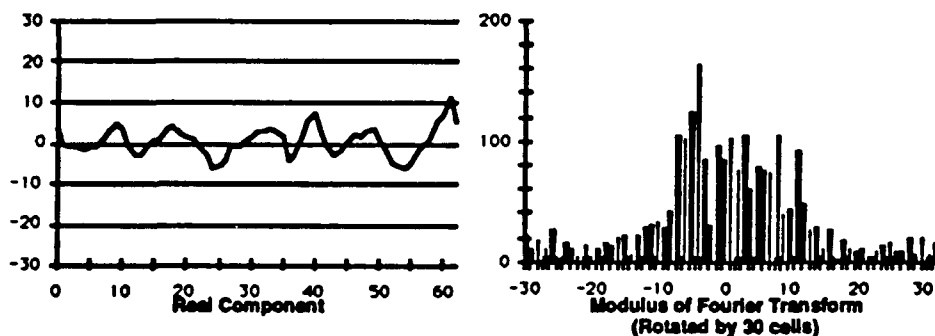


Figure C.6: Phase Unwrapped Data and DFT for M60 Tank Target

The first step requires estimating $W(s, a, b) = \sum_{k=a}^{b-1} W(z, k, k+1)$ from sample values z_k under the assumption that the bandwidth of $z(x)$ is less than half than the sampling rate. In this case either z_k or $(-1)^k z_k$ is a low frequency content signal d_k . Let a_k denote the angle change between d_{k+1} and d_k . Then the average magnitude of a_k is less than 90 degrees. This criteria can be used to select $d_k = z_k$ or $d_k = (-1)^k z_k$. Furthermore, a_k (nearly always) represents either $W(z, k, k+1)$ or $-\pi/2 + W(z, k, k+1)$. Therefore, $W(z, a, b) \approx \sum_{k=a}^{b-1} a_k$ if $d_k = z_k$ else $W(z, a, b) \approx (b-a)\pi/2 + \sum_{k=a}^{b-1} a_k$. Let W denote the total phase winding.

The second step consists of multiplying z_k by the sequence $e^{-iW/(b-a)}$ to obtain $s_k = z_k e^{-iW/(b-a)}$. By the assumptions on z_k and by (C.2), s_k has a low frequency content.

To form a radar image from z_k apply the following steps:

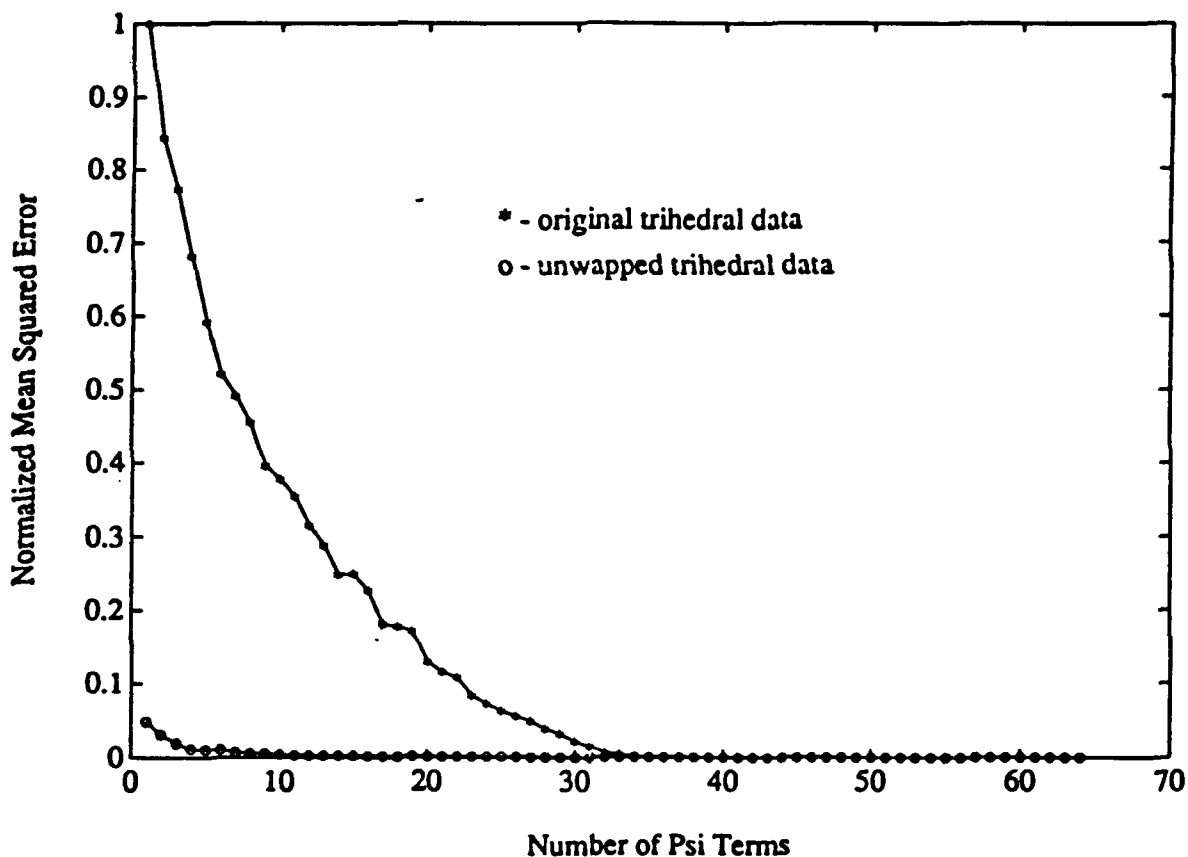


Figure C.7: Comparison of Approximation Error for Trihedral Target for Original and Phase Unwrapped Data

1. estimate W from z_k ,
2. compute $s_k = z_k e^{-iW/(b-a)}$,
3. apply the one-sided recursion method to s_k to form a radar image,
4. if desired, translate this image $W/(2\pi)$ pixels to the right to locate the image in the correct position.

These three steps yield an approximation of the radar image that is formed by computing the (Discrete) Fourier transform of z_k .

Figures C.3 and C.5 are plots of the (raw) real components and DFT for a calibration target and the M60 tank target. Note the oscillatory behavior

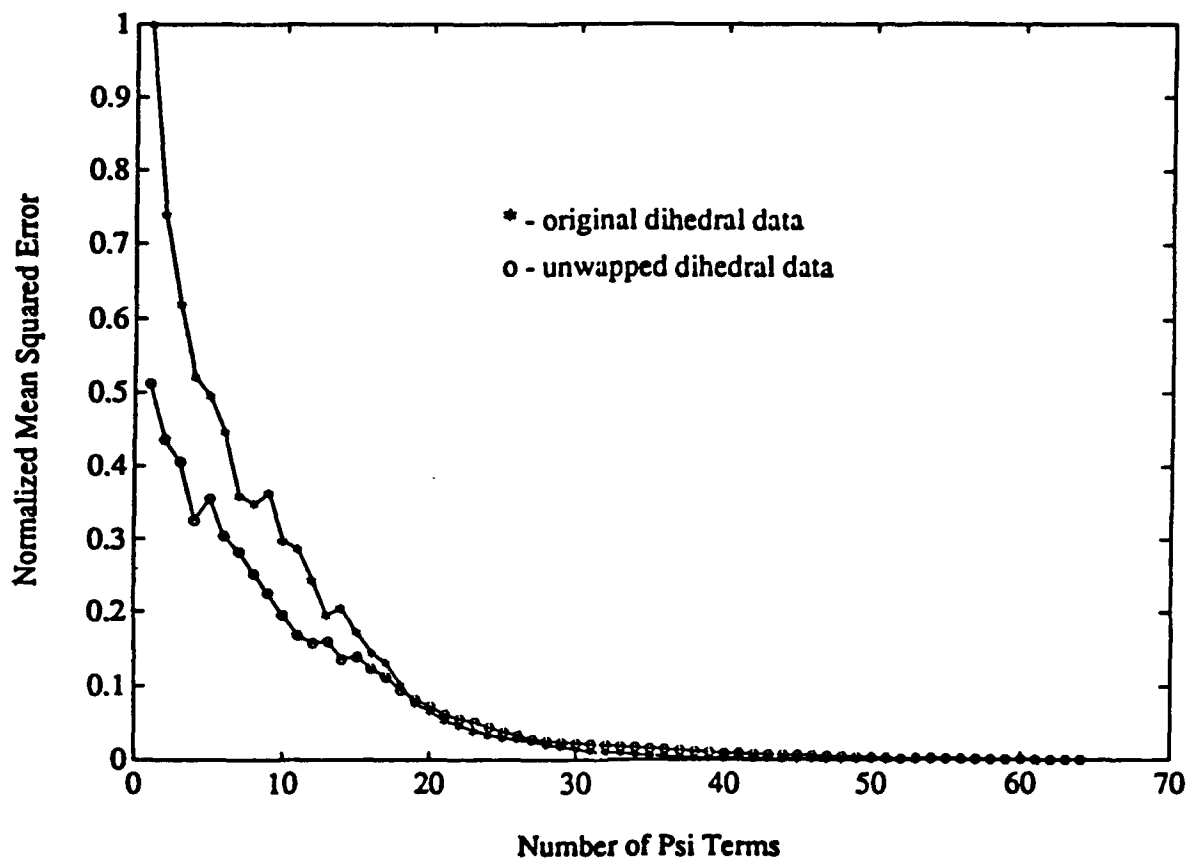


Figure C.8: comparison of Approximation Error for Dihedral Target for Original and Phase Unwrapped Data

of the raw radar data. The results of "phase unwrapping" the radar data for these targets are presented in figures C.4 and C.6. In these figures note the dramatic reduction of oscillatory behavior which allows these function to be well represented by only large scale wavelet terms. There is essentially no loss of shape information caused by the phase unwrapping process indicating that it can be used to reduce the computational complexity without adding any significant artifacts.

Appendix D

Martin Marietta Radar Data and Pulse Compression Processing

This section examines the problem of radar range profile processing that may be amenable to solution by employing wavelet analysis in addition to or in place of conventional Fourier-based analytical methods. The unclassified radar detection processing problem is discussed in detail by Einstein [3] and Skolnik [6].

The problem of obtaining sufficient target signal-to-noise ratio for MMW radar systems with low transmitter power is solved by increasing the duration of the transmitted waveforms, thereby increasing the transmitted energy. Conventional "pulsed" radar systems have their range resolution determined by the pulsewidth of the transmitted waveform and increasing the pulsewidth reduces the range resolution. This limitation is overcome by *coding* the transmitted waveform such that processing (i.e., matched filtering) in the receiver can recover compressed pulse information with an equivalent pulse duration approximately equal to the reciprocal of the spectral bandwidth of the modulated long pulse duration waveform. There are several pulse compression methods available (see [6], §10) however, here we will focus on the problem of processing *time-frequency-coded waveforms*.

D.1 Time-Frequency Pulse Compression

A range finding radar transmitter emits frequency pulses of electromagnetic energy of the form¹

$$u(t) = e^{j(2\pi f_k t + \theta_k + \psi_k(t))} \quad (D.1)$$

where f_k is the (selectable) constant frequency, θ_k is an arbitrary phase angle, and $\psi_k(t)$ represents the phase drift of the oscillator with respect to the constant frequency f_k as a function of time. It is conventional to select the time origin to coincide with the time of emission of the pulse. The emitted frequency will be assumed to serve as the standard reference for the return signal. By definition,

$$\psi_k(0) = 0 \quad \text{and} \quad \frac{d}{dt}\psi_k(0) = 0.$$

The signal reflected from a point target is the original transmitted signal delayed by the transit time and diminished by spherical spreading and the complex reflection coefficient of the target point. Thus the return signal has the form

$$y(t) = A_t u(t - x) e^{j\phi_t} \quad (D.2)$$

where the targets complex reflection coefficient is

$$A_t e^{j\phi_t}$$

and x is the round trip time from the radar to the target. The range r of the target is

$$r = cx/2 \quad (D.3)$$

where c denotes the speed of light.

Upon reception, the reflected signal is mixed with the complex conjugate of the emitted signal to provide

$$v(t) = y(t)u(t) = A_t e^{j\phi_t} u(t - x) \times \overline{u(t)} = A_t e^{-j(2\pi f_k x - \phi_t - \psi_k(t-x) + \psi_k(t))} \quad (D.4)$$

where " $\overline{u(t)}$ " denotes the complex conjugate of $u(t)$.

¹"j" denotes $\sqrt{-1}$.

A pulse of finite duration will attenuate the return: if the pulse shape function is $t \mapsto S(t)$, then the return will be multiplied by $S(t - x)$.

In accordance with Huyghens' principle, a distributed target will produce a return that is the superposition of the point returns. If $\rho(x)$ represents the complex scattering profile (i.e. coefficient) of the target and $s(x)$ represents the transmitted pulse shape, then the received signal due to a differential scattering element $\rho(x)dx$ located at range delay time x will be

$$dE(f_k, t) = \rho(x)s(t - x)e^{j(2\pi f_k(t-x) + \psi_k(t-x) + \theta_k)} dx \quad (D.5)$$

and the received voltage (prior to mixing with the reference signal) is

$$E(f_k, t) = e^{j(2\pi f_k t + \theta_k)} \int_{-\infty}^{\infty} \rho(x)s(t - x)e^{-j(2\pi f_k x - \psi_k(t-x))} dx. \quad (D.6)$$

Einstein [3] shows that $\psi(t - x) \simeq 0$. With this assumption, and after mixing with the reference signal, the complex voltage at the output of the detector becomes

$$V(f_k, t) = e^{-j\psi_k(t)} \int_{-\infty}^{\infty} \rho(x)s(t - x)e^{-j2\pi f_k x} dx. \quad (D.7)$$

Define

$$Q(f_k, t) = \int_{-\infty}^{\infty} \rho(x)s(t - x)e^{-j2\pi f_k x} dx. \quad (D.8)$$

Then the Fourier transform

$$q(x, t) := \hat{Q}(f_k, t) = \rho(x)s(t - x) \quad (D.9)$$

represents the scattering profile $\rho(x)$ of the target, weighted by the pulse shape $s(t - x)$.

Radar returns from stepped frequency pulse trains may be processed either coherently or noncoherently. Coherent processing consists of calculating the Fourier transform of the N coherently detected complex pulse returns from each range cell, where N denotes the number of pulses in the train. The output is a "high resolution" range profile of the scatterers within the range cell.

Noncoherent processing consists of calculating the Fourier transform of the square of the magnitude of the of the pulse returns from a given range

cell, and produces the autocorrelation of the range profile. In both cases the range resolution is determined by the total frequency spread of the pulse train.

Coherent Processing

For coherent processing $q(x, t)$ is realized as the Fourier transform of $Q(f, t)$, i.e.

$$q(x, t) = \int_{-\infty}^{\infty} Q(f, t) e^{j2\pi f x} dx . \quad (D.10)$$

This is *approximated* by (from D.6)

$$\rho(x) s(t - x) \approx \int_{-\infty}^{\infty} V(f, t) e^{j2\pi f x} dx . \quad (D.11)$$

assuming that the phase drift $\psi_k(t)$ of the oscillator is small.

When using a frequency-diverse pulse train the measurements of $V(f, t)$ are not made over a continuum of frequencies but only for a discrete set of frequencies $\{f_k\}$. Thus the continuous transform must be approximated by a discrete (and finite) transform.

For this case Einstein [3] shows that

“The Discrete Fourier Transform (DFT) is a matched filter for the returns from a frequency-diverse pulse train, under the following conditions:

1. Each of the pulse returns is coherently detected by using the transmitted carrier for a given pulse as the coherent reference for that pulse. Thus, a different coherent reference is used for each pulse in the train.
2. The spacing between the different frequencies at which the pulses in the train are transmitted is uniform.
3. There is no relative radial motion between the target and the radar during the transmission of the pulse train.
4. There are no nonlinear differential phase shifts through the radar system between the different carrier frequencies.”

Item #2 is required for application of the DFT to recover a time domain signal from the frequency return signal data. This applies to both coherent and noncoherent processing.

Noncoherent Processing

Noncoherent processing consists of calculating the Fourier transform of the square of the magnitude of the of the pulse returns from a given range cell, and produces the autocorrelation of the range profile. Noncoherent processing offers the following advantages and disadvantages compared with coherent methods:

- The transmitter frequency stability requirements for noncoherent processing are two or three orders of magnitude less than for coherent processing.
- Noncoherent processing is much more robust than coherent processing with respect to relative motion of the target and the radar.
- Coherent processing provides target-to-clutter contrast that is superior to noncoherent processing.

This study does not consider the role of wavelet based signal analysis methods for noncoherent radar data processing.

D.2 Characteristics of the Millimeter Wave Radar Data used in this Study

Millimeter wave radar data was gathered on a test range by Martin Marietta. The radar return signals were coherently detected and the complex data recorded into 3 data sets.

1. Calibration radar reflectors which consisted of an array of two dihedral reflectors and one trihedral reflector. These data were taken with every target measurement, but only 50 records were provided for analysis
2. M60A3 Tank

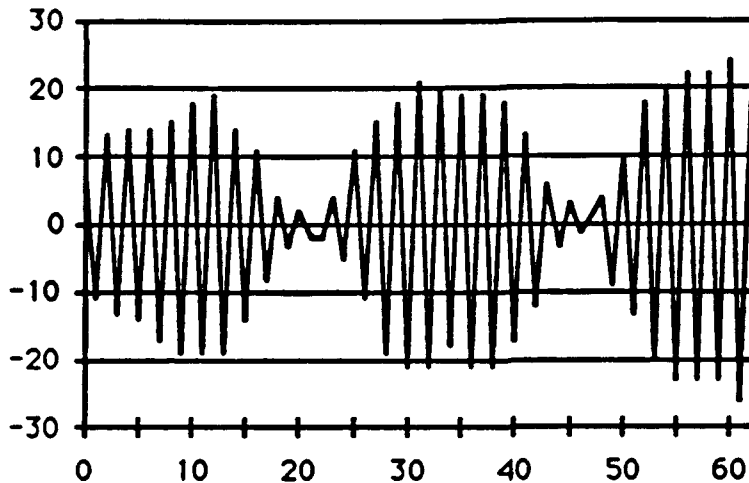


Figure D.1: Real Component of Trihedral Calibration Data

3. M35 Truck.

Figures D.1 to D.6 provide examples of the raw range data and the DFT for the calibration reflectors. Figures D.7 to D.9 are examples of data taken of a military target vehicle, an M60 tank in this case.

The vehicles were located atop a rotating platform adjusted such that the depression (look-down) angle was 15 degrees. The platform rotated at about 1 degree per second.

The data sets for the M35 truck and M60 tank consist of 14,000 records each. A record consists of four complex valued vectors of length 63. Each vector corresponds to a single set of 63 transmitted sinusoidal waveforms (either L or R polarized). The first and second vectors in each record correspond to a L polarized transmission followed by demodulation with a left and right (respectively) polarized waveform. The third and fourth vectors in each record are the data for a R polarized transmission. Thus each record contains, in order, polarization modes LL, LR, RL, and RR.

The time between consecutive sets of transmitted waveforms (i.e. a pair of consecutive rows) equals 6.3μ seconds, therefore, each data set represents 176.4 degrees of rotation.

The frequencies within each transmitted set span a bandwidth of $B = 500$ Megahertz and decrease linearly. Thus the transmitted waveform for the

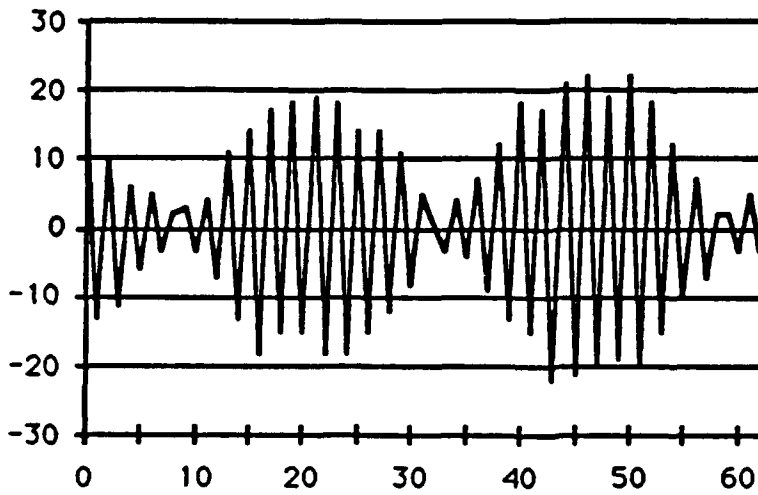


Figure D.2: Imaginary Component of Trihedral Calibration Data

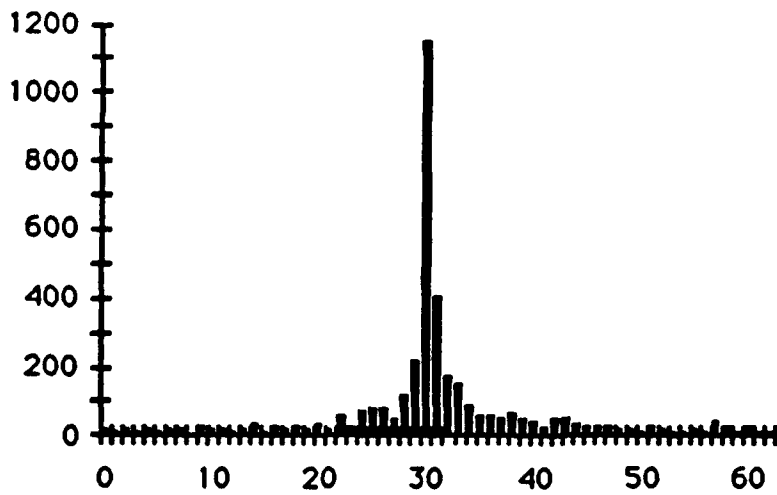


Figure D.3: Modulus of DFT of Trihedral Calibration Data

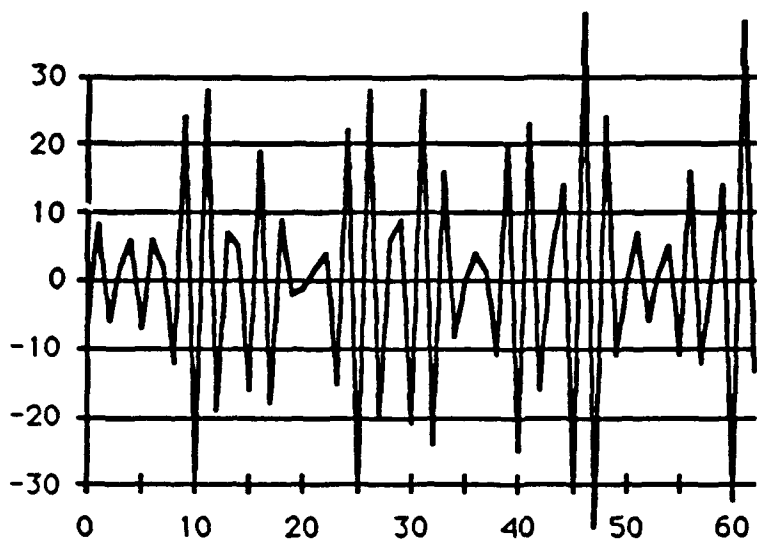


Figure D.4: Real Component of Dihedral Calibration Data

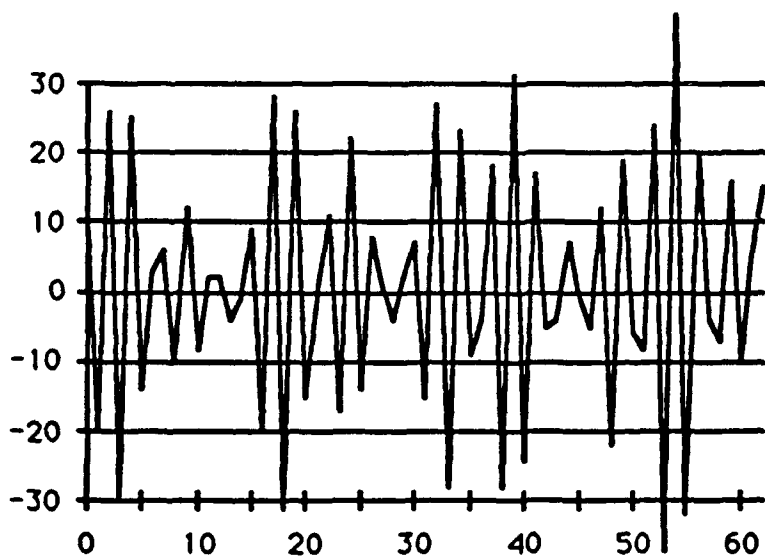


Figure D.5: Imaginary Component of Dihedral Calibration Data

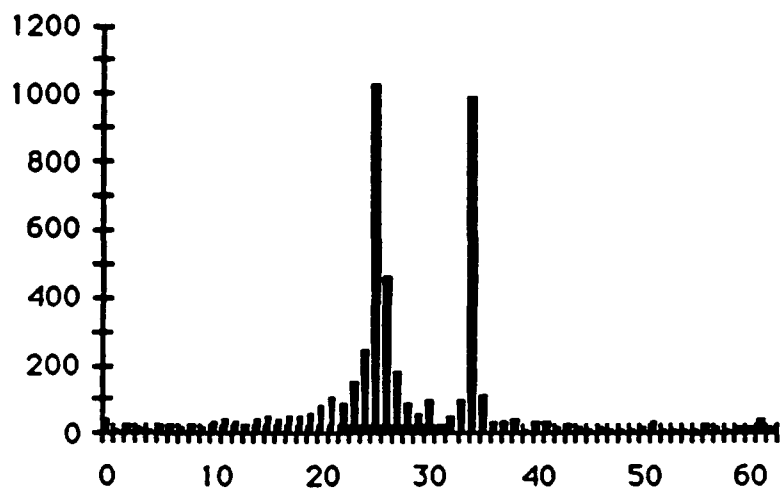


Figure D.6: Modulus of DFT of Dihedral Calibration Data

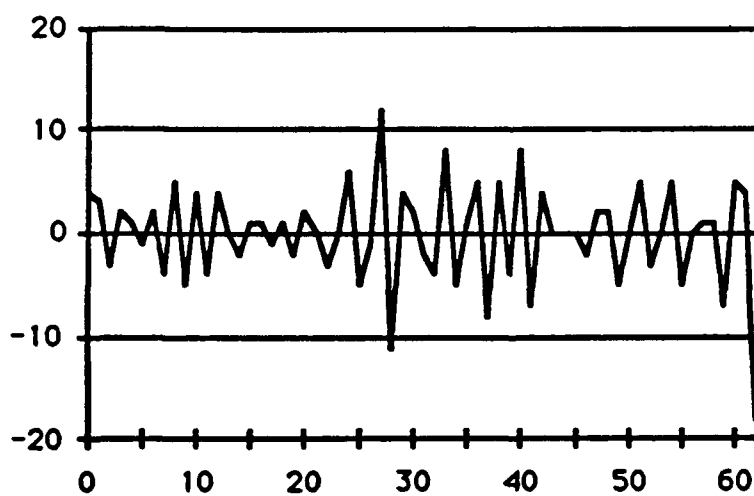


Figure D.7: Real Component of M60 Tank Data (near -20°)

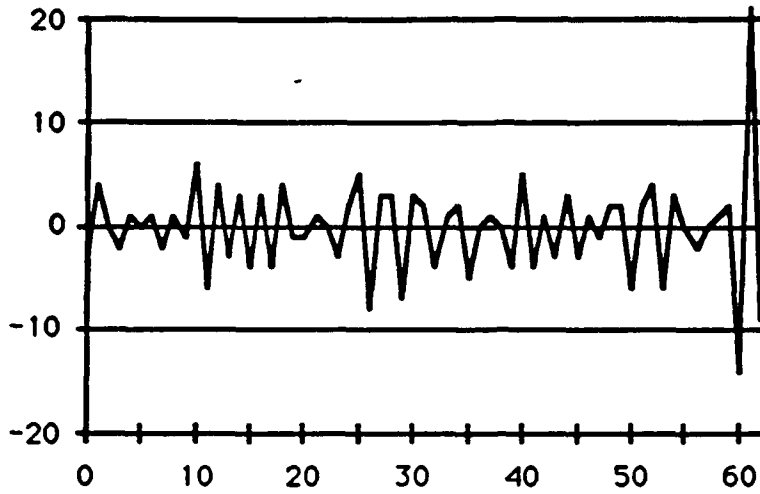


Figure D.8: Imaginary Component of M60 Tank Data (near -20°)

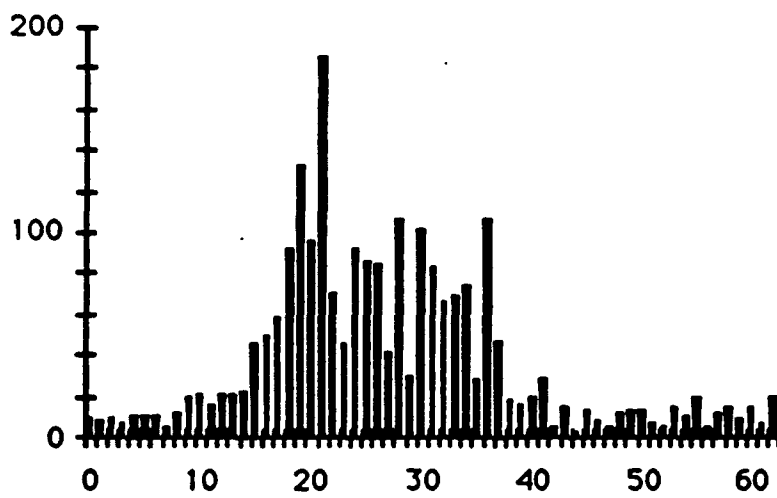


Figure D.9: Modulus of DFT of M60 Tank Data (near -20°)

k -th column within a given pair of rows equals $\sin(2\pi[f_c - (k - 62)B/63]t)$ where f_c equals the reference frequency.

For both vehicles, the angle θ , measured from head-on (0 degrees) counterclockwise, as a function of record index k is given by

$$\theta(k) = ak + b. \quad (D.12)$$

For the tank $a = .0128$ and $b = -23.9$, thus the angle ranges ² from -24 degrees to 156 degrees.

For the truck $a = .0128$ and $b = -34.6$, thus the angle ranges from -35 degrees to 145 degrees.

²The data was divided into "blocks" of 2000 records for ease of shipment on floppy disks. It was discovered late in the study that one "block" of tank data was corrupted. These data were simply skipped leaving 12,000 records of M60 data.

Appendix E

Baseline Target Extent Calculation Method

This section details the baseline method for extracting target extent from a phase history data sequence z_k .

1. compute the Discrete Fourier Transform (DFT) \hat{z}_k of the complex radar data,
2. compute the squared modulus of the transform results $|\hat{z}_k|^2$,
3. establish a threshold $T > 0$,
4. compute an estimate of the noise floor. Since the data provided does not have any "empty" range cells, the average power A calculated from the 16 range cells furthest away from the target, was used as the estimate of the noise floor. This was the best estimate available since the true target position was known to be in the center of the array \hat{z}_k . The first 8 and the last 8 range resolution cells were used to estimate A ,
5. compute the indices I_1 and I_2 of the first and last entries of $|\hat{z}_k|^2$ that exceed $T \times A$,
6. compute target extent as $I_2 - I_1 + 1$.

Bibliography

- [1] C. S. Burrus and T. W. Parks, *(DFT/FFT) and Convolution Algorithms*, John Wiley and Sons, New York, 1985.
- [2] I. Daubechies, "Orthonormal bases of compactly supported wavelets", *Communications on Pure and Applied Mathematics* 1988, Vol. 41, 909-996.
- [3] T. H. Einstein, "Generation of high resolution radar range profiles and range profile auto-correlation functions using stepped-frequency pulse trains," Project Report TT-54, Massachusetts Institute of Technology Lincoln Laboratory, 18 October 1984.
- [4] S. G. Mallat, "A Theory for multiresolution signal decomposition: the wavelet representation", *(IEEE) Transactions on Pattern Recognition and Machine Intelligence*, July 1989, Vol. 11, no. 7, 674-693.
- [5] H. L. Resnikoff and C. S. Burrus, "Relationships between the fourier transform and the wavelet transform", Aware, Inc., AD900609, 1990.
- [6] M. I. Skolnik, *Radar Handbook*, Second Ed., McGraw-Hill, New York, 1990.